The Effect of De-icing Salts on the Chemistry of the Pore Solution in Cement Pastes and Their Influence on Rebar Corrosion

by

Leah Clara Louise Kristufek

A thesis

presented to the University Of Waterloo

in fulfilment of the

thesis requirement for the degree of

Master of Applied Science

in

Mechanical Engineering

Waterloo, Ontario, Canada, 2020

Authors Declaration

I hereby declare that I am the sole author of this thesis. This is a true copy of the thesis, including any required final revisions, as accepted by my examiners.

I understand that my thesis may be made electronically available to the public.

Abstract

Slow moving snow plows and salt trucks are common sights in Canadian winters, especially in parts of Ontario where temperatures hover around zero for much of the winter months. Anti-icing and de-icing salts are an important tool used to increase traction and prevent the formation of black ice. Municipalities may choose to use any of a variety of salts including NaCl, $CaCl_2$ and $MgCl_2$. While all salts depress the freezing point of water, $CaCl_2$ and $MgCl_2$ are effective at lower temperatures making their use more common in Northern Ontario. The use of de-icing and anti-icing salts results in greater traction for vehicles and pedestrians while resulting in increased aesthetics when salt rather than sand is used. These benefits have prompted more northern Canadian municipalities to try using $CaCl_2$ and $MgCl_2$ salts when previously sand and gravel have been used. One example is the City of Edmonton which began using $CaCl_2$ as an anti-icing agent in a pilot project in 2016 but ultimately paused the trial in fall 2019 due to concerns about damage to infrastructure and vehicles[1].

Current research into the effects of road salts on rebar corrosion and concrete focuses mainly on the effects of NaCl salts despite some researchers indicating that $CaCl_2$ and $MgCl_2$ impact concrete and rebar corrosion differently. It is of interest to better understand the hydration products formed in cement exposed to the different salt types since damage to cements can reduce the effective concrete cover depth over rebar. In this research pore solution expression has been used to investigate how different amounts of admixed NaCl, $CaCl_2$ and $MgCl_2$ impact the composition of pore solution from general use Portland cement and by extension the composition of the solid hydration products.

The environment inside cement without salt is protective for reinforcing bars. The pH of expressed pore solution without admixed salts was found to be approximately 13.3. These tests indicate that expressed pore solution from cement paste with admixed NaCl contained significantly more sulphate and chloride than pore solution from pastes which contained $CaCl_2$ or $MgCl_2$. The pH of pore solutions from

pastes containing $CaCl_2$ or $MgCl_2$ also decreased significantly compared to pastes with an equivalent amount of NaCl.

Using the expressed pore solution information about changes in the elemental composition, synthetic pore solutions can be designed which more closely mimic cement exposed to these salts. In this research synthetic pore solutions were prepared from laboratory grade NaOH, KOH, $Ca(OH)_2$ and $CaSO_4$ with additional admixed NaCl, $CaCl_2$ or $MgCl_2$ to investigate rebar corrosion using electrochemical testing techniques. In addition to synthetic pore solutions replicating the pore solution in pastes containing the three salts, other synthetic pore solutions from literature were chosen representing varying elemental compositions and pH values between 12.6 and 13.8.

Acknowledgements

Research never quite goes according to the initial plan. I would like to thank my supervisor, Carolyn Hansson, for her everlasting wisdom, patience and kindness during this process. My ability to critically assess a problem and communicate my findings has improved infinitely with her guidance.

It is not always easy starting a research project, it takes the support of a community to bring a project to completion. Thank you to the members of my lab group, Adam Felinczek, Peter Loudfoot, Marc Johnson, Ibrahim Ogunsanya and Colin Van Niejenhuis. I would also like to thank the technical staff for Mark Griffet, Richard Morrison and Doug Hirst for their help and practical suggestions.

I would also like to thank Joy Hu of the groundwater geochemistry and remediation group for her patience during chemical analysis of my pore solution samples.

Last but not least I would like to thank my family and friends for always being there, even when I haven't reached out recently. In particular the endless support and patience of my boyfriend Donovan who has been amazing.

Table of Contents

List of Figures

List of Tables

List of Equations

List of Abbreviations

Abbreviation	Name
ASTM	American Society for Testing and Materials
β_a and β_c	Anodic and cathodic tafel constants
BFS	Ground granulated blast furnace slag
CE	Counter Electrode
DL	Detection Limit
E_{corr}	Corrosion potential
EDS	Energy Dispersive X-Ray Spectroscopy
FA	Type F fly ash
GU	General Use Cement
HRWR	High range water reducers
IC	Ion chromatography
ICP-OES	Inductively coupled plasma optical emission spectroscopy
ICP-MS	Inductively coupled plasma mass spectroscopy
i_{corr}	Corrosion current density
I_{corr}	Corrosion current
LPR	Linear Polarization Resistance
MTO	Ministry of Transport Ontario
OCP	Open circuit potential
OPC	Ordinary Portland Cement
PS	Pore Solution
QL	Quantification Limit

RE	Reference Electrode
Rebar	Reinforcing bars
RH	Relative Humidity
SCE	Standard calomel electrode
SEM	Scanning Electron Microscope
SEPS	Synthetic Expressed Pore Solution
SCM	Supplementary cementitious materials
SF	Silica Fume
SPS	Synthetic Pore Solution
WE	Working Electrode
w/c	Water to cement (ratio)
XRD	X-ray Powdered Diffraction
XRF	X-ray Fluorescence

Chemical Formulae

Name of Phase/ (cement notation)	Common Name	Formula
C3S	Alite	$3\ CaO \cdot SiO_2$
C2S	Belite	$2\ CaO \cdot SiO_2$
C3A	Aluminate	$2\ CaO \cdot Al_2O_3$
C4AF	Ferrite	$2\ CaO \cdot Al_2O_3 \cdot Fe_2O_3$
Calcium Sulphate	Gypsum	$CaSO_4$
Calcium hydroxide	Portlandite	$Ca(OH)_2$
C-S-H Gel		$3\ CaO \cdot SiO_2 \cdot 4\ H_2O$
Aft	Ettringite	$Ca_6(Al,Fe)_2(SO_4)_3(OH)_{12} \cdot 26\ H_2O$
Afm	Monosulfoaluminate, monosulphate	$Ca_4Al_2(SO_4)(OH)_{12} \cdot 6\ H_2O$
Hydrocalumite	HC	$[Ca_2Al(OH)_6]OH \cdot nH2O$
Hydrotalcite		$Mg_{1-x}(Al,Fe)_x(OH)_2 \cdot [A^{n-}]_{x/n} \cdot mH_2O$ May include the cations: Mn, Mg, Ni, Zn, Al, Fe May include the interlayer anions: OH-, Cl-, CO_3^{2-} and SO_4^{2-}
Oxychloride ($CaCl_2$)		$3\ CaO \cdot CaCl_2 \cdot 15H_2O$
Oxychloride ($MgCl_2$)		$2\ Mg_3(OH)_5Cl \cdot 4H_2O$
Friedel Salt		$Ca_4Al_2Cl_2(OH)_{12} \cdot 4H_2O$
Kuzel Salt		$Ca_4Al_2Cl(SO_4)_{0.5}(OH)_{12} \cdot 6H_2O$
Calcite		$CaCO_3$
Thenardite		Na_2SO_4
Thaumasite		$Ca_6(SiO_3)_2(SO_4)_2(CO_3)_2 \cdot 30H_2O$
Tobermorite		$Ca_5Si6O_{16}(OH)_2 \cdot 4H_2O$
Jennite		$Ca_9Si_6O_{18}(OH)_6 \cdot 8H_2O$
Syngenite		$K_2Ca(SO_4)_2 \cdot H_2O$

1 Introduction

1.1 Background

An estimated 37 million people lived in Canada as of July 1st 2018 with over one third of Canadians residing in either Toronto, Montreal or Vancouver[2]. This means the need to maintain bridges and highways passing through isolated areas with few alternate routes while also meeting the expanding needs of metropolitan areas. In both cases re-routing traffic for repairs can be extremely expensive, especially where bridges and overpasses are in constant use. Designing these structures to last longer coupled with timely maintenance on existing infrastructure is an important part of a sustainable infrastructure system.

The multitude of climates encountered in Canada present a challenge for the durability of concrete structures like bridges, access ramps and elevated highways. In many Ontario cities road salts are applied to combat icy roads due to winter temperatures around that fluctuate around 0 °C. Salts decrease the freezing temperature of water, preventing the formation of black ice and increasing traction for motorists. Due to airflow above and below elevated structures such as bridges these sections of roadways cool more rapidly which makes road salt application in these areas more important.

In addition to preventing accidents the use of de-icing salts results in cleaner roads compared to the use of sand or gravel. This has led to an increasing use of salt including in municipalities with more consistently cold climates like Edmonton[3]. Salt is spread on roadways as either rock salt which is predominantly NaCl, or as salt brines which may contain NaCl, $CaCl_2$ and/or $MgCl_2$. The salt type used affects the useful temperature with NaCl being effective as low as -15 °C, $MgCl_2$ as low as -25 °C and $CaCl_2$ as low as -40 °C.

Salt exposure causes decreased durability in concrete structures. The average age of bridges in Canada was 39 years as of 2016[4]. This was in part because of the construction of 105 new bridges between 2009 and 2014 for highway expansion[4]. In Ontario bridges constructed prior to 1978 have smaller cover depths and less waterproofing on bridge decks making them more susceptible to damage from road salt[4]. Between 1978 and 1996 the MTO required 70 mm cover on surfaces that could be affected by road salt along with improved waterproofing and the use of epoxy-coated rebar. Between 1996 and 2012 further corrosion prevention improvements have been introduced including the use of stainless steel rebar on exposed sections and guidelines limiting the type of concrete used[4]. The required service life of Canadian bridges has since been increased from 50 to 75 years[5].

The shift from the use of rock salt to brine solutions has changed both the types of salts used and how chloride diffuses into cement potentially resulting in shorter time to corrosion initiation. The use of different salt types may also have significant effects on the concrete of highway bridges and potentially result in corrosion related damage more quickly making service life prediction more challenging. In bridges exposed to high amounts of chloride alternatives to the common black steel rebar must be considered despite higher costs to allow the 75-year service life to be achieved.

Accelerated testing, is required to inform future bridge designs. Investigation of cement pore solutions and corrosion in synthetic pore solutions are some of the possible options.

1.2 Research Objectives

Understanding the relationship between synthetic pore solution compositions used to investigate chloride induced corrosion and the actual pore solution of cements exposed to salts is important for future investigations of alternative reinforcement, such as stainless steel. Thus, the specific objectives of the current research were:

1. To investigate pore solution from general use Portland (GU) cements with admixed NaCl, $CaCl_2$ and $MgCl_2$. Salt contents corresponding to those expected to cause corrosion of carbon steel and stainless steel were investigated.
2. To evaluate the corrosion behaviour of carbon (black) steel rebar immersed in various synthetic pore solutions with admixed NaCl.
3. To evaluate the corrosion behaviour of black steel rebar in synthetic pore solution created replicating the expressed pore solution from cement pastes with admixed NaCl, $CaCl_2$ or $MgCl_2$.

1.3 Scope

- Pore solution composition was investigated over a large range of admixed chloride representing pore solution for cement exposed to low and high chloride concentrations. The low levels (0.25, 0.50, 0.75 and 1.00 wt. % Cl by mass of cement) represent the chloride concentration where carbon steel corrosion is expected to initiate. The high levels (2.50, 5.00 and 7.50 wt. % Cl by mass of cement) are representative of the range where corrosion is expected to initiate in stainless-steel reinforcement. However stainless-steel corrosion has not been investigated in this thesis.
- An extensive investigation of the effects of sulphate released from the cement components into pore solution on steel corrosion was not conducted. Different sulphate concentrations are included in the synthetic pore solutions in lower concentrations corresponding to the low levels expressed from pastes with admixed $CaCl_2$ and $MgCl_2$ and in higher levels from pastes with admixed NaCl.
- It is recognized that the effects of admixed chloride are not directly comparable to the effects of salt diffusion into hardened cement paste or concrete, but only admixed chloride has been investigated in this thesis.

2 Literature Review

2.1 Cements

Concrete is a commonly used building material. The cement component undergoes chemical reactions when water is added to form hardened cement paste that holds the aggregates together creating concrete. Hydration reactions continue throughout the life of the concrete however they occur rapidly in the first 24 hours while cement hardens and gains strength. It is standard in industry to perform cement testing at 28 days due to ongoing hydration reactions during the first month.

The calcium aluminate phase (C3A) dominates initial reactions as it reacts rapidly with water. Gypsum ($CaSO_4$) is added to cement to prevent an initial flash set and allow the placement of concrete. Gypsum reacts to form ettringite which protects parts of the C3A from exposure to water eventually forming the monosulphate (Afm) phase[6]. Formation of the C-S-H gel is the most important hydration product as it provides structure to the cement.

Table 2.1-1: Common products from cement hydration

Clinker Phase	**Chemical Formula**	**Hydration Product**	**Chemical Formula**
Alite (**C3S**)	$3\ CaO \cdot SiO_2$	C-S-H + Portlandite	$3\ CaO \cdot SiO_2 \cdot 4\ H_2O$ $Ca(OH)_2$
Belite (**C2S**)	$2\ CaO \cdot SiO_2$	C-S-H + Portlandite	$3\ CaO \cdot SiO_2 \cdot 4\ H_2O$ $Ca(OH)_2$
Aluminate (**C3A**) Gypsum (CaSO4)	$2\ CaO \cdot Al_2O_3$ $CaSO_4$	Monosulphate (Afm) Ettringite (Aft)	$Ca_4Al_2(SO_4)(OH)_{12} \cdot 6\ H_2O$ $Ca_6(Al)_2(SO_4)_3(OH)_{12} \cdot 26\ H_2O$
Ferrite (**C4AF**) Gypsum (CaSO4)	$2\ CaO \cdot Al_2O_3 \cdot Fe_2O_3$ $CaSO_4$	Monosulphate (Afm)* Ettringite (Aft)*	$Ca_4Fe_2(SO_4)(OH)_{12} \cdot 6\ H_2O$ $Ca_6(Fe)_2(SO_4)_3(OH)_{12} \cdot 26\ H_2O$

* Contain Fe in addition to Al

As hydration occurs the clinker which is primarily Ca, Si, Al and Fe interacts with trace type elements resulting in substitutions by Mg, P, S, K, and Na[7]. The most common hydration products in Portland cement are shown in Table 2.1-1 below. Small amounts of calcite($CaCO_3$), hydrotalcite ($Mg_{1-x}(Al,Fe)_x(OH)_2{\cdot}[A^{n-}]_{x/n}{\cdot}mH_2O$) and monocarboaluminate ($3CaO{\cdot}Al_2O_3{\cdot}CaCO_3{\cdot}xH_2O$) may also occur[8,9] when cement is exposed to carbonate which can be introduced to clinker through condensation[10].

Small amounts of calcite ($CaCO_3$), hydrotalcite ($Mg_{1-x}(Al,Fe)_x(OH)_2{\cdot}[A^{n-}]_{x/n}{\cdot}mH_2O$) and monocarboaluminate ($3CaO{\cdot}Al_2O_3{\cdot}CaCO_3{\cdot}xH_2O$) may also be present[8,9] when cement is exposed to carbonate which can be introduced to clinker through condensation[10].

The composition and particle size distribution of cement and concrete have undergone significant changes over the past century. The way the clinker phases are prepared, the water to cement (w/c) ratios used and the additions of supplementary cementitious materials (SCM)'s and chemical admixtures have allowed concrete to become a highly specialized construction material. The most commonly used SCM's are blast furnace slag (BFS), fly ash (FA) and silica fume (SF), wheras the chemical admixtures can include high range water reducers (superplasticizers) [11] and air entraining agents.

Cement chemistry research has become increasingly prevalent because of the growing need to address CO_2 emissions from the cement industry[12,13], to understand nuclear waste containment[8,9,14–18] and to understand the impact of road salts on concrete structures such as highway bridges[19,20]. This thesis focuses on the impact of NaCl, $CaCl_2$ and $MgCl_2$, introduced to roadways as de-icing and anti-icing brines, on cement and reinforcing bars to better understand how the use of these salts by municipalities will impact the durability of highway bridges and other structures.

2.1.1 Importance of W/C Ratio

The idea that the amount of water added to cement could affect its structural performance was first introduced by D.A. Abrams in the late 1910's[21]. Since then manipulation of the w/c ratio has allowed cement to be tailored to various applications and environments.

A w/c ratio of 0.42 is the theoretical minimum water required for complete hydration of cement[22] while maintaining its workability. The advent of high range water reducers (HRWR) also known as "super plasticizers" has allowed increasingly low w/c ratios to be used, ensuring concrete that can flow into form work and around reinforcement while still having the benefit of low porosity. In colder climates, air-entraining agents are often used to introduce air voids into cement which allow for expansion of the pore solution on freezing, thereby limiting damage from ice formation.

The terms w/c, w/cm and w/b are used depending on whether extra binders, such as SCM's, are used. The choice of w/c ratio impacts the types of hydration products formed, the pore structure and, by extension, how easily undesired materials, such as de-icing salts or sulphate, will diffuse into the structure. While the research in this thesis uses a w/c ratio of 0.50 cement research has been conducted using a variety of ratios. An awareness of the w/c or w/b ratio used is important due to the different material properties resulting from the hydration of the cement.

The excess water present in the pore system of cement contains a variety of ions. This pore solution in contact with reinforcing bars is responsible for the passivity of rebar due to its high pH. However, pore solution can become less protective when contaminated by chloride from de-icing salts resulting in corrosion of the steel and in high volume corrosion products which threaten the durability of cement.

In a 2009 study[23], Tritthart investigated the pore solution of cement with different w/c ratios and 1 wt% chloride by mass of cement in the form of NaCl and $CaCl_2$. The results, shown in Figure 2.1-1, illustrate differences between chloride in the pore solutions. Tritthart suggests that since full hydration is reached

around a w/c of 0.4, chloride ions in cement with higher w/c ratios are diluted by extra water[23]. However, the significant difference between the two salts, especially at lower w/c indicates differences in equilibrium between the solid and liquid phases in these cements.

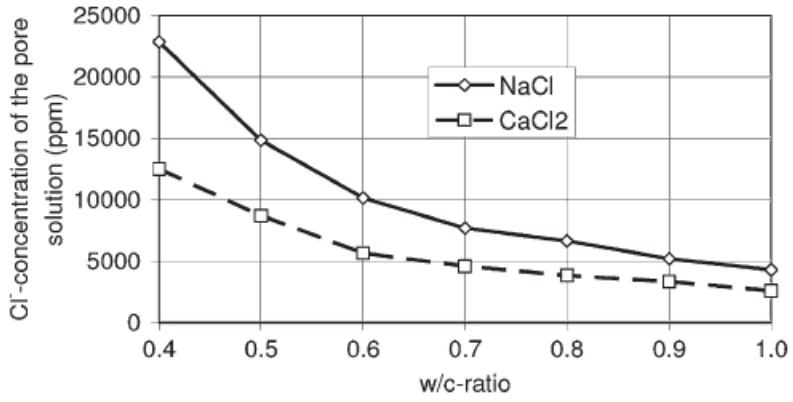

Figure 2.1-1: Impact of w/c ratio and salt type on chloride binding[23]

2.1.2 De-Icing Salts and Concrete

De-icing salts are applied to roads when temperatures are expected to cause icy driving conditions, typically below 5°C. Over time repeated salt applications result in increasingly high concentrations of salt diffusing into concrete[24] in addition to increasing concentrations of salt in nearby soils and ground water. Many factors affect the diffusion rate and depth of chloride penetration into concrete including wet-dry cycles, concrete mixture design and reactions within the cement. High concentrations of chloride at the surface of cement do not always indicate significant chloride at the surface of reinforcement.

Salts on roadways diffuse into cement from the surface. The salt concentrations, temperatures and amount of moisture at that surface fluctuate daily and seasonally. Laboratory research into the effects of salt solutions on concrete and reinforcement frequently isolate specific conditions experienced by these structures to understand both concrete degradation and corrosion. These tests include (i) subjecting samples to freeze-thaw cycles; (ii) subjecting them to wet and dry cycles with exposure to salt solutions during the wet cycle; (iii) constant immersion of samples in salt baths and (iv) direct mixing of salt into

concrete (admixed salt) to study their effects on the hydration phases or conduct more rapid investigation of reinforcing bar (rebar) corrosion. Admixed chlorides in cement can also be used for the purpose of expressing and analyzing the pore solution (section 2.1.2.2) allowing corrosion of rebar in realistic synthetic pore solutions. In this research the impact of different salt types on cement will be investigated through pore expression and synthetic pore solutions are used to investigate rebar corrosion.

Chlorides in cement remain mainly dissolved in the pore solution, but a portion become chemically bound or adsorbed in the diffuse layer of C-S-H ($3CaO{\cdot}SiO_2{\cdot}4H_2O$)[6,9,23,25,26]. Common chloride binding compounds that may form include Friedel salt ($Ca_4Al_2Cl_2(OH)_{12}{\cdot}4H_2O$)[6,23,27,28], Kuzel salts ($Ca_4Al_2Cl(SO_4)_{0.5}(OH)_{12}{\cdot}6H_2O$)[27,29] and other chloroaluminate hydrates (C-A-H)[9,30,31]. A variety of other compounds can bind chlorides as partial substitutions including many double layered hydroxides like Afm[32]. Sulphate can be released by these reactions resulting in varying amounts of dissolved sulphate in pore solution. The salt cation used also effects chloride binding with more chloride binding occurring from $CaCl_2$ and $MgCl_2$ than NaCl or KCl[33,34]. Anecdotally Tritthart[23] observed that rainwater on cement structures failed to remove the high volumes of salt it was initially exposed to indicating that chloride binding often occurred.

Some researchers have concluded that more salt is bound into cement when it is admixed rather than exposed externally[30,34]. This is thought to be because of the preferential formation of phases which chemically bind chlorides, as well as chlorides becoming physically trapped in C-S-H[30].

Cement pore solution exists in equilibrium with the solid phases. When cement is hydrated for a period of time prior to salt exposure the amount of Friedel or Kuzel salts formed are limited by availability of aluminum, sulphate and chloride. Availability of these ions in pore solution is limited in mature cement paste by the stability of Afm, ettringite and other phases which may dissolve back into solution. When salts are admixed, aluminum, sulphate and, obviously, chloride are more available. In testing of both

admixed and external chlorides Arya et al.[34] found in both cases chloride binding increased with increases in curing temperature, w/c and cement maturity. However, for externally introduced chlorides it was also found that the C3A content had little effect on chloride binding after two days[34] indicating high stability of the Afm phase.

2.1.2.1 Chloride Diffusion into Hydrated Cements

Studies of chloride ingress into cement pastes[9,28,35] and mortar[26,36] samples have been conducted to better understand the damage associated with different de-icing salts. A shift to the use of brines instead of rock salt is thought to increase infrastructure damage because of increased rates of chloride ingress[36,37]. In Ontario, brines may contain NaCl, $CaCl_2$ and/or $MgCl_2$, increasing the need to understand the impact of all three salts[37].

There are many interdependent factors that contribute to chloride ingress into cement with no single factor controlling the depth of chloride penetration. However, the salt cation type can affect the types of hydration products formed and the amount of hydration encountered.

In a 2013 study, Peterson et al. found that cement samples immersed in NaCl solutions for a specific period had deeper chloride penetration than those submerged in $CaCl_2$ or $MgCl_2$[35]. Two different w/c ratios (0.45 and 0.55) and two different salt exposure concentrations (~7 and ~17 g salt/ Kg water) were investigated. For samples exposed to NaCl higher concentration salt solutions directly equated to deeper chloride penetration in cements with both w/c contents. Samples exposed to the higher concentration $CaCl_2$ and $MgCl_2$ solutions experienced lower chloride penetration. This indicates that despite 28 days of salt free hydration prior to exposure to salt these salts facilitate further hydration reactions which have the effects of both chemically binding chlorides and blocking pores.

Exposure to NaCl salts do not result in significant additional hydration. Loser et al. 2010 investigated cement pastes with different w/c ratios submerged in a 2.8 M NaCl solution for 50 days found that chloride binding in samples was a less significant factor for depth of chloride ingress than sample porosity[28].

Pore coarsening was observed by Gegout et al.[9] in w/c 0.37 OPC cement exposed to chloride solutions with an unspecified cation over a three-year period. Cement was stored in aggressive chloride solutions with pH either 11.5 or 13.0. While chloride binding was initially equivalent over time they noted that in the lower pH solution chloride resulted in calcium leaching from the C-S-H, portlandite ($Ca(OH)_2$) and chloroaluminate (CAH) phases. It was further concluded that the effects of chloride could increase or decrease the effects of pH.

The C-S-H phase has a variable composition[38,39] which can be quantified by the Ca/Si ratio[39]. Calcium leaching of C-S-H results in a decreased Ca/Si ratio and a modified structure[40]. In samples with available sulphate calcium leached from C-S-H has been found to facilitate the formation of ettringite and gypsum[39].

The lower diffusion rate of chlorides as $CaCl_2$ and $MgCl_2$ salts, especially at higher concentrations, has been attributed to reactions that decrease the pH of the pore solution. As concentrations of these salts increase, more $Ca(OH)_2$ and $Mg(OH)_2$ precipitate, and these can have the effect of blocking pores[37]. In a 1997 review article, Justnes suggested the following reactions occur depending on salt type[1]. While the NaCl reaction (Equation 2.1-1) introduces hydroxide to the pore solution with no decrease of pH, limited calcium solubility in solution causes the formation of $Ca(OH)_2$ when exposed to $CaCl_2$ causing a reduction in pH. $MgCl_2$ feeds into the $CaCl_2$ reaction through the suggested mechanism in Equation 2.1-2[6,33,41] which also proceeds spontaneously to the right. These reactions are controlled by the solubility limit of Ca^{2+} in pore solution due to the common ion effect.

Equation 2.1-1: NaCl reaction in Cement[6]

$$2\,NaCl(aq) + 4Ca(OH)_2(s) + 12\,H_2O = CaCl_2 * 3Ca(OH)_2 * 12\,H_2O(s) + 2\,NaOH\,(aq)$$

Equation 2.1-2: $MgCl_2$ reaction in cement[6,33,41]

$$MgCl_2(aq) + 3Ca(OH)_2(s) = CaCl_2(aq) + Mg(OH)_2(s)$$

$CaCl_2$ and $MgCl_2$ are also associated with the formation of oxychlorides in cement[24,32,35,36]. Oxychlorides and hydroxychlorides are expansive and can be highly damaging. An unidentified compound identified by CuKα radiation at 9.56 and 5.46 Å was observed by Chatterji in 1978 upon exposure of Portland Cement to $CaCl_2$ solutions. This compound was observed for cement exposed to 15% $CaCl_2 \cdot 2H_2O$ solution at 5 °C as well as cement exposed to a 30% $CaCl_2 \cdot 2H_2O$ solution at 5 °C and 20 °C but not at 40 °C[42]. Mortar bars exposed to solutions containing 28% $CaCl_2$ and 25% $MgCl_2$ respectively for 45 days underwent sufficient reactions to result in catastrophic cracking of the bars[36]. This was attributed to the formation of oxychlorides which form more rapidly at low temperatures and destabilize quickly as temperatures increase resulting in the loss of water[35,36]. This compound is the most stable around 5°C[35] with the magnesium variation being the most stable at laboratory temperatures[35,36]. Calcium oxychloride hydrate and magnesium hydroxychloride are thought to form through the mechanisms shown in Equation 2.1-3 and Equation 2.1-4 below. Balonis et al. [32] suggest that the formation of Friedel salts is favoured until a threshold of 3 M Cl (~10.6 %Cl by weight solution) is reached. Glasser et al. [15] suggested that some forms of Friedel salts require thresholds of 4 M Cl or 9 M Cl (14.2 and 31.9 wt% Cl of solution respectively) further noting that these concentrations would only occur at surfaces where evaporation has concentrated the salt. Experiments of synthesized oxychlorides by Galan et al. 2015 it was found that when isolated from carbonation in the air, pure oxychloride is stable between 5 and 55 °C. Both synthesized versions co-existed with Friedel salt at 25 °C but only one variation was stable when $Ca(OH)_2$ is present. All researchers agree that oxychlorides can vary in composition with various amounts of associated water, depending mainly on the temperature and chloride concentrations[15,24,32,35,36].

Equation 2.1-3: Formation of Calcium Oxychloride Hydrate from $CaCl_2$[35]

$$CaCl_2(aq) + 3\ Ca(OH)_2(s) + 12\ H_2O = 3\ CaO * CaCl_2 * 15\ H_2O(s)$$

Equation 2.1-4: Formation of Magnesium Hydroxychloride from $MgCl_2$[35]

$$6\ MgCl_2(aq) + 5\ Ca(OH)_2(s) + 8\ H_2O = 2\ Mg_3(OH)_5Cl * 4\ H_2O(s) + 5\ Ca^{2+}(aq) + 10\ Cl^-(aq)$$

2.1.2.2 Admixed Chlorides

Salts are often cast into specimen by dissolving them in the water which is then mixed with the cement, mortar or concrete. This is especially valuable for short term corrosion tests, when it is useful to know the chloride concentration at the surface of a rebar specimen. However, because salts are present during initial hydration there are limitations when relating results from admixed salt specimens to the real world where salt slowly diffuses into hydrated cements as discussed in section 2.1.2.

Changes to the microstructure of cement discussed in section 2.1.2.1 are amplified with admixed salts resulting in a different distribution of hydration products. Both the w/c and the amount and type of salt used have a significant impact on the final pore structure. A 1985 study of a 0.5 w/c OPC mortar containing mild steel rebar by Hansson et al. investigating admixed NaCl, KCl and $CaCl_2$ reported a more open pore structure than in salt-free samples from all salts with the most significant increase resulting from $CaCl_2$[43]. A 1995 study of a 0.7 w/c OPC Mortar by Suryavanish et al. with admixed NaCl and $CaCl_2$ found an overall decrease in pore volume due to a shift from coarse pores to finer pores[40]. They determined that this shift was due to changes in the C-S-H gel morphology in which it changed from fibrous to a more dense structure decreasing the amount of larger pores which previously formed between fibers[40]. The additional available water in the 0.7 w/c cement would have reduced pockets of unhydrated clinker allowing new hydration products to fill spaces which may remain empty in lower w/c cements.

pH is a critical factor affecting the equilibrium between solid phases and the pore solution. This is most easily studied through pore expression of cement samples with a known amount of salt added during

mixing where the pH is tested in freshly expressed solution. The mechanisms in the previous section only tell part of the story, failing to capture changes to the C-S-H as well as Friedel salt formation. In his 1997 review article, Justnes proposed the following reaction (Equation 2.1-5) for the formation of Friedel salt. He noted that since $Ca(OH)_2$ becomes less soluble as pH increases it could become rate limiting[6]. With admixed chlorides Friedel salts can form consuming alumina that would otherwise be used to form ettringite[44]. More recently Glasser et al., have noted an absence of research concerning the Friedel equivalent from C4AF[15]. This iron bearing equivalent is thought to have the form $C3F{\cdot}10H_2O$ in cement chemist notation which is approximately $((CaO)_3Fe_2O_3{*}CaCl_2{\cdot}10H_2O)$ [45].

Equation 2.1-5: NaCl interaction with C3A to form Friedel Salt[6]

$$2\ NaCl(aq) + C_3A + Ca(OH)_2(aq) + 4\ H_2O = Ca_3Al_2O_6 * CaCl_2 * 10\ H_2O(s) + 2\ NaOH\ (aq)$$

The presence of NaCl has been found to cause in a slight pH increase at some chloride concentrations rather than the continuous pH decrease reported in samples exposed to $CaCl_2$ and $MgCl_2$[46]. especially at lower NaCl concentrations. This follows the formation of NaOH through the mechanisms shown in Equation 2.1-1 and Equation 2.1-5 where $Ca(OH)_2$ may be rate limiting[6] resulting in a maximum pH. Results from De Weerdt et al. identified a pH peak around 0.25 M free chlorides (0.5 M NaCl exposure solution) in OPC samples exposed to NaCl[41,47]. Tritthart 2009 studied admixed chlorides in various cements with w/c 0.6. For CEM I samples the $[OH^-]$ was found to peak while a low C3A sulphate resistant cement sample with NaCl exhibited a much lower $[OH^-]$ with no peak[23]. Tritthart also investigated cement with admixed $CaCl_2$ and found that the pH values that decreased continuously[23].

$CaCl_2$ and $MgCl_2$ salts have been found to decrease the pH of pore solutions relative to comparative chloride concentrations from NaCl[33,41]. It has been suggested that adsorption of Cl^- onto C-S-H plays a large role in this phenomenon in addition to the precipitation reactions described earlier. These salts have been found to result in an increased Ca/Si ratio in C-S-H[41] which alters the adsorption of both Cl^- and OH^- onto

C-S-H. Tritthart proposed that, when the pore solution pH decreases, it liberates adsorption sites for chloride binding[23]. His results showed decreased free chlorides and hydroxide concentrations in pore solution from $CaCl_2$ in comparison to NaCl. He concluded that this mechanism was solely dependant on the pH with no difference between admixed and ingressed chloride sources[23]. Following this, [Cl-]/[OH-] ratio has been suggested as a metric for rebar corrosion and is discussed in more detail in section 2.4.1. More recently Bernard et al. found that adding $MgCl_2$ to a synthetic C-S-H with a Ca/Si ratio of 0.8 resulted in a significant pH decrease and the formation of M-S-H at pH values below 12[25]. While M-S-H is stable below pH 12 it forms extremely slowly above pH 10 and so is felt to be improbable in the scope of this thesis. The role of C-S-H on chloride adsorption is of particular interest for modeling of cement systems.

2.1.3 Sulphate in Cement

Sulphates in cement come from a variety of sources including the water used to make the cement, gypsum which is added to prevent rapid set from the C3A phase and external contaminants such as groundwater[48,49], soils[44], runoff[48] and de-icing brines[37,50,51]. The C2S, C3S and to a lesser extent C4AF clinker contain some SO_3[52]. Sulphate introduced as gypsum usually reacts with C3A and C4AF within 24 hours to form ettringite (Aft)[8,53] and eventually monosulphoaluminate (Afm). As the concentration of sulphate ions increases in cement pore solution as a result of initial gypsum reactions, precipitates of gypsum, ettringite and a mineral called thaumasite ($Ca_6(SiO_3)_2(SO_4)_2(CO_3)_2 \cdot 30H_2O$) may form in the solid cement causing expansion and weakening of the cement[15,44]. This type of damage has been observed in concrete structures in highway infrastructure[51,54,55] and sulphate has been reported as part of de-icing salt mixes spread on North American roads[50,51].

2.1.3.1 Sulphate and Chloride Interactions in Cement

Sulphates have been found to bind preferentially to available sites in the C-S-H and Friedel salts[6,26,47]. This leaves more chlorides in the pore solution. This has been seen in structures exposed to sea water and

contaminated ground water[6] as well as in lab settings[6,26,47]. However, investigations of chloride ingress by De Weerdt et al., 2019 of 6% SF mortars exposed to ~0.55 mol Cl/L through either NaCl or seawater (~27 mmol S/L), showed that sulphate had no significant impact on chloride ingress.

Chloride binding also helps prevent sulphate attack because Friedel salt formation decreases the aluminum available to form ettringite[44]. Chloride ions diffuse into cement more quickly than sulphate giving chloride the opportunity to form Friedel's salts[44,56]. Additionally, ettringite and gypsum are more soluble in chloride solutions than in chloride-free solutions[49] with ettringite being approximately 3x more soluble in chloride solution than water[56]. Because less ettringite precipitates out of salt containing solution it decreased the severity of sulphate attack[56]. Work by Al-Amoudi[49] corroborated this in studies of cement exposed to solutions containing only sulphates or both chloride and sulphate finding that less ettringite formed in samples exposed to the salt containing solution. Sulphate was in the form of Na_2SO_4 or $MgSO_4$, however $MgSO_4$ continued to breakdown the C-S-H gel[49], Note that Al-Amoudi did not specify the cation used for chloride additions.

Studies by De Weerdt et al. in 2014 found that for hydrated cement samples exposed to $MgCl_2$, the amount of bound chlorides increased as pH decreased. However, when cement was exposed to a solution of $MgCl_2$ and $MgSO_4$ less variation in chloride binding was observed during changes in pH[47].

2.1.4 Impact of Calcium Interactions in Cement

Calcium solubility increases as pH decreases[53,57] resulting in changes to the hydration products and in extreme cases full decalcification[9,15,26,58]. Dissolution of portlandite ($Ca(OH)_2$) has been observed. Chatterji 1978 studied the effect of $CaCl_2$ on ordinary cement paste and discovered that the degree of dissolution of $Ca(OH)_2$ was linked to both the chloride content in contact with the cement and the temperature. Complete $Ca(OH)_2$ dissolution was observed for cement powder in contact with a 30% $CaCl_2 \cdot 2H_2O$ solution as well as cement exposed to a 15% $CaCl_2 \cdot 2H_2O$ solution at 5 °C. Cement in contact with 5% $CaCl_2$

· $2H_2O$ solution Ca(OH)2 was detected for 5 °C, 20 °C and 40 °C however the extent of depletion was unspecified[42].

De Weerdt et al. 2019 identify calcium availability as a critical aspect of chloride binding in cement due to its role in C-S-H morphology. De Weerdt suggests that decreasing calcium in the pore solution also decreases chloride binding and vice versa[26]. It is possible that the link is one of correlation rather than causation since lower pH increases the solubility of calcium and pH is lowered as cement is exposed to more $CaCl_2$ or $MgCl_2$. Decreased chloride binding in C-S-H may, in fact, be due to a breakdown in the C-S-H structure rather than changes in the amount of available binding sites as Bensted alludes to when describing C-S-H decalcification as 'silicate debonding'[59].

2.2 Expression of Concrete Pore Solutions

Pressure is used to extract solution from the pores of cement specimen. This allows the impact of various factors such as chloride and sulphate content to be studied. This technique has been used extensively in concrete research especially where SCMs or salts are admixed[60].

The pore expression technique was first developed by Longuet et al in 1971 and was later refined by Barneyback and Diamond and published in 1981[61]. At the time, the small volume of liquid obtained from this method was a challenge for thorough elemental analyses. Barneyback and Diamond were able to identify the pH of the solutions by titration as well as the elements Na, K, Li, Si, Al, Fe, Mg and Ca using flame photometry and atomic absorption spectrometry which were the standard technique at that time. The sulphate content in this study was determined using $BaSO_4$ precipitation technique[61]. More recently elemental compositions are determined using Inductively coupled plasma optical emission spectroscopy (ICP- OES) and Inductively coupled plasma mass spectroscopy (ICP-MS and Ion chromatography (IC) which allow more accurate elemental analysis with small volumes[62].

An additional measure evaluated by Barneyback and Diamond was to determine what component of the original water used to mix the cement (i.e. from w/b ratio) remained in samples as liquid in the pore system. They determined that the non-evaporable water content in cement would remain bound in the sample between 105 °C and 1050 °C above which temperature the material would ignite[61]. Moisture content tests involving weighing a sample before and after drying it at 105 °C for 24 hours are frequently used by researchers[40,43,63]. It was felt that this information allowed the movement of elements between the solid phases and the pore solution to be better quantified for greater understanding of the rate of secondary reactions, like the formation of ettringite or Friedel Salts[61].

Pore solution expression is important as an evaluation technique and is a useful input for developing models of cement hydration. The concentrations of K, Ca, S and OH- of mature cement depend most heavily on the w/c ratio and the cement composition. For cements with higher pH increased concentrations of SO_4^2, Si, Al and Fe are expected[57]. Changes in the expressed pore solution can be related to saturation conditions where precipitation might occur.

Large changes in pore solution composition have been found when a large range of admixed chlorides is investigated. Pore expression of general use (GU) cement with a 0.5 w/c by Van Niejenhuis and Ogunsanya[64] found that the sulphate concentration increased 33x from the chloride free to samples with 7.50 wt% admixed chloride in the form of NaCl.

2.3 Synthetic Concrete Pore Solutions

Excess water from cement hydration remains in a system of pores within the cement. This liquid is highly concentrated solutions of ions in equilibrium with solid phases. The high pH of this pore solution in contact with rebar is responsible for the formation of a protective passive film on the bars. Carbonation, which decreases the pH of pore solution, often accompanies increased Chloride concentrations at the rebar surface due to the time required for the ingress of these ions and in some cases interactions of the

salt cation with the pore solution. The inability to form and or maintain a robust passive film on the surface of rebar has been attributed in varying degrees to the amount of Cl^- ions and the pH in the pore solution and will be discussed further in section 2.4. Changes in pore solution composition, like increased chloride and sulphate, can either protect the rebar or make it more susceptible to corrosion. In particular the role of sulphate in this process is not fully understood.

The creation of synthetic pore solutions (SPS) allows the suitability of rebar to be investigated for given conditions. In particular, the use of SPS allows relatively rapid and consistent testing since salts can be dissolved into solution at known concentrations without needing to wait for chloride to diffuse into concrete. However, the types of pore solutions that have been used vary drastically.

Saturated calcium hydroxide has been used by many researchers[20,65–70]. Saturation gives a pH of approximately 12.6 and is easily maintained over long time periods despite potential evaporation from the solution. However, this relatively low pH solution is not sufficient to fully replicate rebar passivation in cement. In an investigation of rebar passivation in both saturated calcium hydroxide and a higher pH synthetic pore solution, Poursaee found that the passive film formed in calcium hydroxide solution was much less protective, resulting in different corrosion results after salt was added[68]. Passive films are discussed further in section 2.4.1.

Synthetic pore solutions are often made of $Ca(OH)_2$, KOH and NaOH with some researchers also including sulphate[20,37,68,69,71–73], often in the form of $CaSO_4$ since the $[Ca^{2+}]$ is already present in excess. Other forms of sulphate have also been used including K_2SO_4[74] and Na_2SO_4[65,75]. The amount of $Ca(OH)_2$ required for saturation varies depending on whether it is added to water or an existing solution. Often $Ca(OH)_2$ is simply added until precipitates appear on the bottom of the container. Saturation amounts are often specified for water but that concentration for saturation changes when other molecules are present. The concentrations of the different hydroxides used vary between solutions, as do the pH of solutions.

Low pH values are often used to replicate the effects of carbonation while high pH solutions are used for highly protective films. For example, ASTM A955 specifies a solution with pH ~13.8 for testing stainless steel.

Chloride addition to synthetic pore solutions alters the pH depending on the salt cation used and the composition of the solution. In thesis research by Mathew Hunt[76], rebar corrosion was tested in synthetic pore solutions with different types of salt added incrementally in the form of NaCl, $CaCl_2$ and $MgCl_2$. Hunt found that the pH of the solution with added NaCl experienced very little pH change remaining around pH 13 while the solutions with added $CaCl_2$ and $MgCl_2$ behaved similarly until approximately 0.90 wt% admixed Cl by weight solution. At higher chloride contents the solution with added $MgCl_2$ experienced a significant pH decrease reaching a pH of 9.1 at approximately 2.00 wt% Cl. Hunt attributed this pH change to the replacement of $Ca(OH)_2$ with $Mg(OH)_2$[76]. This illustrates the importance of understanding reaction kinetics and stability when evaluating synthetic pore solutions.

High chloride concentrations in concrete from chloride diffusion or admixed chlorides significantly impact the cement pore solution composition. This is due to dissolution or precipitation of hydration phases to maintain equilibrium with negative chloride ions. Significant changes to solid phases with increased chloride modeled by De Weerdt et al. 2019 illustrate these changes (Figure 2.3-1). This means that pore solutions that accurately replicate pore solution in chloride free cement may not be adequate for high chloride content cement.

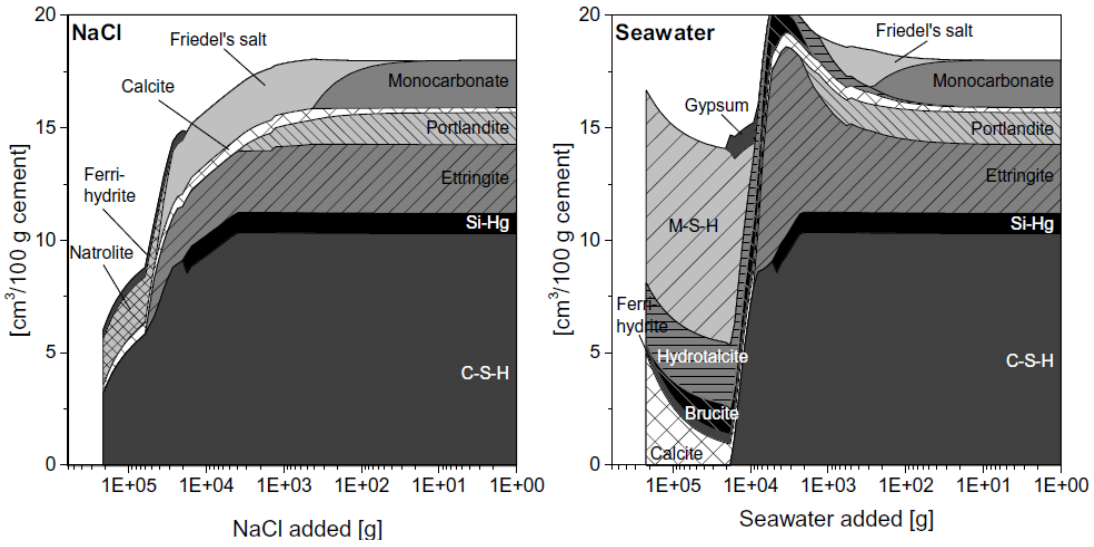

Figure 2.3-1: Modeled phase volumes of PC paste exposed to NaCl (Left) and Seawater (Right) from De Weerdt et al. 2019[26]

2.3.1 Impact of Pressure on Pore Solution

The pressure used to express pore solutions has been found to impact the anions and cations in the expressed solution. It is possible that heat generated by compression might change the equilibrium of the pore solution causing solids to dissolve in to the solution and be collected[57]. The impact of applied pressure has a greater effect on cements with lower w/c ratios. For a w/c of 0.5 it has been found that there is no significant change in alkali concentrations of pore solutions expressed using pressures up to 560 MPa[77] which is quite high. However, when a w/c close to 0.4 is used, alkali concentrations change depending on the maximum pressure applied to express the pore solution. For OPC this effect has been found to be moderate between 60 and 330 MPa for most elements with the exception of sulphate for which the concentration steadily increases with increasing pressure[62]. Significant changes in composition can be found above 500 MPa for cements using w/c 0.4[57] including increases in expressed sulphate[57]. This use of high pressures to extract pore solutions has not been found to be significant for ordinary Portland cement mortars with a 0.5 w/c[57,62].

2.3.2 Alternatives to Pore Solution Expression

Alternative techniques to pore water expression have been investigated. One option, extraction using water or ethanol, was investigated by Tritthart in 1989 but was found to result in too much dilution[78]. Isotherms for chloride binding and sorption have also been used[6] to learn how much chloride can be bound by a hydrated cement sample. In this method the cement sample is ground to a powder then placed in a chloride solution with a known concentration. The solution is stirred constantly for a period of time, after which the remaining liquid is tested to determine how much salt was bound to the cement[6]. This technique is limited to determining the amount of salt that can be bound and does not give insight into other elements. More recently a similar technique has been used by De Weerdt et al.[41] in which they created a 0.4 w/c cement, allowed it to hydrate at controlled temperatures, crushed the sample and mixed it with another 40% water to ensure complete hydration for an approximate w/c of 0.96. The hydrated cement was consequentially exposed to chloride solutions. Cement was removed from solution, dried to the consistency of wet sand and centrifuged to isolate pore solution[41]. De Weerdt et al. further investigated the chloride solution after it had reached equilibrium with the cement paste to determine a pH and the elements Al, Ca, Cl, Fe, K, Na, Mg, S and Si[41].

Several tests have become increasingly common in conjunction with pore expression experiments. Investigation of the hydrated cement is frequently performed using XRD, SEM and Thermogravimetric analysis (TGA)[41,47]. These techniques are especially useful for gathering data for the development of models for cement kinetics and thermodynamics.

2.4 Corrosion of Rebar

The high pH environment found in concrete allows the formation of a protective passive film on carbon steel reinforcing bars. However, over time, increased concentrations of chloride ions which have diffused into the cement attack the passive film ultimately resulting in corrosion initiation. This process is

often linked with pH, which often decreases due to carbonation or is initially lower due to the use SCM's. The roles of chloride ions and changes in pH are not directly linked and corrosion can be seen to initiate under a variety of chloride concentrations and pH values. The formation of corrosion products exerts pressure on the surrounding concrete resulting in spalling. It has been suggested that more corrosion resistant materials be used for rebar in vulnerable places in the structure with plain carbon steel only being used deeper in the structure[79]. The option to simply place rebar well below the surface is unfeasible because reinforcement helps prevent cracking caused by internal and external stresses on the concrete[80]. Current MTO guidelines require a 70 mm cover depth over reinforcement for bridge decks coupled with waterproofing on the surface[4] to increase durability.

Rebar can be monitored using electrochemical tests including linear polarization resistance (LPR) and cyclic polarization tests. ASTM C876 outlines the criteria for testing and monitoring of reinforcement bars in concrete through evaluating the electrical potential over a section of rebar. This test suggests that for carbon steel reinforcement in concrete corrosion is likely when potentials are more negative than -0.29 mV SCE. Another important criterion is the corrosion current density (i_{corr}) which indicates the amount of movement of ions to and from the surface of the bar.

Defining a threshold i_{corr} above which corrosion is probable has been of interest for non-destructively evaluating corrosion. In their 2016 experiments investigating mild steel rebar corrosion in synthetic pore solutions Scott and Alexander used an i_{corr} threshold of 0.1 $\mu A/cm^2$ noting that [this threshold] "is generally taken as the level beyond which active corrosion has begun"[74]. Alternately in studies of corrosion initiation of steel rebar in an OPC mortar Alonso et al identified the same threshold stating that "Active corrosion is considered when, in a small exposed area, the corrosion rate of the rebar is higher than 0.1 $\mu A/cm^2$"[81]. This threshold was based on previous research from this laboratory group. In a 1980 paper referenced corrosion performance of high strength steel rebar in mortar was investigated where the cement mix was varied (no additives, 2 wt% $CaCl_2$ or 3 wt% $NaNO_2$) and the storage environment was varied by changing

relative humidity (RH) and causing carbonation [82]. Since electrochemical testing is often employed over a section of rebar rather than at the precise point where corrosion is occurring, and rebar passive states can vary, the use of a hard threshold does not capture the variability that can be encountered. Rather three possible ranges should be considered, a range where corrosion is very unlikely, a range where both corrosion and passive behaviour can not be determined and a range where significant corrosion is highly likely. This is not reflected in the use of a i_{corr} threshold like 0.1 μA/cm^2.

Corrosion occurs when iron undergoes the following reactions (Equation 2.4-1) which occur simultaneously with the reduction of dissolved oxygen (Equation 2.4-2) at the steel surface. These reactions lead to the formation of ferrous hydroxide $Fe(OH)_2$ which precipitates from solution. Further reactions with the environment result in a variety of corrosion products.

Equation 2.4-1: Anodic reaction of Iron

$$Fe \rightarrow Fe^{2+} + 2e^{-}$$

Equation 2.4-2: Cathodic reaction for corrosion in high pH environment

$$H_2O + \frac{1}{2}O_2 + 2e^{-} \rightarrow 2OH^{-}$$

When chloride is present in solution the negative chloride ion is attracted to the positive Fe^{2+} anion (Equation 2.4-3). The chloride ion essentially catalyses the formation of corrosion products and positive hydrogen ions as part of HCl. Because H^+ is formed instead of OH^- the site of corrosion becomes less alkaline. When depassivation begins to occur in cement the portlandite ($Ca(OH)_2$) can buffer this reaction to maintain the pH in solution, KOH and NaOH can also contribute to buffering this reaction and re-establishing the passive film[83]. Pitting corrosion occurs when the rate of the chloride reaction with Fe^{2+} can no longer be buffered.

Equation 2.4-3: Acidification reaction due to chloride attack during pitting corrosion[84]

$$Fe^{2+} + 2H_2O + 2Cl^- \rightarrow Fe(OH)_2 + 2HCl$$

2.4.1 Passivation of Steel and the Effect of Surface Treatments

Carbon steel rebar is typically covered in a dark oxide layer called 'mill scale' which consists of wustite (FeO), magnetite (Fe_3O_4) and hematite (α-Fe_2O_3)[85–87]. This layer can vary between manufacturers and even within batches. Several surface treatments have been used to prepare laboratory samples including sandblasting[88], chemical pickling[89,90] and cleaning with a wire brush. Mill scale is thought to alter the time to corrosion initiation. Several researchers have suggested that mill scale decreases the chloride threshold where corrosion initiation occurs because it creates a less uniform surface and introduces more locations for pitting corrosion to initiate due to the presence of cracks and crevices[71,88,89,91]. In particular, Gouda and Mourad suggested that an anodic reaction occurs within the oxide[92]. Modeling work by Karadakis et al. found that crevices in mill scale could cause significant pH decreases at the metal surface compared to bulk pore solutions[91]. Decreases in pH have been found to increase the severity of rebar coorrosion[65]. Research by Ahlström et al.[87] investigated steel mill scale consisting of pure wustite, magnetite and hematite prepared through heating and quenching a hot rolled steel plate. Through electrochemical testing in saturated $Ca(OH)_2$ solution with 0.0 and 0.6 M NaCl they concluded that magnetite and wustite acted as strong cathodic surfaces compared to hematite. They further deduce that the mill scale would act as a cathode resulting in chloride being attracted to the more negative steel surface in locations where there are cracks in the mill scale[87].

Nakagawa and Ono[93] investigated the impact of KCl on wustite (FeO), magnetite (Fe_3O_4) and hematite (α-Fe_2O_3) in CO and CO_2 environments due to accumulation of alkali compounds in blast furnaces. They discovered that KCl accelerated the reduction of these iron oxides. Nakagawa and Ono's experiments were not performed in solution and employed a higher temperature. No research was found investigating

the possibility that the presence of NaCl, NaOH and KOH in cement pore solution might accelerate the reduction of the oxides in mill scale.

At an industrial level, the removal of mill scale adds extra cost. Additionally, the use of harsh chemicals to pickle bars has its own environmental impact. Depending on the process used chemical pickling can also have its own corrosion issues[90]. For this reason, it is important to understand the corrosion behaviour of rebar in its as received state complete with mill scale.

Most rebar is formed with diagonal ribs to increase the surface area in contact with concrete and provide a mechanical bond. The manufacturing process results in different grain structures in the main body of the rebar compared to the ribs due to heat dissipation during cooling. Some researchers choose to remove the ribs[70,81] for the purpose of electrochemical testing to better isolate passive film behaviour.

Rebar forms a thin protective passive film in concrete consisting mainly of Fe_3O_4 and Fe_2O_3 [75]. A stable film has been found to form in synthetic pore solution after the first 48 hours and the level of protectivity has been found to correlate to pH[68,89]. High pH solutions result in the formation of more protective passive films[68,69] with a stable protective passive film being formed as low as 11.5[75]. Gouda and Halaka assessed rebar corrosion using galvanostatic polarization measurements, monitoring changes in potential over time and through visual assessments. Their findings led them to suggest that the film formed is similar whether it is formed in cement or synthetic pore solution[94]. Corrosion can result either when something inhibits the formation of a passive film or causes de-passivation of an established passive film. In the case of exposure to sufficient concentrations of chloride ions pitting corrosion occurs. Among possible contributors to passive film inhibition or depassivation, the role of sulphate ions is not as well understood. While chlorides have been viewed as an issue for a long-time, issues with sulphate are only recently being investigated.

Vigneshwaran et al[70] conducted pore solution tests investigating passive film formation in saturated $Ca(OH)_2$ solution with additions of sodium sulphate (Na_2SO_4). They found that sulphate impaired passive film formation if initially present in pH 12.6 but less so in pH 13.0. If a passive film was allowed to form prior to the introduction of sulphates, subsequent sulphate additions to the solution did not increase corrosion in the absence of chloride. The form of sulphur in pore solution may also be important. Investigations of the impact of SCM's and sulphates on rebar corrosion by Scott and Alexander 2016[74] using pore expression and synthetic pore solution corrosion experiments had several interesting findings. In characterization of expressed OPC cement without chlorides, mainly sulphates rather than thiosulphate or sulphide were found, while the opposite was true for cement containing slag. They suggest that thiosulphate and sulphides create a reducing environment that result in a less protective passive film and increased corrosion rate. However, they concluded that decreases in the initial pH due to the presence of SCM's had a much bigger impact on corrosion rate at a given chloride concentration compared to sulphide.

Gouda 1966[89] found that 1 wt% admixed chloride (as NaCl) was required to cause corrosion of steel reinforcement in a 0.6 w/c Portland cement mortar. For samples cast without chlorides passivation was found to occur after 2 to 3 days depending on the storage conditions. This was a surprise as Gouda expected passivation to have taken place in conjunction with $Ca(OH)_2$ saturation which occurs after one to two minutes. This delay was attributed to the presence of sulphate as gypsum breaks down which inhibited passive film formation until the sulphate concentration in pore solution was sufficiently low. Cements mixed using sea water rather than tap water also had difficulty forming passive films. Gouda notes that the alkali content of cement, which controls the pH of pore solution beyond $Ca(OH)_2$ saturation, does appear to impact the time to passivation.

When corrosion initiates, an increasing corrosion current density and a corresponding decreasing half cell or open circuit potential are expected. However, judging corrosion behaviour based solely on changes in the potential and current is not always a reliable metric. In a study of galvanically coupled samples in

two chloride solutions Gouda and Mourad[95] observed slightly more positive potentials on steel in a 1 M chloride solution compared to that in a 0.1 M chloride solution (both NaCl) in a pH 12 solution. They suggest that this is the result of chloride initially filling gaps in the passive film having a healing effect; however, over time pitting corrosion becomes favoured in high pH solutions. A case study by Gouda, Abdul Azim and El Sayed[96] found that general corrosion occurred when SO_4^{2-} was present while pitting occurred with Cl^- and S^{2-} in reinforcement in several concrete structures in Cairo, Egypt. However, in field studies Wimpenny and Slater[55] found pitting corrosion in the presence of chloride and sulphate noting that soft, black corrosion products were deposited in the pits.

The Cl^-/OH^- ratio of pore solutions has previously been suggested as an appropriate criterion for the susceptibility of reinforcing bars to corrosion[15,23,33,43,97,98]. It has been used to describe the pint where the pore solution can no longer buffer chloride reactions with the steel resulting in corrosion in a localized area[83]. It has more widely been used as a means to specify the critical amount of chloride required to cause significant corrosion on rebar in a given environment, typically under laboratory environments. In a 1967 paper, Hausmann proposed that corrosion would only occur above a ratio of Cl^-/OH^- of 0.6[98]. However, the added complexity of cements since 1967 including the ability to use lower w/c ratios and include SCM's has resulted in a larger range of Cl^-/OH^- ratios that indicate a corrosion initiation threshold[15,43,74,81,97]. Alonso et al. summarized the work up until 2000 showing significant variations in the chloride concentrations at the point of corrosion initiation[81]. Scott and Alexander, suggested that the initial hydroxyl concentration is more important than the Cl^-/OH^- ratio because it impacts the quality of the passive film formed[74].

Other limitations of the Cl^-/OH^- ratio are the measurement variability of $[OH^-]$[99]. When $[OH^-]$ calculated from a measured pH is compared to that measured by titration there can significant discrepancies. Goñi and Andrade[99], who identified this issue, demonstrated that it can be as large as a discrepancy of $[OH^-]$ = 0.032 M. In a study of cement exposed to salt solutions. Jiang et al. found that $CaCl_2$ and $MgCl_2$ resulted

in much higher Cl^-/OH^- ratios than samples exposed to solutions containing the same amount of chloride as KCl or NaCl, due to the decrease in pH in the former solutions despite lower free chloride content. Jiang et al.[33] further investigated different w/b ratios and the use of different SCM's. They note that the in the specimen containing fly ash and ground granulated blast furnace slag resulted in lower critical free chloride content when $CaCl_2$ and $MgCl_2$ were used while samples exposed to NaCl and KCl were unchanged[33].

In 1970 Gouda et al[75] proposed a linear relationship between the chloride concentration and pH (Equation 2.4-4). Gouda related the relationship to the ion exchange equilibrium between the solution and the rebar oxide surface. For her research, the constant, n was found to be 0.83 and K was unspecified.

Equation 2.4-4: Relationship between pH and [Cl-] proposed by Gouda 1970[75]

$$pH = n\log C_{Cl^-} + K$$

The concept that a chloride threshold exists, above which there will be active corrosion has been proposed frequently. As has been discussed, a universal threshold would need to consider and quantify many factors including pH, types of ions in pore solution, rebar surface treatment and temperature. Recently in 2019 Ogunsanya and Hansson[100], investigated a methodology following one used by Williams et al.[101] for the investigation of magnesium in a corrosive chloride solution. The test involves determining the corrosion and pitting potentials of samples at different chloride concentrations and extrapolating the data to the value of chlorides at which the two potentials are equal.

3 Experimental Methods

3.1 Testing Methods

3.1.1 X-Ray Powdered Diffraction (XRD)

A Bruker D8-Advance X-ray diffractometer was used to analyse powdered cement pastes. In this technique, x-rays irradiate a sample from known angles. Diffracted x-ray beams are captured by a detector and the intensity of the captured x-rays are plotted versus the angle of incidence, θ.

Crystals diffract the X-rays in destructive and constructive interference patterns resulting in peaks corresponding to the ordered arrangement of atoms indicating crystal faces. Amorphous materials do not have uniform crystalline structures and form broad, indistinct peaks. Braggs law (Equation 3.1-1) is used to identify crystal structures based on the wavelength of x-rays used as illustrated in Figure 3.1-1. CuKα radiation was used for all tests performed in this thesis work. Dynamic Beam Optimization (DBO), a software built into this model of XRD machine, was used to remove background noise.

Equation 3.1-1: Braggs Law[102]

$$2d\sin\theta = n\lambda$$

Where θ is the angle of the incident beam, d is the space between diffracting planes, λ is the wavelength of the x-ray beam used and n is an integer. All XRD scans performed for this thesis started at 2θ = 10 degrees.

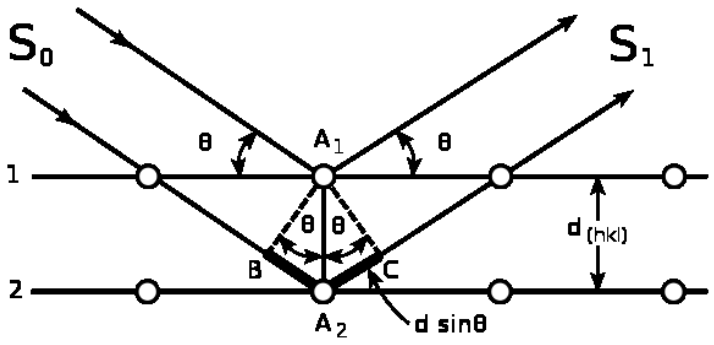

Figure 3.1-1: Schematic of diffracted X-rays following Bragg's law[103]

3.1.2 Scanning Electron Microscopy (SEM) and Energy Dispersive X-Ray Spectroscopy (EDS)

SEM use electrons to excite the atoms in a sample resulting in the emission of secondary electrons (SE) which can be used to image the surface. A Jeol JSM-6460 SEM was used for this research with a thermionic electron gun source.

3.1.3 X-Ray Fluorescence (XRF)

XRF excites atoms through the use of x-rays and gamma rays. Characteristic x-rays are emitted and used to identify elements in a sample. A handheld NITON XL3t 900 Analyzer was used for XRF scans.

3.1.4 Elemental Analysis of Expressed Pore Solution

Ion chromatography mass spectroscopy (IC-MS) was used for the chloride and sulphate concentrations. The remaining elements, and elemental sulphur, were determined using Inductively coupled plasma optical emission spectroscopy ICP-OES or Inductively coupled plasma mass spectroscopy where element concentrations were low.

In expressed pore solution Si, Al, Mg and Fe are often present in low concentrations[62]. It is important to compare these values to the detection limit (DL) and the Quantification Limit (QL). Samples between the DL and the QL are considered to indicate only the presence of that element in the sample. Values

greater than the QL can be taken as quantitative values. The limits for tested samples are in Table 3.1-1 below.

Table 3.1-1: Detection Limits for elements sampled using IC and ICP-OES techniques

Element	Al	Ca	Cl	Fe	K	Mg	Na	S	SO_4^{2-}	Si
DL (mg/L)	0.00004	0.2	0.01	0.00006	0.1	0.00004	0.2	0.2	0.01	0.07
QL (mg/L)	0.0001	0.6		0.0002	0.4	0.0001	0.5	0.7		0.2

3.1.5 Electrochemical Testing

3.1.5.1 Half Cell Potential

The half cell potential is measured between the specimen and a saturated Calomel electrode (SCE) using a voltmeter. Different SC electrodes can give slightly different readings depending on how they are used. To minimize this effect on results the same SCE was used for all half cell potential readings. The consistency of this SCE was monitored by comparing it to a reference SCE which is only used in a saturated KCl solution.

3.1.5.2 Linear Polarization Resistance (LPR)

This potentiostatic technique is used to monitor the corrosion current density without exposing the specimens to significant potential excursions (ASTM.G59)[104]. All LPR measurements used in this thesis research was conducted by imposing an anodic potential of 10 mV for three minutes followed by a cathodic potential of 10 mV relative to the initial open circuit potential (OCP) and monitoring the steady state current. Rebar specimens are arranged as shown in Figure 3.1-2 below. Rebar specimen act as the working electrode (WE), stainless steel coupons act as counter electrodes (CE) and a Saturated Calomel electrode (SCE) was used as the reference electrode (RE).

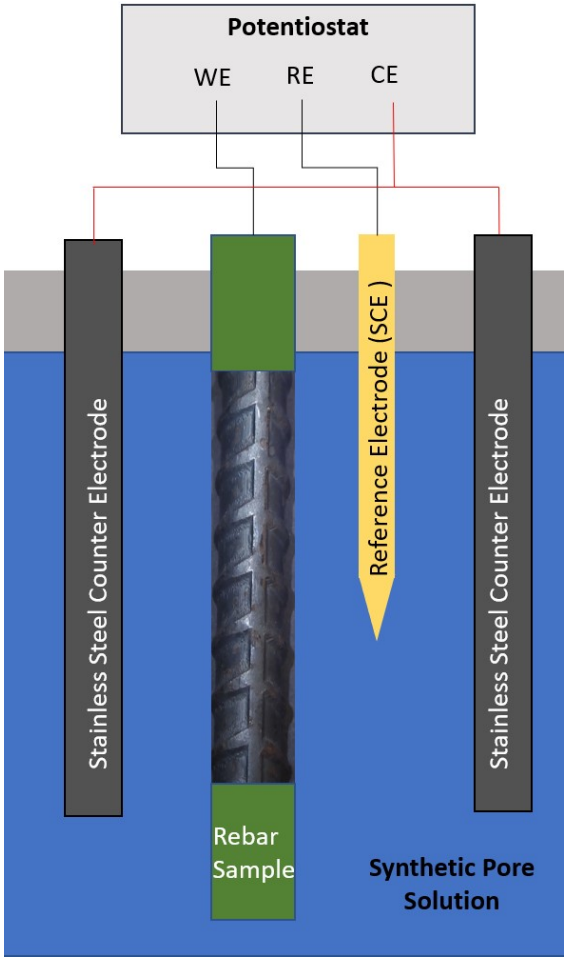

Figure 3.1-2: Schematic of corrosion cell used for Rebar tests

The Stern-Geary equation is used to calculate the corrosion current density of specimen following Equation 3.1-2 below.

Equation 3.1-2: Stern-Geary Equation[105]

$$\Delta E/\Delta I = \frac{B}{I_{CORR}} \quad \text{where } B = \frac{\beta_a \beta_c}{2.3\,(\beta_a+\beta_c)}$$

Where β_a and β_c are anodic and cathodic Tafel constants which are determined experimentally. The constants are typically approximated by B equals 0.026 V as discussed in ASTM G59[104]. This can be re-arranged to solve for the corrosion current (I_{corr}). The corrosion current density (i_{corr}) can then be calculated from the active area of the specimen[84].

LPR tests can have a short-term effect on other specimens in the same solution as the specimen being tested. Therefore, all LPR results reported in this thesis have been conducted with a 30-minute minimum wait time between the end of one test and beginning of the next if specimen are in shared containers.

3.2 Materials

3.2.1 Carbon Steel

Carbon steel rebar specimens have a nominal 16mm diameter and were prepared with a 125 mm (5 inch) exposed length. Two batches of rebar were used for some synthetic pore solution tests. The surface finish and rib pattern were different as shown in Figure 3.2-1 below. Rebar A was tested in all solutions while rebar B was used as two of the five bars in each container of the second set of long-term corrosion tests.

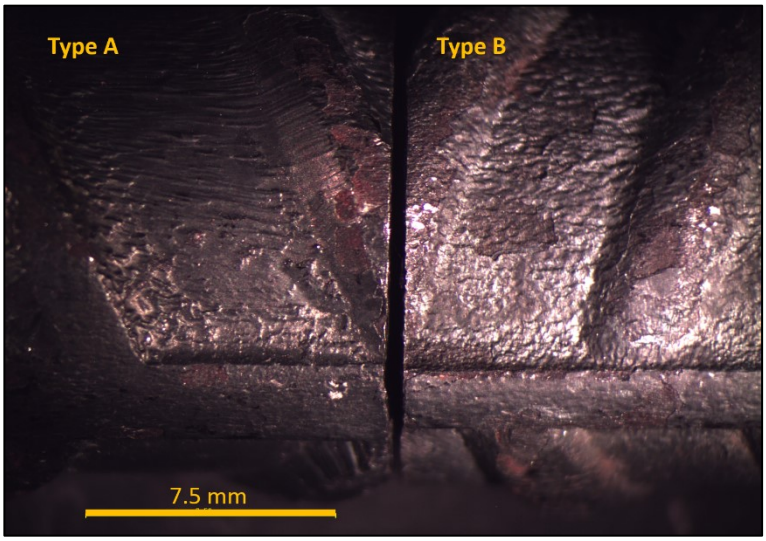

Figure 3.2-1: Photomicrograph image of Type A and Type B rebar specimens used for SEM Testing

3.2.1.1 As Received Steel Cross Sections

It was of interest to investigate whether there was a difference between different locations on rebar that might make them more susceptible to corrosion. A cross-section specimen was prepared for each steel type by cutting an as received piece of rebar, polishing it using aluminate polish and applying a Nital

etchant. The microstructure at various locations was examined as well as the mill scale along the edges of the specimen.

3.2.2 Chemicals

Deionized water was used to prepare the synthetic pore solutions used. Deionized water was also used for hydration of cement specimen for pore solution expression.

Laboratory grade chemicals were used in all synthetic pore solutions and as admixed chlorides.

3.2.3 Cement

A general use Portland (GU) cement with the composition provided by the manufacturer shown in Table 3.2-1 and Table 3.2-2 below, was used for pore solution expression experiments. A water to cement ratio (w/c) of 0.5 was used.

Table 3.2-1: Mill Certificate for GU Cement Used

Component	Wt%	Mol%	Component	Wt%	Mol%
SiO_2	19.80	20	K_2O	0.48	<1
Fe_2O_3	2.60	1	Na_2O	0.26	<1
Al_2O_3	4.50	3	TiO_2	0.27	<1
CaO	62.50	67	*Total Alkali as* Na_2O	0.58	1
Free CaO	1.10	1	*loss on ignition*	2.4	
MgO	3.30	5	*Insoluble residue*	0.23	
SO_3	3.40	3			

*Table 3.2-2: Mill Certificate Cement Phases**

Compound	Wt % Present
C2S	17.0
C3S	52.0
C3A	8.0
C4AF	8.0
$CaSO_4$	5.8

** $CaSO_4$ content calculated by author*

3.3 Experimental Procedure

3.3.1 Pore Solution Expression

The cement paste pore solution expression method is used to allow synthesis of test solutions with a composition simulating that experienced by rebar in concrete. Since the materials used to make the paste, the cement, salt and water to cement ratios, are all known, inferences can also be made about the cement phases in equilibrium with the pore solution

Cement cylinders, 50 mmØ x 100mm, consisting of GU cement with a w/c of 0.5 and additions of NaCl, $CaCl_2$ or $MgCl_2$ were prepared with chloride amounts corresponding to: 0.00, 0.25, 0.50, 0.75, 1.00, 2.50, 5.00 and 7.50 wt% of cement. The cylinders were prepared by mixing 2000 g of GU cement with 1000 g of de-ionized water in a small concrete paddle mixer. The desired amount of salt was dissolved into the water prior to mixing. Each batch of cement was mixed for three minutes, allowed to rest for three minutes and mixed for an additional three minutes. The slurry was then poured into the plastic cylinders, compacted and capped such that minimal air was included in the cylinder. Compaction was performed by lightly tapping the sides of the cylinders. In the case of 5.00 and 7.50 wt% admixed $CaCl_2$ and $MgCl_2$, an accelerated set was observed. These cylinders were slammed down on the table to eliminate any excess bubbles. All cylinders were rotated slowly for 24 hours to prevent bleeding. One cylinder was then

demoulded while the remaining 6 were stored in their plastic moulds in laboratory conditions for 27 days. The cylinder demoulded after 24 hours was used to investigate changes in the cement such as cracking which may be caused by the formation of oxychloride compounds.

Seven 50 mm Ø × 100 mm cylinders were prepared for each condition. Three cylinders were used for pore expression at 28 days after casting; one was demoulded after 24 hours to observe any early age cracking and one was used to determine the moisture content of the hardened cement paste. The remaining two cylinders were extras in case of error. For admixed salt concentrations less than 1 wt% Cl by mass of cement one of the extra cylinders was expressed at 56 days.

Pore solution was expressed 28 days after casting using the equipment in Figure 3.3-1 which is used in a compression chamber. The paste cylinder is placed in the chamber followed by an 8 mm PTFE disk and an 8 mm nylon disk. These ensure that expressed solution remains in the chamber and pressure from the piston is evenly distributed.

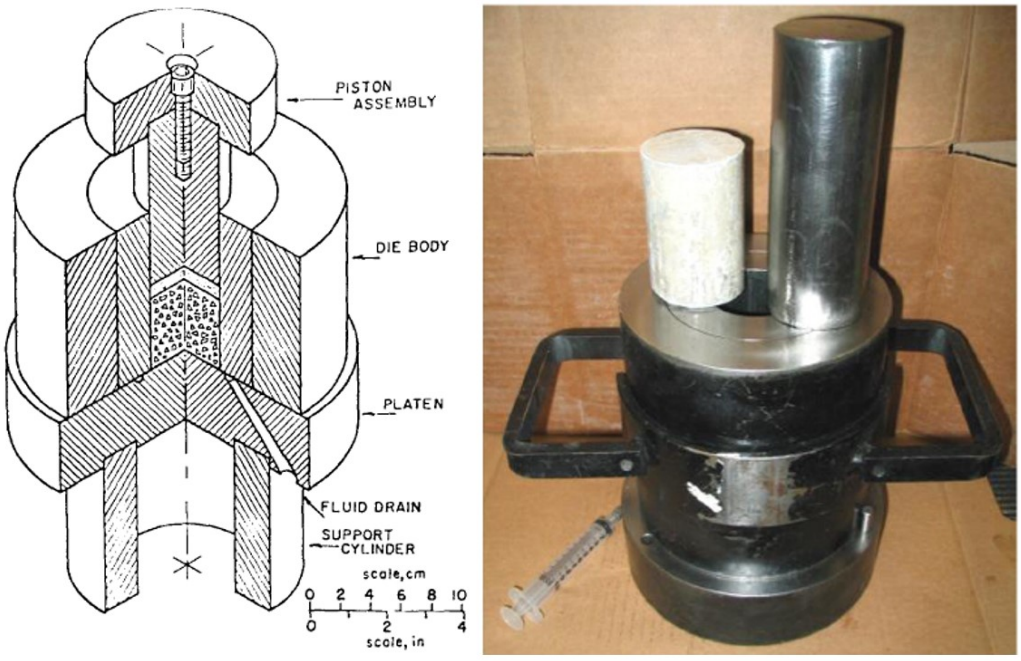

Figure 3.3-1: Pore Expression apparatus specifications[61] *(a) and device* [106]*(b)*

The force on the cement paste was held at 300 KN for 3 minutes, at 400 KN for 3 minutes and at 500 KN for 5 minutes for specimens with less than 2.5 wt % admixed chloride. At higher admixed chloride contents, the cylinder was compressed at 300 KN for 3.5 minutes, at 400 KN for 3.5 minutes, at 500 KN for 5 minutes, and at 600 KN, 700, 800 or 900 KN for 5 minutes each as needed. In some cases, pore solution was slow to be forced into the syringe. This may be due to the presence of larger pores in the cement paste which were initially filled partially with air. As cylinders were compressed water may have filled these pores before the fluid was under sufficient pressure to be expressed into the syringe. In such cases where there was limited pore solution in the syringe pressure was held at each force for an additional 30 to 60 seconds. Increasing the force on the cylinder incrementally allowed pores to be compressed without blocking passages within the cement and allowed pore solution to travel towards the bottom of the cylinder with the help of gravity.

The cylinder of the pore expression apparatus was gently sand blasted between each cylinder to clean off cement pressed into the walls by the applied pressure. The bottom plate, including the hole used to collect the pore solution, were rinsed with deionized water followed by isopropanol and were dried using compressed air.

Expressed pore solution was collected in a syringe fitted with a 0.45 μm filter to eliminate any cement particles. Between 5 and 10 mL of pore solution were obtained for most cylinders however for pastes with admixed $CaCl_2$ and $MgCl_2$ greater than 2.5 wt% Cl^- by weight cement less solution was obtained as discussed further in the results Section 4.1. Expressed pore solution was transferred into a 2.5 mL plastic vial prior to pH testing to avoid contamination. Vials were then stored in a fridge prior to testing using inductively coupled plasma (ICP) analysis for the cations and ion chromatography (IC) for the anions.

The pH of each expressed pore solution was measured using a pH probe within 30 minutes of pore expression to avoid carbonation and any changes caused by storage at a lower temperature. Because of

the limited pore solution after transferring some pore solution into a vial for further testing the pH was measured in the syringe. The electrode was calibrated using buffers for pH 4, 7 and 10. The temperatures of solutions were found to be between ~20 C and ~ 27 C. The pH meter used for the majority of tests up to 1.00 wt % Cl^- was an ORION Star A321. Due to a power source malfunction in the original meter, specimens with 2.50, 5.00 and 7.50 wt% chloride were tested using an ORION 290A pH meter. Comparison between meters resulted in very similar precision. When both pH meters were used on the same expressed por solution sample the pH reported was the same up to the second decimal place.

3.3.1.1 Measurement of Cement Paste Moisture Content

Samples for moisture content determination was as follows. The cylinders were demoulded 28 days after casting, individually placed in a plastic bag and crushed using a hammer. Powdered pastes and small chunks were then extracted from the bag and further ground using a mortar and pestle to create two 10 g samples. An example of the powders formed are shown in Figure 3.3-2 below. Despite rotating cylinders for the first 24 hrs. after casting, some separation was still observed in cylinders (Figure 3.3-3). By crushing the entire cylinder, it allowed for a more representative sample.

Figure 3.3-2: Cement powder prepared for moisture content testing

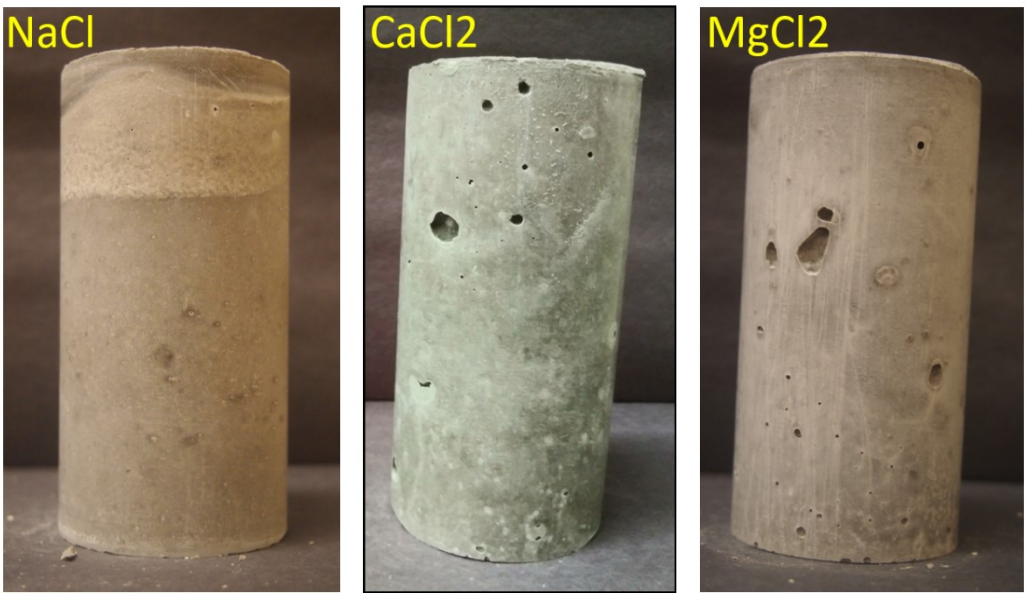

Figure 3.3-3: Examples of freshly demoulded cylinders containing 5.00 wt% admixed Cl by weight cement

Powdered samples were placed on glass sample holders with the weight of the powder and holders being recorded before and after being placed in an oven at 105 C for 24 hours. The percentage weight difference was then calculated between the fresh and dried powder weights with the weight decrease due to drying representing evaporated water. No neutral gas atmosphere was used in the oven.

3.3.2 Corrosion Tests of Carbon Steel Rebar in Synthetic Pore Solution

Carbon steel rebar begins to corrode when exposed to sufficient concentration of chlorides. Corrosion initiation has been found to vary depending on the composition of the synthetic pore solution used to evaluate future rebar performance.

3.3.2.1 Rebar Preparation

All rebar specimens used in this research were 5M bars (nominally 16 mm in diameter. Rebar specimen were cut to length from 6 m bars and were prepared for testing by drilling a hole in one end where copper wire was soldered in place. Both ends of rebar specimen, including the wire connection, were coated in an electroplating stop-off lacquer to create a known exposed area. Through the course of

this research it was found that the initial approach where tape was used to create a straight line of lacquer caused increased incidents of crevice corrosion. As a result, subsequent specimens were prepared with an uneven lacquer edge. The exposed area dimensions were found by measuring the exposed length at 4 equally spaced locations. A minimum of two layers of lacquer were applied with adequate time between layers to allow sufficient drying. Specimens were cleaned using a sponge and a small amount of dish soap to remove traces of oils from handling, rinsed in distilled water, then dried using an air gun. This was performed prior to the application of the lacquer as well as just prior to placement in the solution. All specimens were photographed and weighed prior to use.

Rebar specimens were immersed in synthetic pore solutions for four months with additional chloride being added weekly. Four synthetic pore solutions were prepared. These solutions are listed in Table 3.3-1. NaCl was added to all four solutions while Solution 4 was repeated with admixed $CaCl_2$ and $MgCl_2$ and the corresponding amounts of sulphate determined in the pore solution analysis. Five replicates of steel rebar specimens were immersed in each of the six cells and were monitored electrochemically through weekly LPR tests after which 0.05 wt% Cl/ L pore solution were added. This translates to 0.83 g ± 0.01g NaCl/L, 1.01 g ± 0.07g $CaCl_2 \cdot 6H_2O$/L and 1.44 g ± 0.07g $MgCl_2 \cdot 6H_2O$/L each week. Rebar specimens were allowed to passivate for one week prior to the first salt addition.

The first three pore solutions were chosen to capture the least and most protective conditions reported in the literature, as well as an intermediary pore solution based on the work of Randstrom et al. 2010[107]. The cations Ca^{2+}, Na^{+} and K^{+} are readily present in expressed pore solution so investigating the potential effect of neglecting some of these cations as in solutions 1 and 3 was of interest.

For the fourth solution, the carbon steel rebar corrosion tests focussed on the impacts of sulphate and the different salts on corrosion. The concentration of KOH, NaOH and $Ca(OH)_2$ and the corresponding sulphate was chosen based on the results of pore expression tests discussed in Chapter 4.

Each synthetic pore solution for the 4-month corrosion tests was prepared in a container containing 2.6 L. Due to evaporation, the amount of liquid fluctuates somewhat and water is periodically added to ensure the pore solution volume is approximately constant. The pH was tested using litmus paper to ensure it was above pH 12.00. Rebar specimens were prepared as discussed in section 3.3.2.1. After LPR tests were performed at a concentration of 0.80 wt% Cl, bars were removed from solution and photographed and corrosion products were then removed using a 30% HCl solution.

3.3.2.2 Synthetic Pore Solutions

Pore solutions 1, 2 and 3 were tested first. The pore solution 4 tests with varying salt types were tested the following year after the pore solution compositions had been obtained. There were two major changes in the experiment conditions. The first was the need to partially switch to rebar from a different manufacturer. It was decided to use two specimens of the new rebar type and three of the original rebar types in each solution. The second change was the time of year that the experiments were being run. Due to changing seasons there is a potentially non-negligible change in temperature as air conditioning is turned off and winter heating is turned on. For this reason, the 3rd synthetic pore solution, which showed the closest grouping of I_{corr} values in LPR tests in the first iteration, was chosen as a control test solution to be repeated in the second test set.

The amount of sulphate added to solutions, 4, 5 and 6 was chosen from the results of the pore solution expression using linear trend lines based on the results shown in Figure 4.1-26 (for admixed NaCl) and Figure 4.1-27 (for admixed $CaCl_2$ and $MgCl_2$). Since sulphate increases almost negligibly in pore solutions from cements with admixed $CaCl_2$ and $MgCl_2$, sulphate is only added when the amount needed exceeds 0.38 g $CaSO_4$*$2H_2O$/L. On weeks seven and twelve approximately 0.04 g $CaSO_4$*$2H_2O$/L was added to the $CaCl_2$ solution while no additional sulphate was required for the solution with added $MgCl_2$. For the NaCl pore solution, sulphate is added weekly at the same time as the salt addition. The total accumulated sulphate added is summarized in Table 3.3-2.

Table 3.3-1: Synthetic Pore Solution Compositions

	Solution	KOH mol/L	$CaSO_4.2H_2O$ mol/L	NaOH mol/L	$Ca(OH)_2$ mol/L OH^-	Mol/L OH^-	Calculated pH
1	***Saturated Calcium hydroxide***	0	0	0	>0.046	0.046	**12.66**
2	***ASTM Std.***	0.336	0	0.447	0	0.783	**13.80**
3	***Tri-hydroxides (Randstrom et al, 2010)***[107]	0.161	0	0.065	0.005	0.231	**13.36**
4	***Expressed Pore Soln*** *(from current project)*	0.225	Correlates to expressed Pore Solution	0.175	0.002	0.404	**13.61**

Table 3.3-2: Sulphate Additions to Synthetic Pore Solution 4

Solution 4 admixed salt	NaCl	CaCl2	MgCl2
Initial g $CaSO_4*2H_2O$/L	0.58	0.36	0.32
Subsequent Addition Frequency	Weekly	Twice	NA
Accumulated g $CaSO_4*2H_2O$/L added throughout test	2.33	0.43	0.27

4 Results

4.1 Pore Solution Expression

4.1.1 pH and Moisture Content Results

It is difficult to obtain accurate pH measurements at high pH. Changes to the equilibrium of the pH meter as well as the presence of alkali metals in the pore solution can alter a pH reading or cause gradual drift in the results if many measurements are performed at once. Measurements were performed using a hand-held, Orion low maintenance triode pH probe which was calibrated just prior to testing each sample using pH 4, 7 and 10 buffer solutions. A check with a 0.1 M KOH solution (theoretical pH 13) resulted in a pH reading of 12.83. The pH values presented in Figure 4.1-1 have not be adjusted to account for this difference. Increasing [Na+] in the pore solution, which is especially prevalent in the samples with admixed NaCl, may result in additional underprediction of the pH[62] because Na^+ can result in an overestimation of H^+.

Due to the limited volume of pore solution, the pH of most samples was tested in the syringe. Where the pH was not tested in the syringe a small glass beaker was used. It is common practice to gently stir solutions while doing pH tests however due to the small volume this was not possible.

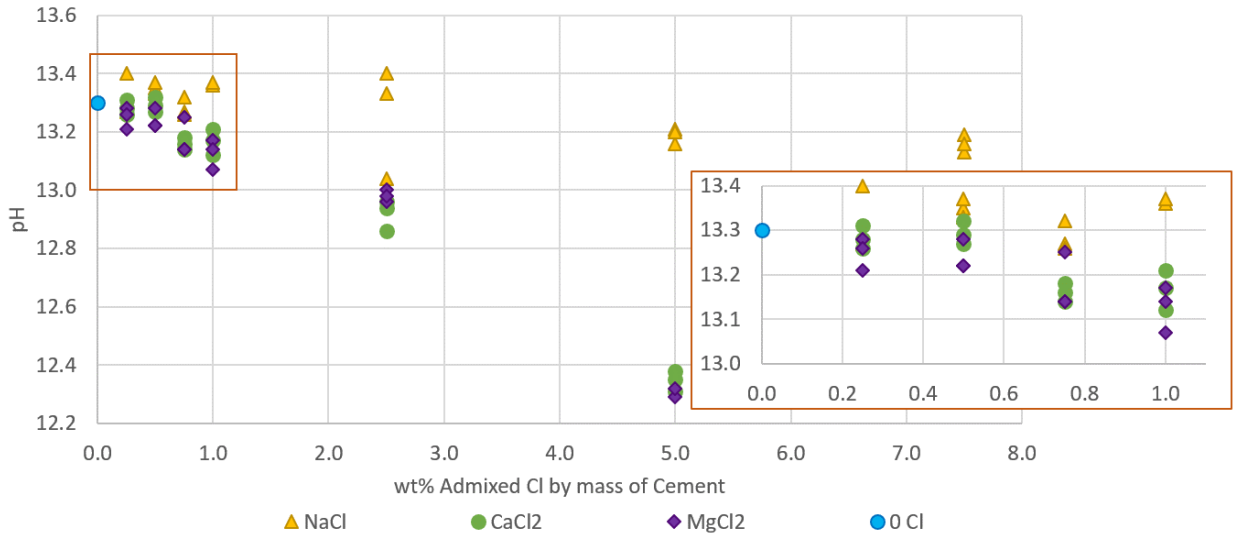

Figure 4.1-1: Experimental pH of expressed Pore Solutions. Inset shows the data for admixed Cl ≤ 1% on an expanded scale

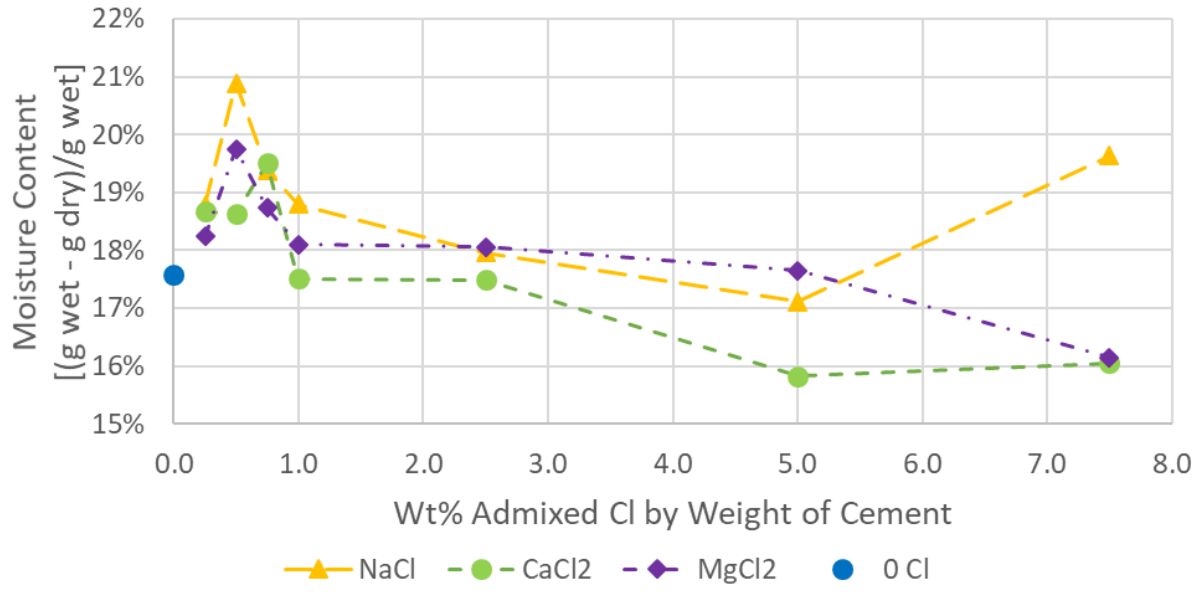

Figure 4.1-2: Moisture content of cement cylinders (average of two powder samples)

The moisture content (Figure 4.1-2) was determined experimentally as described in Section 3.3.1.1 and did not always correlate well with the amount of pore solution that could be extracted. This was especially evident at higher concentrations of admixed chloride in the $CaCl_2$ and $MgCl_2$ pastes. Moisture content shown in Figure 4.1-2 is based on two powder samples and in most cases the moisture content

was very close (within 0.1 %). In particular for the 0.50 wt% Cl NaCl sample the individual moisture contents were 20.2% and 21.6% respectively and for the 0.75 wt% Cl $CaCl_2$ sample moisture contents were 19.8 and 19.2% respectively. This means the sharp increases for moisture content for these samples may not be completely representative. The variability of all moisture content is included in Table A 1 in Appendix A.

In the 5.00 wt% admixed chloride cylinders the amount of expressed solution was 6.3 ± 0.5 mL for the NaCl pastes, 4.5 ± 0.5 mL for the $CaCl_2$ pastes and 3.8 ± 0.8 mL for the $MgCl_2$ pastes. The moisture content data shown in Figure 4.1-2 would suggest that the amount of expressed pore solution from most to least would be $MgCl_2$> NaCl > $CaCl_2$. Table A 1 in Appendix A shows the average moisture content compared to the average volume of pore solution obtained for each condition. As pore solution became more difficult to extract, the maximum applied load was increased. It must be noted that for earlier cylinders the average amount of pore solution is conservative because a lower load was applied and there was no difficulty obtaining the minimum volume required for testing.

At 7.50 wt% admixed chloride, insufficient pore solution for elemental analysis or pH testing could be extracted from the $CaCl_2$ and $MgCl_2$ cylinders while the moisture content from powdered samples actually increased slightly in the $CaCl_2$ compared to the 5.00 wt% samples.

The NaCl pastes had both higher moisture contents and larger volumes of expressed pore solution for comparable chloride content and duration of applied loads. The moisture content and volume of expressed pore solution increased between 5.00 and 7.50 wt% admixed chloride. This increase in moisture content has been previously observed for admixed NaCl[64].

4.1.2 Visual Observations of Cylinders

One cylinder from each admixed salt concentration was demoulded 24 hours after casting and stored in room conditions. No cracking was observed in any cylinders with less than 2.5 wt% admixed chlorides.

Only those cylinders with cracking are discussed in this section. Each batch of cement cylinders was prepared on different days but visual inspections were performed on all stored cylinders at once. For this reason, the number of days stored since demoulding varies between pastes.

4.1.2.1 NaCl Cylinders

Cracking was initially observed in the 2.50 wt% Cl by weight cement NaCl paste but appeared to heal over time as seen in Figure 4.1-3. In cylinders with higher chloride concentrations, salt was found to crystalize out resulting in a rougher surface. This is most visible in the 7.50 wt% Cl by weight cement NaCl cylinder shown in Figure 4.1-4. Salt crystallization was not apparent until the cylinder has been demoulded for a period of time as can be seen in the comparison between a cylinder demoulded after 28 days (sample A) and a cylinder from the same batch that was demoulded after 24 hours and left in the laboratory at room temperature for 171 days. Visible salt crystallization is likely the result of water evaporating from the system of pores resulting in insufficient liquid to fully dissolve the salt.

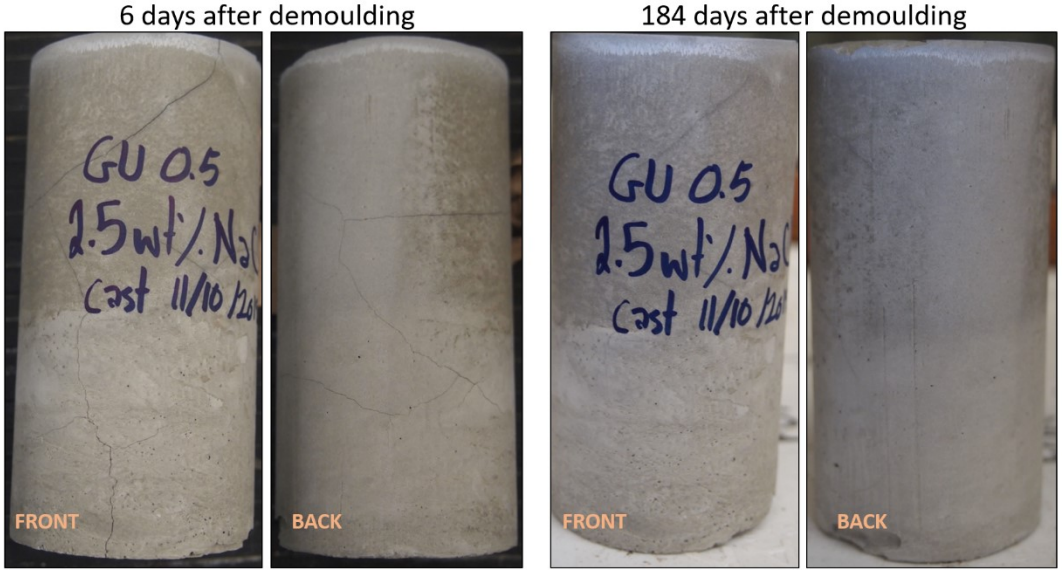

Figure 4.1-3: Cracking in cylinder with 2.5 wt% admixed Cl by weight of Cement (NaCl)

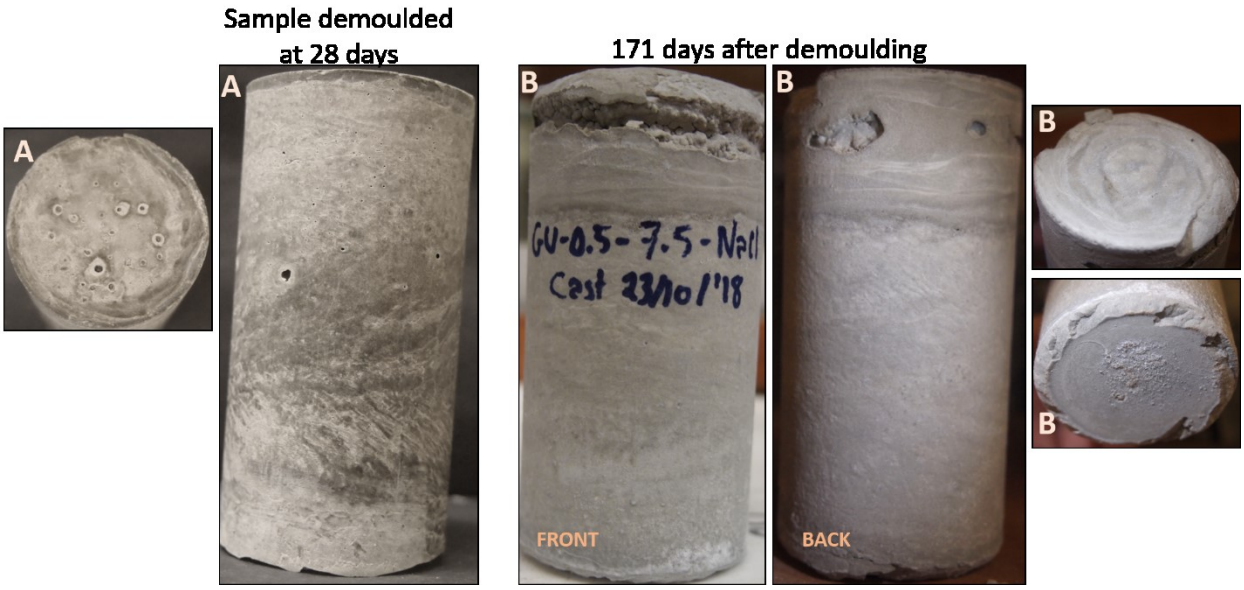

Figure 4.1-4: Cylinders with 7.5 wt% admixed Cl^- (NaCl) by weight of cement where sample A is shown shortly after being demoulded after 28 days and sample B is shown after being stored at room temperature for 171 days.

4.1.2.2 $CaCl_2$ Cylinders

Cracking was observed on the 2.5 wt% Cl ($CaCl_2$) by weight cement cylinders shortly after demoulding with some cracks becoming more visible after 180 days. Cracks appear to penetrate the cylinder as seen in the top and bottom images of Figure 4.1-5. However, cracking in cylinders with 5.0 and 7.5 wt% Cl was limited to the surface with the amount of visible cracking decreasing as the amount of admixed salt increases as seen in Figure 4.1-6. This trend where damage appears to decrease as the admixed chloride increases may suggest a shift from a higher volume (lower density) hydration product to a lower volume (higher density) product.

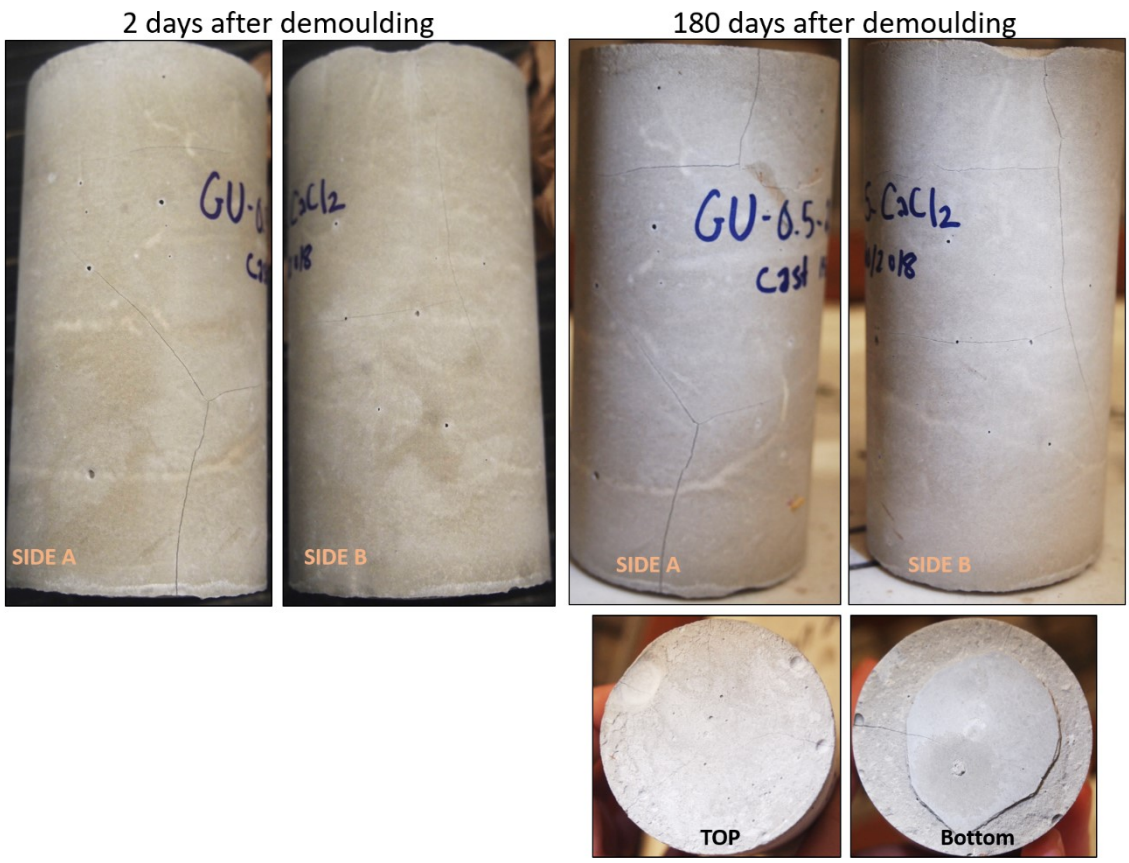

Figure 4.1-5: Cracking in cylinder with 2.5 wt% admixed Cl (as $CaCl_2$) by weight of Cement

$CaCl_2$ is known to accelerate set which was an issue when preparing cylinders with 5.00 and 7.50 wt% admixed Cl by weight cement. This resulted in large voids, especially for the 5.00 wt% Cl cylinders where the rapid set was less expected. While most voids are empty some appear to be filled with a lighter coloured hydration product as indicated in the void circled in red in Figure 4.1-6.

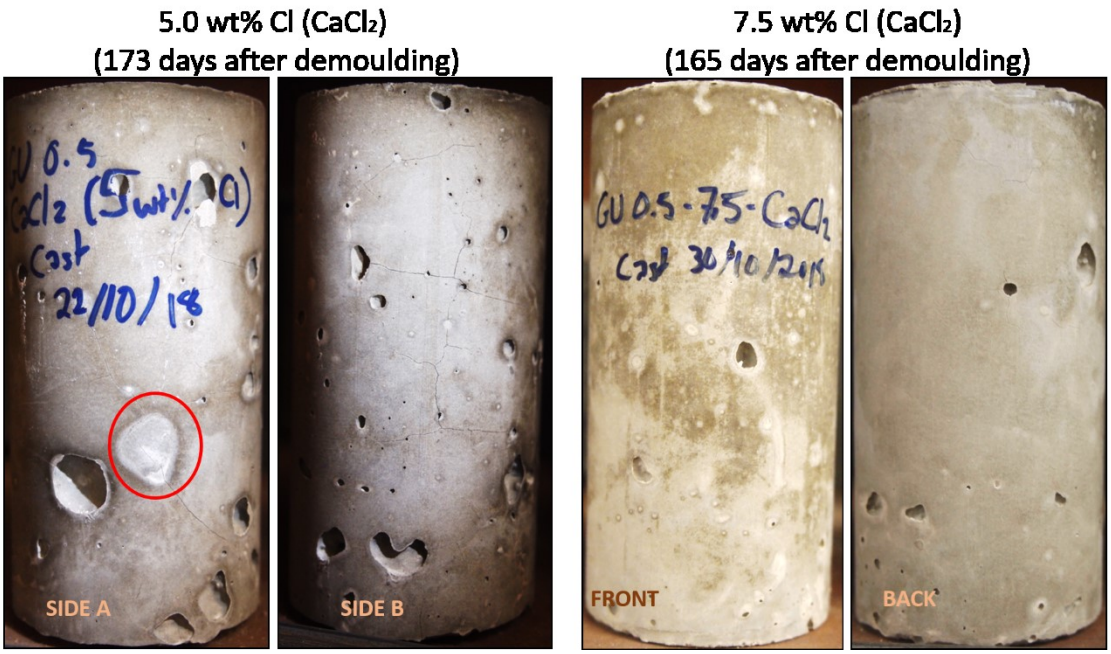

Figure 4.1-6: Cracking in cylinders with 5.0 and 7.5 wt% admixed Cl by weight of Cement ($CaCl_2$)

XRF analysis was used to investigate $CaCl_2$ cylinders shown in Figure 4.1-6. Elemental data obtained for the white section inside the large pore may include background data from the general cement resulting in the minimal variations observed in Table 4.1-1. The elements Ca, Cl and K appear to have the most variation. In the 7.50 wt% Cl cylinder it is unsurprising that the amount of calcium detected has increased since more calcium is introduced by $CaCl_2$ however the amount of chloride was expected to increase.

Table 4.1-1: XRF data for Paste with admixed $CaCl_2$ (wt%)

	Al	Ca	Cl	Fe	K	S	Si	Mg
5.00 wt% Cl ($CaCl_2$) (area circled)‡	1.6	36.5	15.6	1.2	2.0	1.7	6.3	<LOD
5.00 wt% Cl ($CaCl_2$) ‡	1.2	33.8	10.7	1.0	2.0	1.6	5.6	<LOD
7.50 wt% Cl ($CaCl_2$)	1.2	41.0	7.8	0.9	0.2	1.4	4.2	<LOD

‡ Average of two XRF readings

4.1.2.3 $MgCl_2$ Cylinders

Cracking in the cylinders with admixed $MgCl_2$ was found to be most severe in the cylinders with 2.50 and 7.50 wt% Cl ($MgCl_2$) by weight cement where cracks extended to the interior of the cylinders. Surface cracking was visible on all three cylinders with 2.50, 5.00 and 7.50 wt% Cl by weight cement.

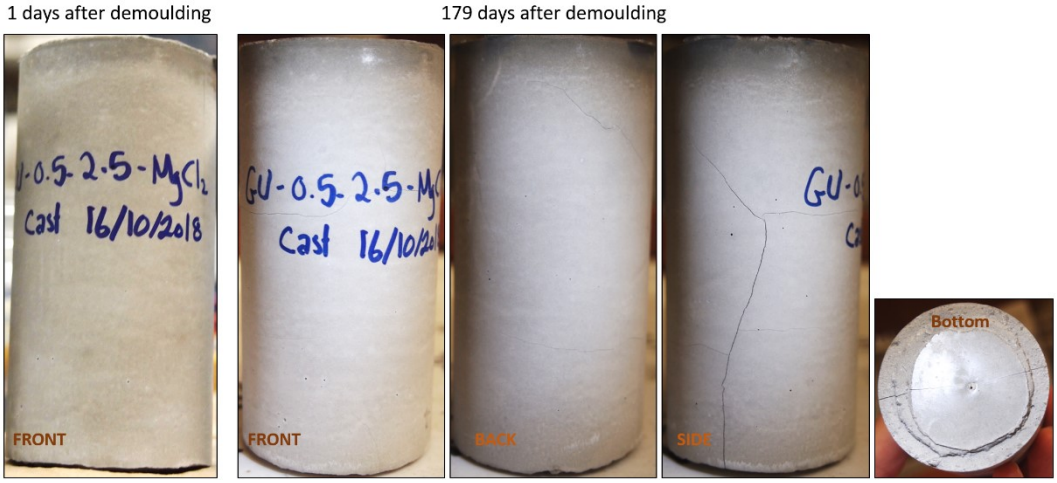

Figure 4.1-7: Cracking in cylinder with 2.5 wt% admixed Cl by weight of Cement ($MgCl_2$)

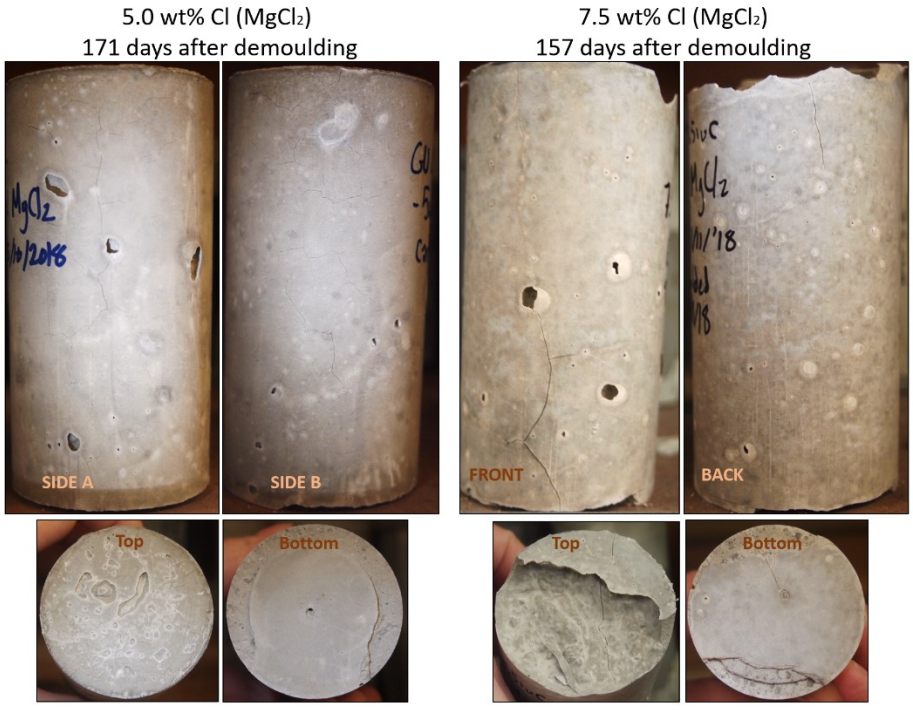

Figure 4.1-8: Cracking in cylinders with 5.0 and 7.5 wt% admixed Cl by weight of Cement ($MgCl_2$)

XRF was used to investigate possible differences between the amount of admixed salt as well as the location with significant cracking shown in the front view of the cylinder with 7.50 wt% Cl by weight cement. None of the filled voids were sufficiently large for an independent XRF scan. Only small differences occurred as shown in Table 4.1-2. The lack of detected magnesium is surprising because there are significant amounts introduced as $MgCl_2$ and very little magnesium was expressed in pore solution (Figure 4.1-20).

Table 4.1-2: XRF data for Paste with admixed $MgCl_2$ (wt%)

	Al	Ca	Cl	Fe	K	S	Si	Mg
5.00 wt% Cl ($MgCl_2$)	1.2	36.8	5.0	0.8	0.6	1.1	5.5	<LOD
7.50 wt% Cl ($MgCl_2$)	1.1	34.5	8.2	0.9	0.2	1.5	5.7	<LOD
7.5 wt% Cl ($MgCl_2$) (Near big cracks)	0.9	36.0	6.4	0.8	0.4	1.4	5.3	<LOD

4.1.3 Chemical Analysis of Pore Solution

Expressed pore solution was analyzed by Joy Hu in the Groundwater Geochemistry and Remediation group at the University of Waterloo. Expressed pore solution samples were refrigerated to minimise equilibrium changes which might result in precipitation and where possible testing was performed within two weeks of expression. Results from IC and ICP tests are summarized in the figures below. Some elements are especially susceptible to storage conditions, in particular calcium has been found to precipitate out of solution easily[62]. Storing samples at lower temperatures increases the solubility of Ca^{2+} although some precipitation may still occur during testing, lowering reported concentrations.

A check of the quantification limit (QL) showed that all elements but Mg are significant. For magnesium some points were above the QL but even within expressed pore solution with the same amount and type of admixed salt only one or two of the three had quantifiable amounts of magnesium. These values have been included because despite the addition of significant quantities of $MgCl_2$ salts this

was not evident in the expressed solution. Although pore solutions were diluted during IC and ICP testing, high concentrations of chlorides relative to other elements may decrease the accuracy of results as chloride content increased.

Note that elements are present in concentrations on the order of mols, mmols and µmols. Sulphur, which was determined from ICP-OES, and sulphate, which was determined using IC-MS, are both presented. The concentration of an element may differ significantly depending on the specific admixed salt so two graphs may be used to capture the behaviour of these elements. Results are plotted against both the admixed chloride and pH to better understand equilibrium conditions and solubility in pore solutions. Some elements, such as calcium, have a clear dependence on the pH of the solution. Other elements, such as aluminum and iron, are not saturated in solution and the concentrations in pore solution are a function of reactions occurring in the pastes for a given admixed Cl and salt type. Please note: there are no results for 7.50 wt% Cl from $CaCl_2$ and $MgCl_2$ due to insufficient pore solution.

4.1.3.1 Aluminum

Aluminum is introduced to cement in the C3A and C4AF phases which form monosulphate (Afm) and ettringite (Aft) after hydration. The cement used for this research had an aluminum oxide (Al_2O_3) content of 4.50 wt% (Table 3.2-1). Since a w/c ratio of 0.50 was used, this is equivalent to approximately 1.7 mol Al/L if all aluminum were dissolved into the pore solution instead of forming solid hydration products. Since the aluminum found in the expressed pore solution was on the order of µmol/L (Figure 4.1-9) the majority of aluminum is in the solid phase. Similar trends occur for all salt types as the amount of chloride is increased. Although these values are above the quantification limit (Table 3.1-1), the high concentrations of chloride in solution may decrease measurement accuracy. The amount of chloride rather than decreases in pH appear to have the biggest impact on aluminum concentrations, in particular exhibiting similar aluminum content at 5.00wt% admixed Cl for all admixed salt types (Figure 4.1-9) despite very different pH values in these solutions (outliers in Figure 4.1-10).

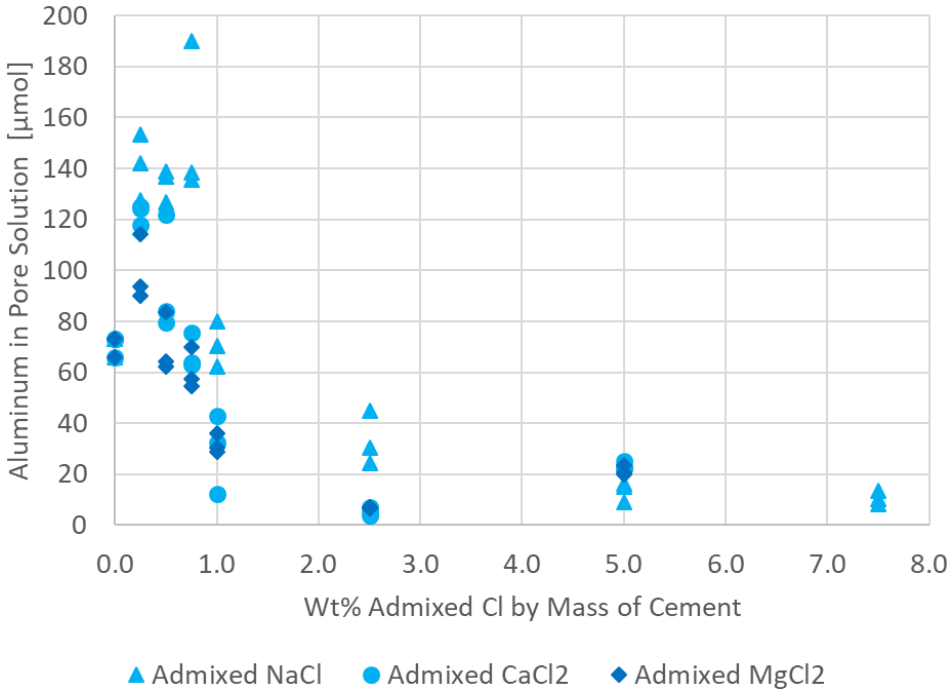

Figure 4.1-9: Al in expressed pore solution as a function of admixed Cl

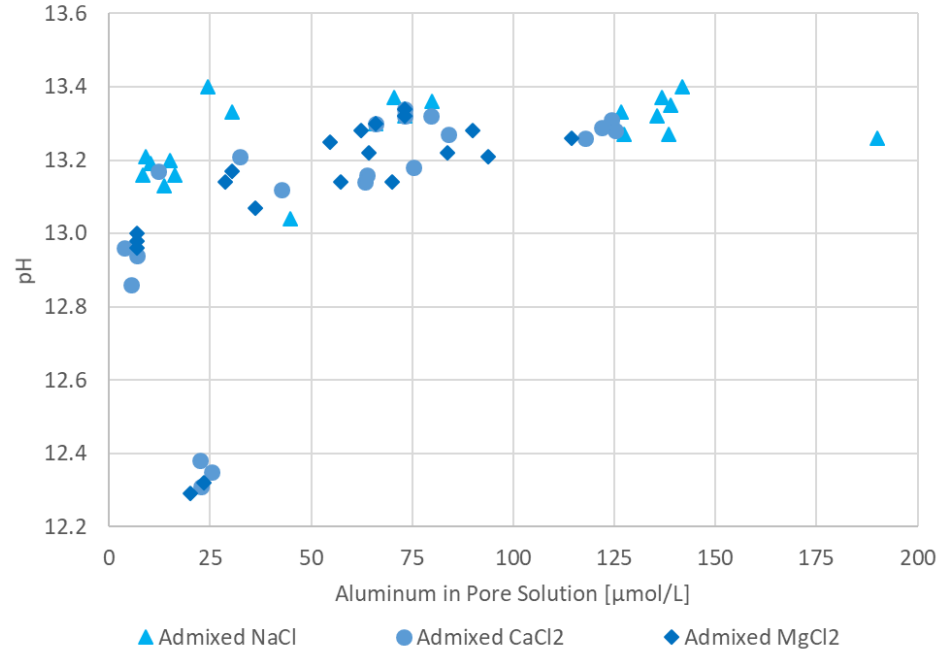

Figure 4.1-10: pH as a function of Al in the expressed pore solution

4.1.3.2 Calcium

Calcium is the most important element in cement and is present in all clinker phases. It is part of all hydration products formed with Portlandite ($Ca(OH)_2$) being the most easily dissolved in solution. The cement used for this research had a calcium oxide (CaO) content of 62.5 wt% (Table 3.2-1). Since a w/c ratio of 0.50 was used, this is equivalent to approximately 22.7 mol Ca/L if all calcium were dissolved into the pore solution instead of forming solid hydration products. Note that the calcium concentrations in expressed pore solution were found to be in mmol/L. The concentration of calcium expressed pore solution exhibits different trends depending on the type of admixed salt with significant increases for increased admixed $CaCl_2$ and $MgCl_2$ (Figure 4.1-11) and minor changes as chloride increases in the form of NaCl (Figure 4.1-12 shows the lower calcium concentrations in more detail). The calcium concentration can be seen to increase as the pH decreases (Figure 4.1-13), which is thought to be due to increased $Ca(OH)_2$ solubility at lower pH values

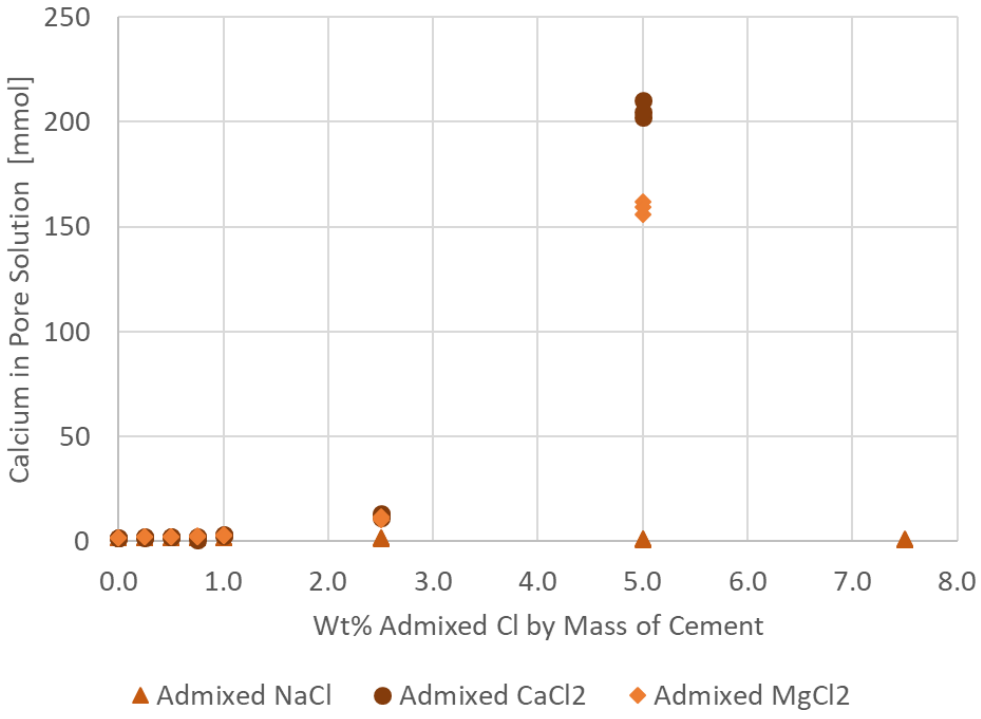

Figure 4.1-11: Ca in expressed pore solution as a function of admixed Cl

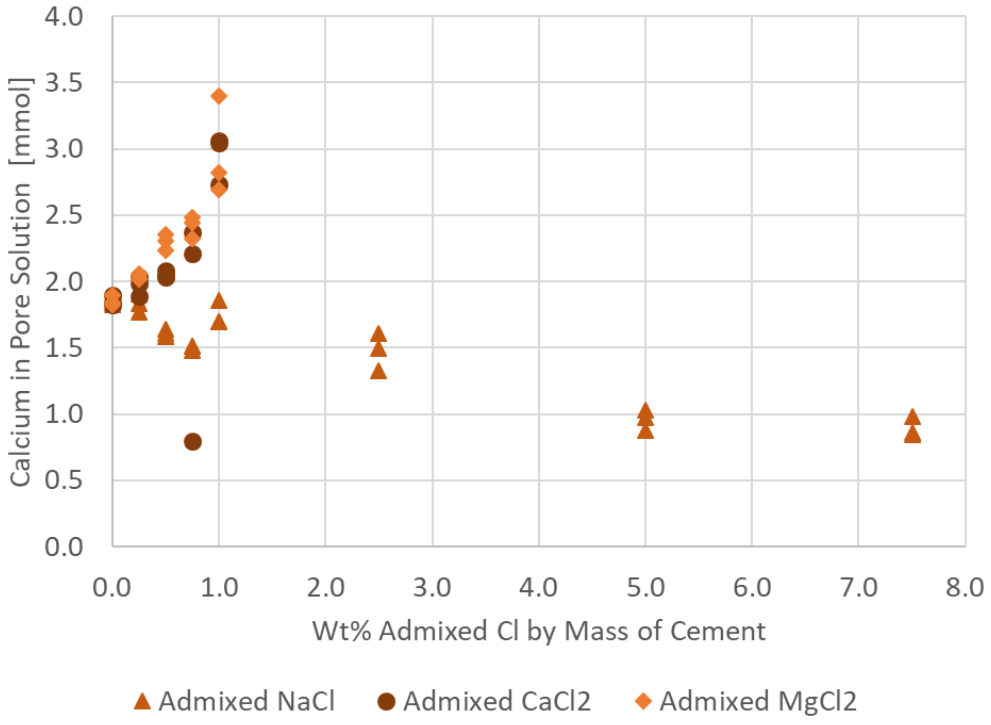

Figure 4.1-12: Ca in expressed pore solution as a function of admixed Cl with an expanded ordinate scale

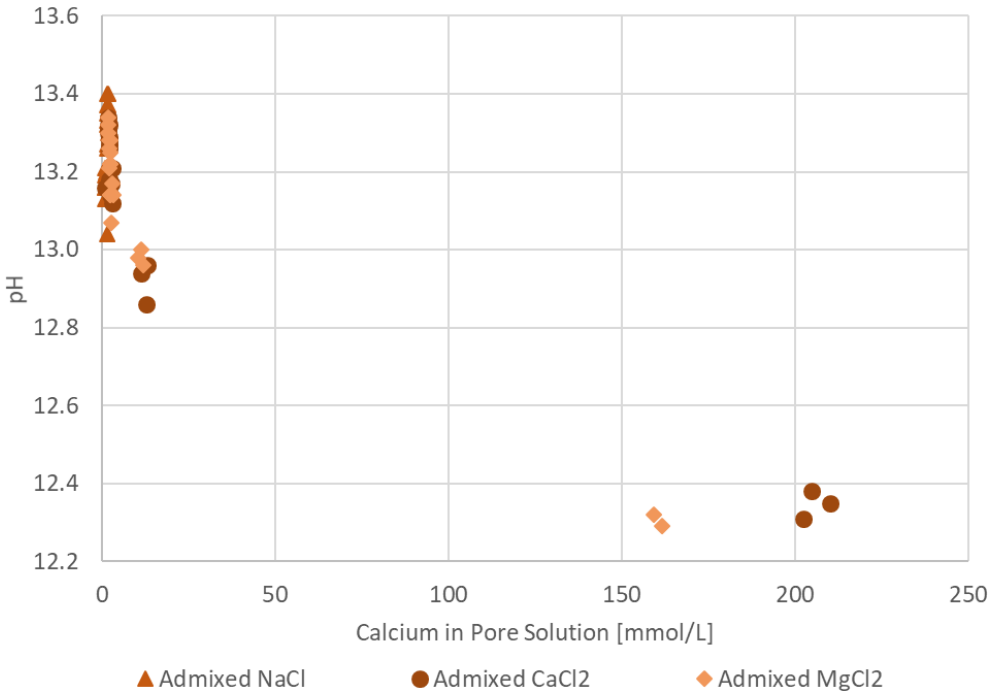

Figure 4.1-13: pH as a function of Ca in the expressed pore solution

4.1.3.3 Chloride

Chloride is introduced to the pastes as either NaCl, $CaCl_2$ or $MgCl_2$, a small amount of chloride, approximately 2 mmol Cl/L, was found to be present in the cement initially. More chloride is in expressed pore solution from pastes with admixed NaCl than from pastes with admixed $CaCl_2$ and $MgCl_2$ (Figure 4.1-14) indicating that more chlorides are bound into the solid hydrated phases in the pastes containing $CaCl_2$ and $MgCl_2$. The chloride content in the pore solution does not appear to be related to pH as the concentrations of chloride continue to increase in all pastes (Figure 4.1-15).

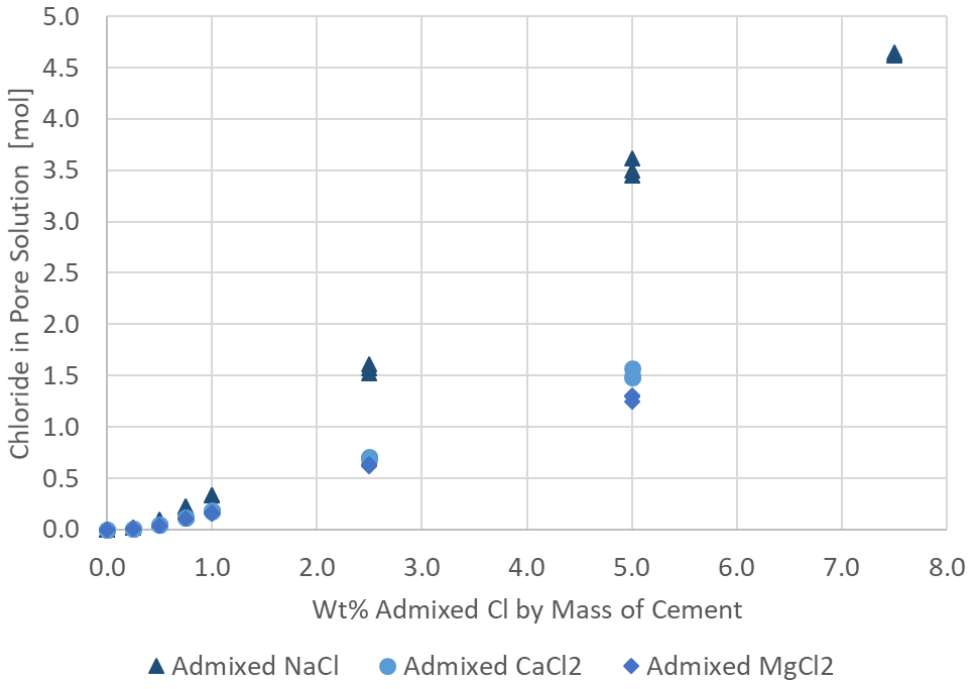

Figure 4.1-14: Cl in expressed pore solution as a function of admixed Cl

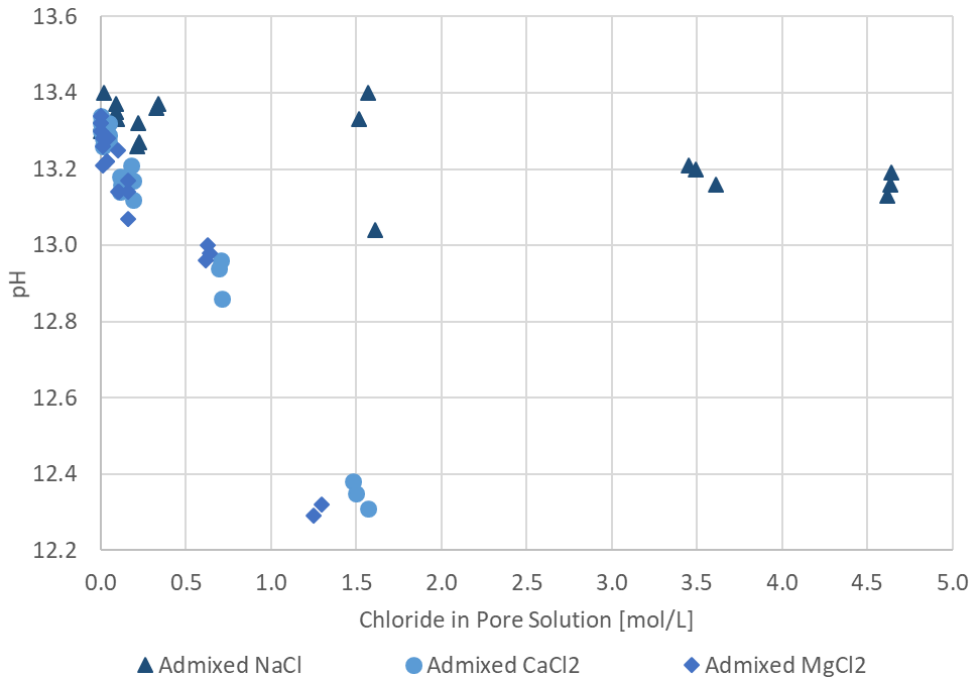

Figure 4.1-15: pH as a function of Cl in the expressed pore solution

4.1.3.4 Iron

Iron is introduced to cement in the C4AF phase and forms monosulphate (Afm) and ettringite (Aft). The cement used for this research had an iron oxide (Fe_2O_3) content of 2.6 wt% (Table 3.2-1). Since a w/c ratio of 0.50 was used, this is equivalent to approximately 0.65 mol Fe/L if all iron were dissolved into the pore solution instead of forming solid hydration products. The iron in expressed pore solutions was in the order of µmol. As mentioned for the aluminum, high concentrations of chloride might decrease the accuracy of elemental measurements despite measured concentrations being above the quantification limit (Table 3.1-1). Unlike the aluminum values, iron concentrations show different trends for admixed NaCl compared to admixed $CaCl_2$ and $MgCl_2$ (Figure 4.1-16). When iron concentrations are compared relative to the pH of the expressed pore solution there appears to be a trend where iron solubility increases as pH increases (Figure 4.1-17).

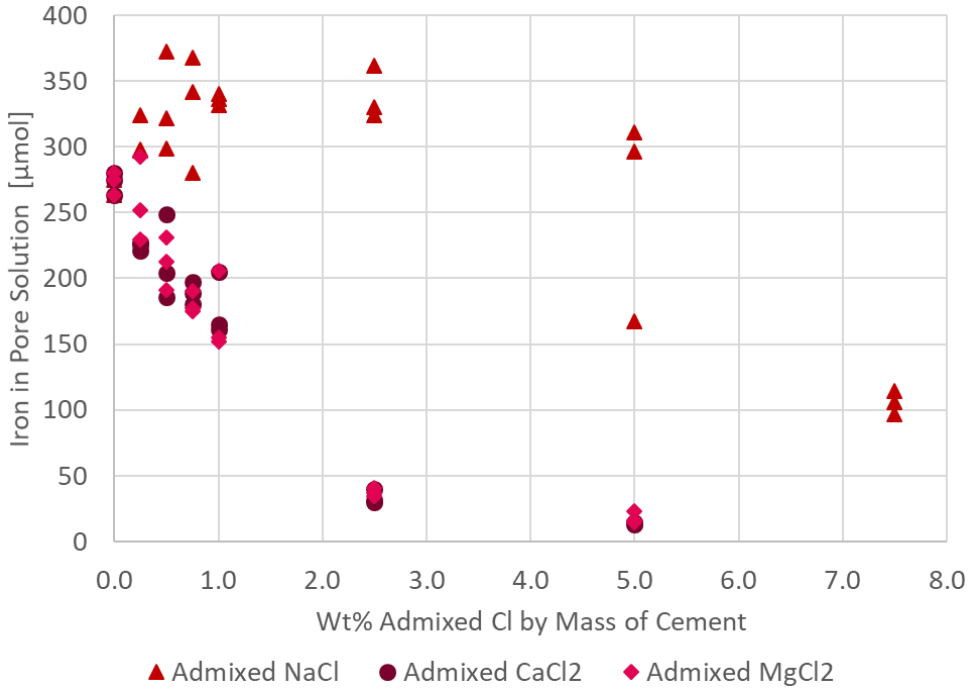

Figure 4.1-16: Fe in expressed pore solution as a function of admixed Cl

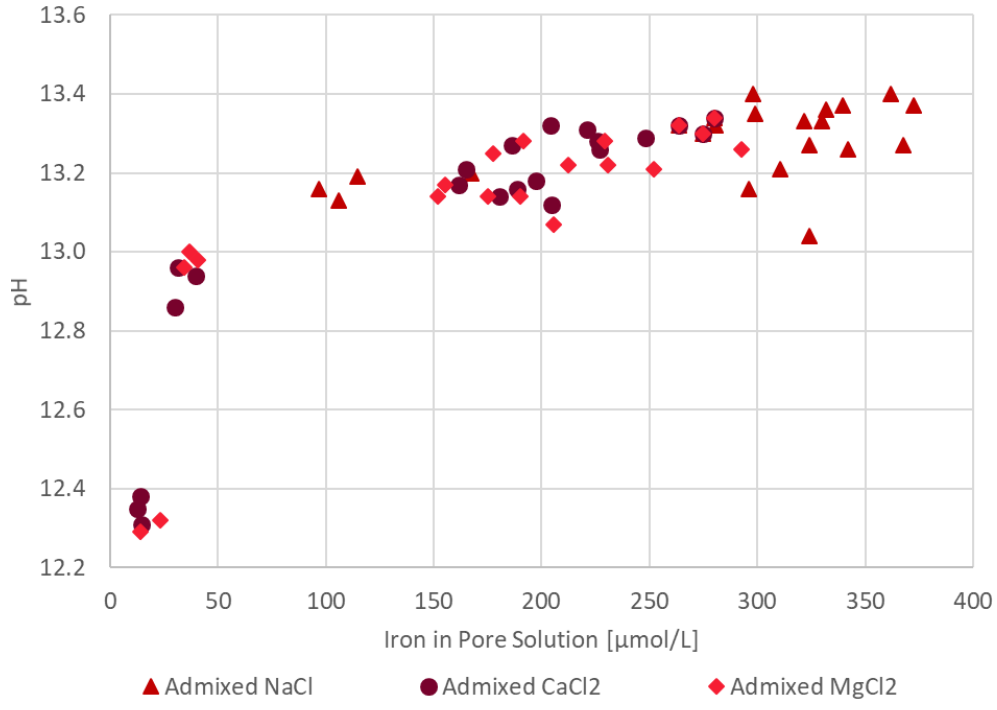

Figure 4.1-17: pH as a function of Fe in the expressed pore solution

4.1.3.5 Potassium

Potassium is introduced as a trace element in the clinker phase. The cement used for this research had a potassium oxide (K_2O) content of 0.48 wt% (Table 3.2-1). Since a w/c ratio of 0.50 was used, this is equivalent to approximately 0.20 mol K/L if all potassium were dissolved into the pore solution instead of being chemically or physically bound in the solid phase. The potassium in expressed pore solutions was in this range initially, however more potassium was expressed as the amount of admixed salt increased. The highest concentration of potassium, approximately 0.60 mol/L corresponds to approximately 1.4 g K_2O instead of 0.48 g K_2O reported in the mill certificate. Smaller amounts of materials are harder to identify accurately which may explain the higher concentration in pore solution compared to the expected amount based on Table 3.2-1. Similar to iron, potassium concentrations indicate different trends for pastes with admixed NaCl than pastes with admixed $CaCl_2$ and $MgCl_2$ (Figure 4.1-18). In this case there appears to be a trend where the solubility of potassium increases as the pH decreases (Figure 4.1-19).

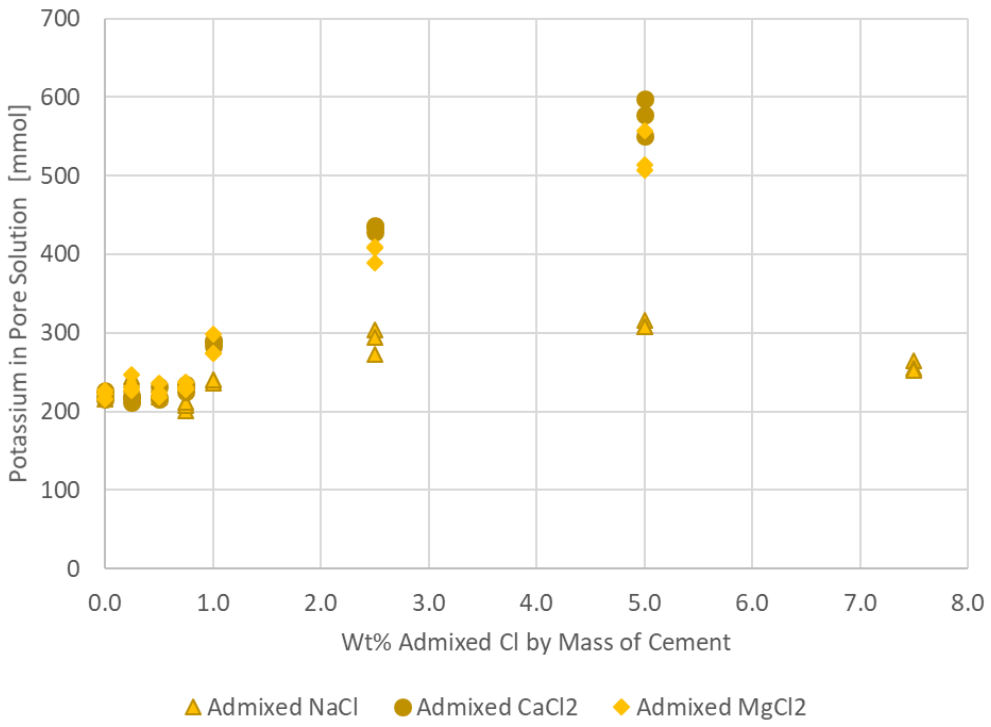

Figure 4.1-18: K in expressed pore solution as a function of admixed Cl

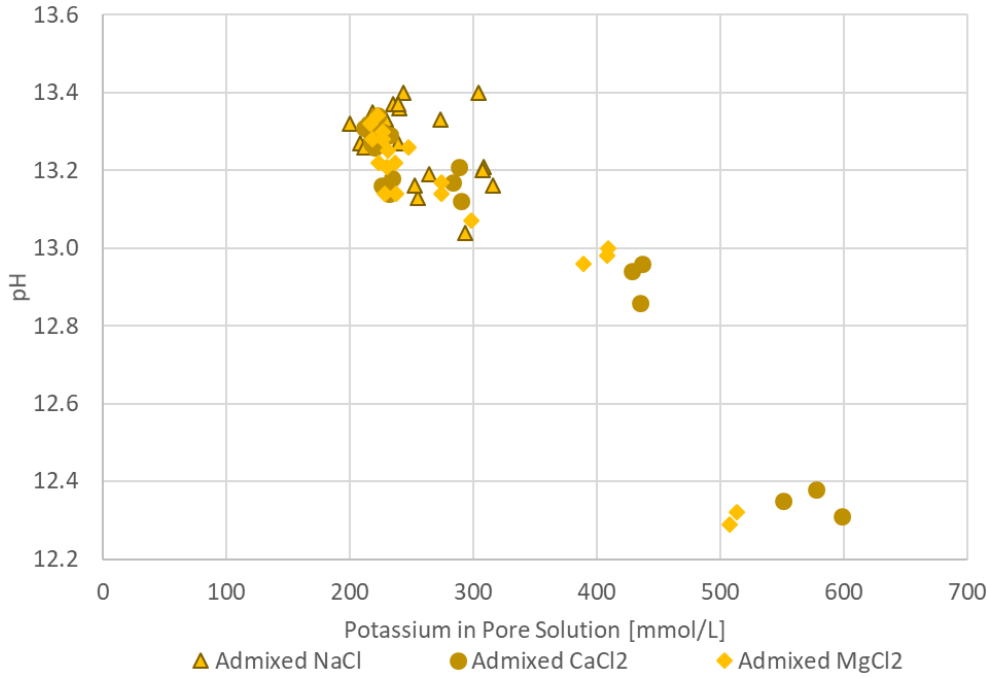

Figure 4.1-19: pH as a function of K in the expressed pore solution

4.1.3.6 Magnesium

Magnesium is introduced as a trace element in the clinker. The cement used for this research had a magnesium oxide (MgO) content of 3.3 wt% (Table 3.2-1). Since a w/c ratio of 0.50 was used, this is equivalent to approximately 1.6 mol Mg/L if all magnesium in the cement were dissolved into the pore solution instead of instead of being chemically or physically bound in the solid phase. The magnesium in expressed pore solutions was in the order of µmol and in many cases the magnesium was below the detection limit (Table 3.1-1). Although there was additional magnesium in pastes with admixed $MgCl_2$, this did not increase the amount of expressed magnesium in pore solution. This is attributed to the very low magnesium solubility resulting in solid products like brucite ($Mg(OH)_2$). There is not enough data to comment on possible trends in the concentration of magnesium with increased admixed salts (Figure 4.1-20) or in comparison to pore solution pH (Figure 4.1-21).

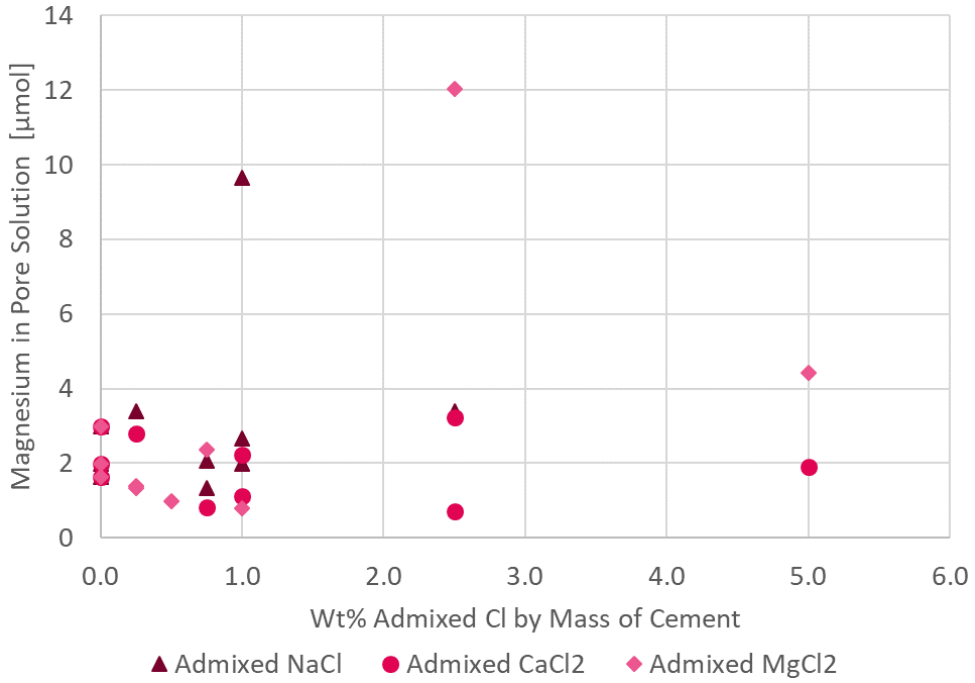

Figure 4.1-20: Mg in expressed pore solution as a function of admixed Cl

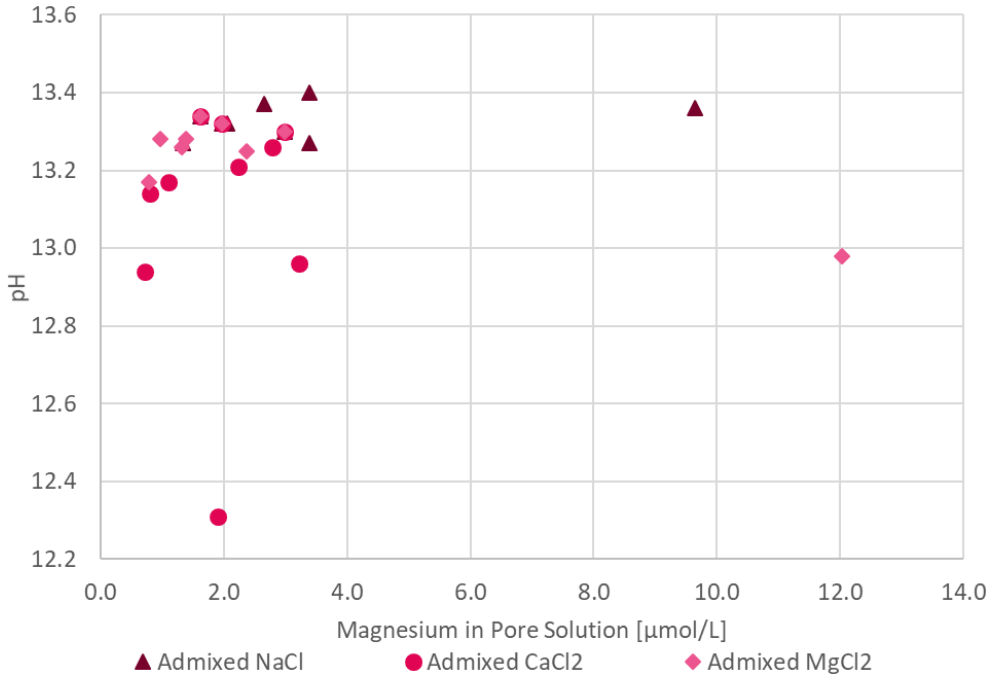

Figure 4.1-21: pH as a function of Mg in the expressed pore solution

4.1.3.7 Sodium

Sodium is introduced as a trace element in the clinker phase as well as through the addition of NaCl. The cement used for this research had a sodium oxide (Na_2O) content of 0.26 wt% (Table 3.2-1). Since a w/c ratio of 0.50 was used, this is equivalent to approximately 0.5 mol Na/L if all sodium were dissolved into the pore solution instead of being chemically or physically bound in the solid phase. Compared to previous elements much less sodium is bound in the solid phases. For pastes with admixed $CaCl_2$ and $MgCl_2$, sodium increases from 0.15 mol Na/L in paste with no added salt to approximately 0.45 mol Na/L in paste with 5.00 wt% admixed Cl^-. Similarly, most of the sodium introduced as NaCl remains in the pore solution (Figure 4.1-22 but does not appear to be linked to the pH (Figure 4.1-23).

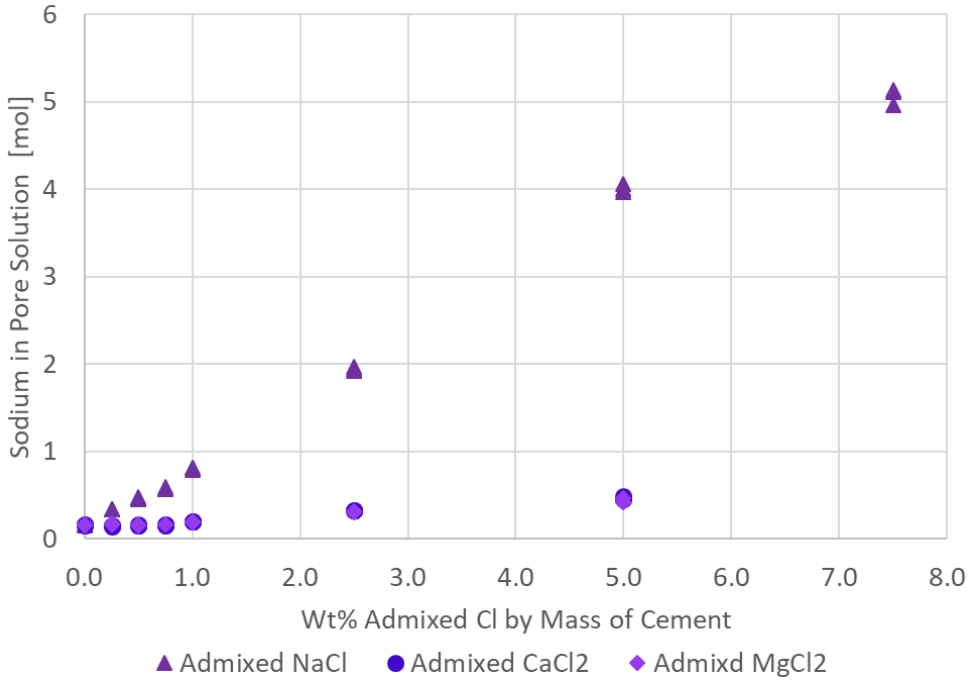

Figure 4.1-22: Na in expressed pore solution as a function of admixed Cl

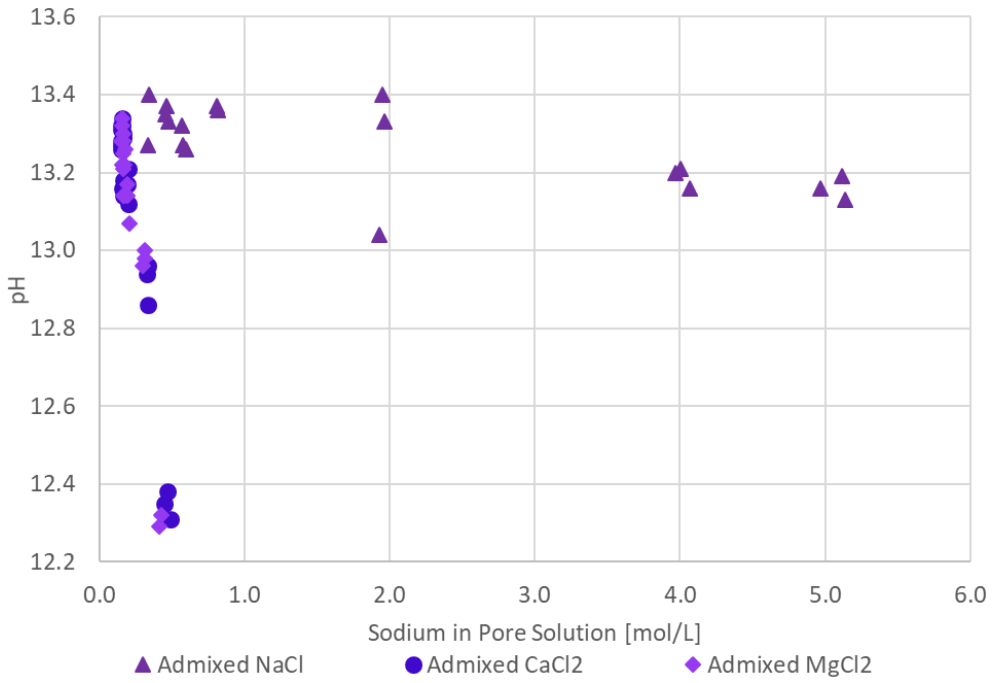

Figure 4.1-23: pH as a function of Na in the expressed pore solution

4.1.3.8 Silicon

Silicon is introduced to cement in the C2S and C3S phases and forms C-S-H. The cement used for this research had a silicon oxide (SiO_2) content of 19.8 wt% (Table 3.2-1). Since a w/c ratio of 0.50 was used, this is equivalent to approximately 6.6 mol Si/L if all silicon were dissolved into the pore solution instead of forming solid hydration products. The silicon concentrations in expressed pore solution were found to be in µmol/L indicating that most of the silicon is used in the solid phase. At these low concentrations' measurements are more subject to error, especially as the chloride content in solution increases. A general trend can be observed where pore solution from pastes with admixed NaCl have higher concentrations of silicon than pastes with admixed $CaCl_2$ and $MgCl_2$ (Figure 4.1-24). When compared to the pore solution pH it can be seen that silicon concentrations increase with increasing pH (Figure 4.1-25).

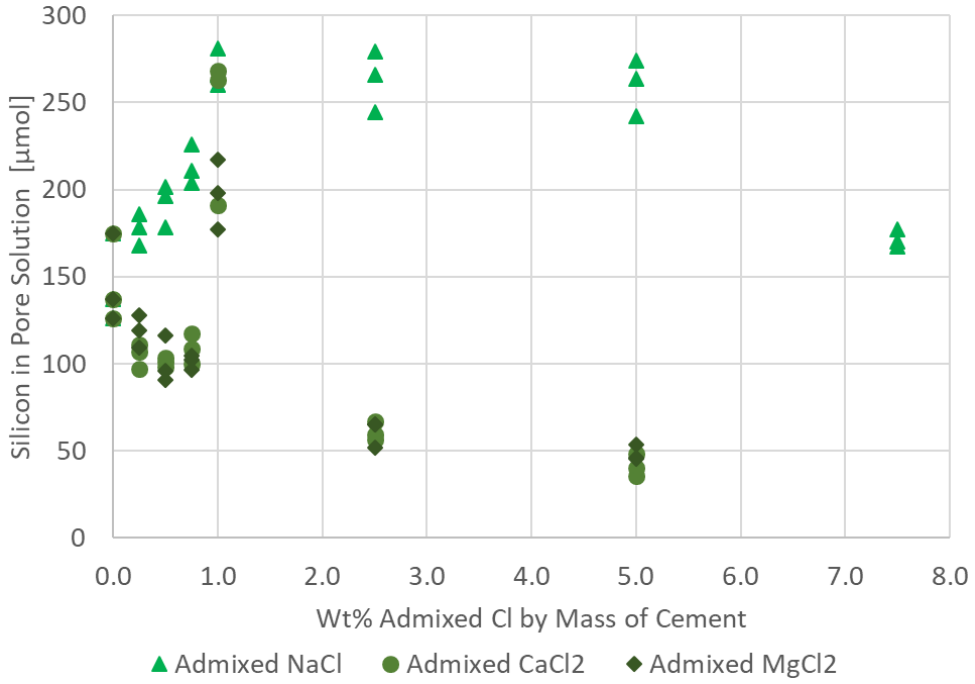

Figure 4.1-24: Si in expressed pore solution as a function of admixed Cl

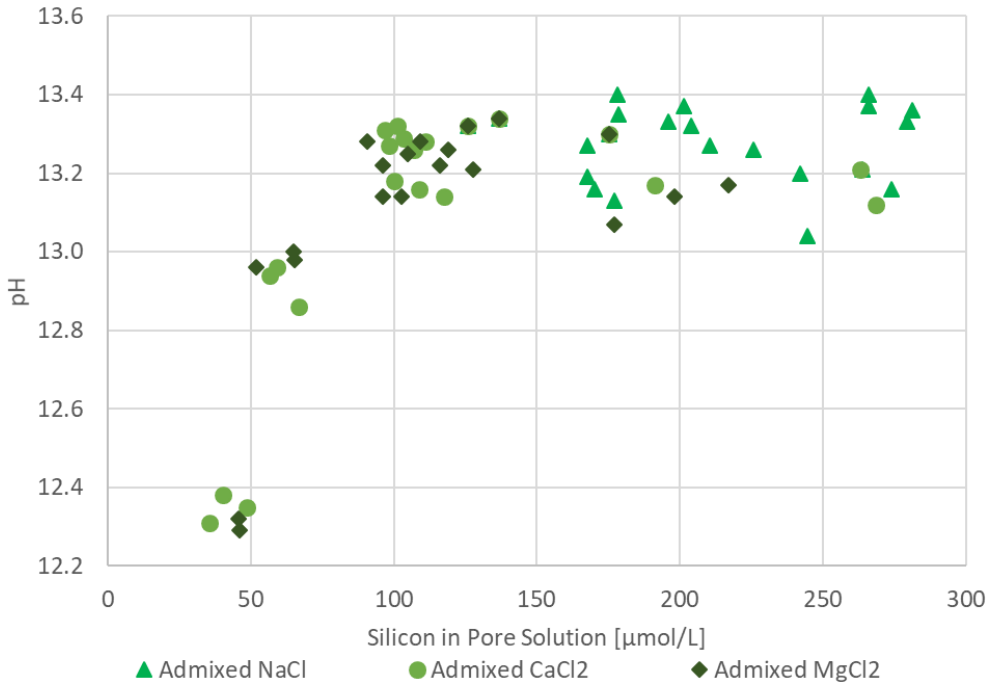

Figure 4.1-25: pH as a function of Si in the expressed pore solution

4.1.3.9 Sulphur (S) and Sulphate (SO_4^{2-})

Sulphate is introduced to cement as gypsum which reacts with the C3A and C4AF to form monosulphate (Afm) and ettringite (Aft) during hydration. The cement used for this research had a sulphur trioxide (SO_3) content of 3.40 wt% (Table 3.2-1). Since a w/c ratio of 0.50 was used, this is equivalent to approximately 0.6 mol SO_4^{2-}/L if all sulphate were dissolved into the pore solution instead of forming solid hydration products. The amount of sulphate in pore solution increased significantly with increased admixed chloride for pastes with NaCl (Figure 4.1-26) compared to pastes with $CaCl_2$ and $MgCl_2$ (Figure 4.1-27). Tests were performed on each sample to determine both the sulphur content (by ICP) and the amount of sulphur which formed sulphate since the types of sulphur in solution may have an impact rebar corrosion[74]. There was good agreement between sulphur and sulphate values for all expressed pore solutions except 5.00 wt% Cl pastes with admixed $CaCl_2$ and $MgCl_2$ (Figure 4.1-27), a trend that is expected to continue for 7.50 wt% Cl. Similar sulphate and sulphur concentrations indicate that the majority of sulphur in pore solution is in the form of sulphate. Sulphate concentrations do not appear to be influenced by pH (Figure 4.1-28, Figure 4.1-29).

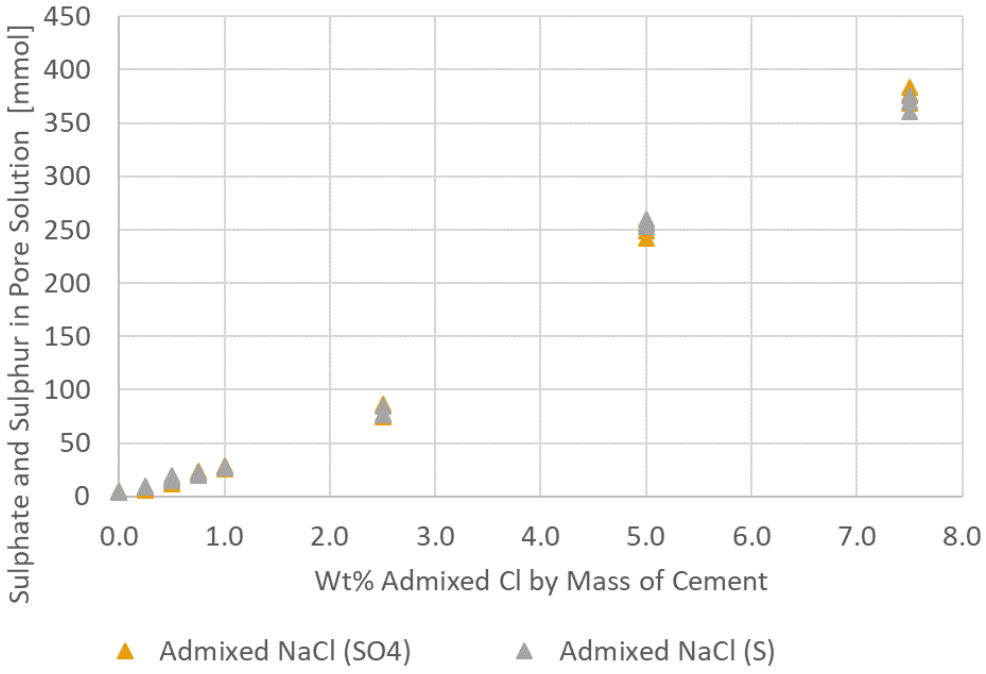

Figure 4.1-26: S and SO_4 in expressed pore solution as a function of admixed Cl (NaCl)

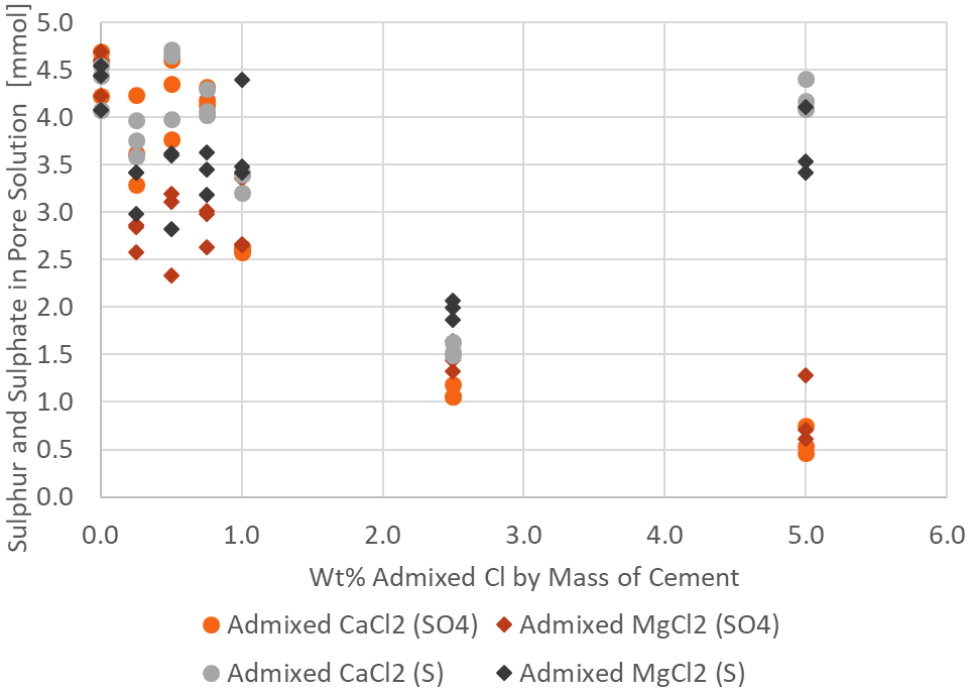

Figure 4.1-27: S and SO_4 in expressed pore solution as a function of admixed Cl ($CaCl_2$ and $MgCl_2$)

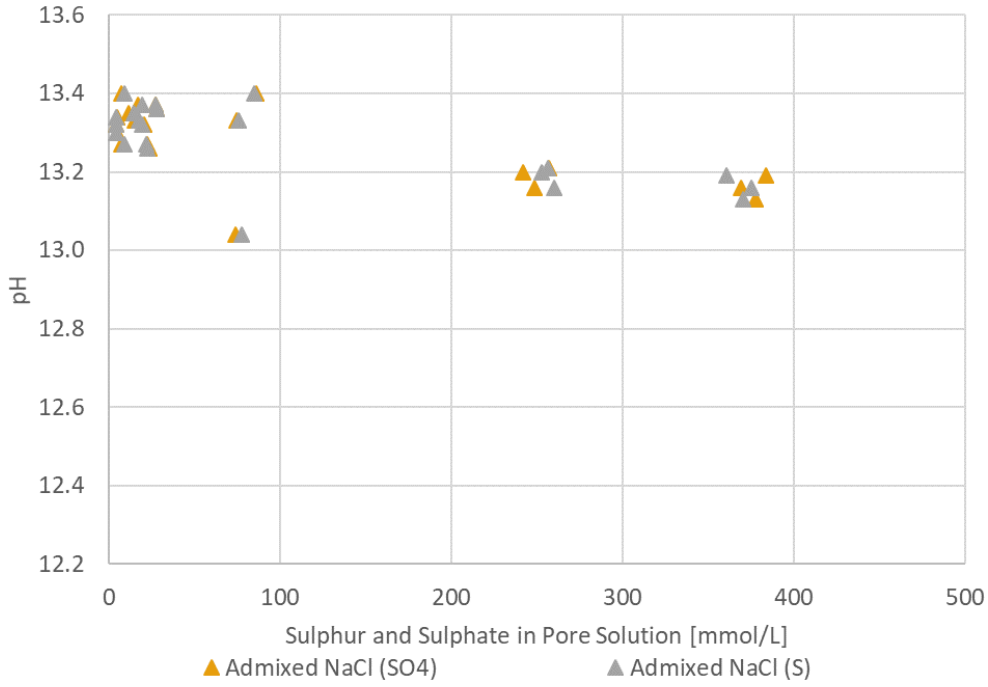

Figure 4.1-28: pH as a function of S and SO_4 in the expressed pore solution (NaCl)

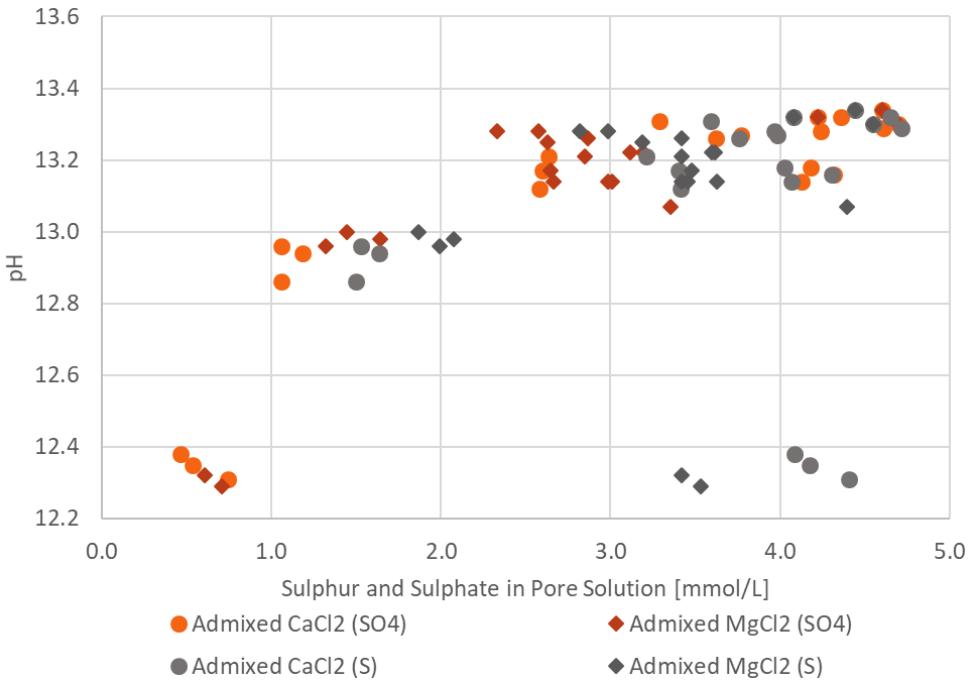

Figure 4.1-29: pH as a function of S and SO_4 in the expressed pore solution ($CaCl_2$ and $MgCl_2$)

4.1.4 Investigation of Cement Composition

XRD (Cu Kα) was used to investigate cement pastes containing 7.5 wt% admixed Cl by weight cement and compare to a chloride free paste. Insufficient pore solution was obtained for pastes with 7.50 wt% admixed chloride as $CaCl_2$ and $MgCl_2$ suggesting that more water was chemically bound in the cement or that sufficient precipitates formed to block liquid movement through pores. Possible precipitates include $Mg(OH)_2$ and calcium- or magnesium-oxychlorides, so XRD was performed on the pastes to compare with diffraction peaks found in literature. At the time of testing salt containing pastes were between 42 and 50 days old while the chloride free cylinder was 147 days old as specified in the next paragraph. Freshly demoulded cylinders containing 7.5 wt% Cl^- (NaCl, $CaCl_2$ and $MgCl_2$) and the chloride free cylinder were ground to a powder for the scan. Cracking in cylinders has been found to occur several days after demoulding (Section 4.1.2) so these results will only provide a partial explanation for the cracking but will be fairly representative of the cylinders when pore solution is being expressed.

The chloride-free cylinders were cast 147 days before XRD was performed while the 7.5 wt% Cl^- $CaCl_2$, $MgCl_2$ and NaCl cylinders were tested 42, 40 and 50 days respectively after being cast. Since cement continues to hydrate over a long time, albeit at a decreasing rate, this extra time could impact the results. A review paper by Vollpracht et al[62] which included elements expressed from CEM I cement with a 0.5 w/c reported that most elements in expressed pore solutions increased with increasing hydration but the mean values remained approximately constant between 10 to 500 days hydration. For this reason, comparison between all four sets of pastes in the current project are considered to be adequately representative.

An additional consideration when viewing the diffraction spectra is possible shifts in the peak angles. Small offsets can be caused by the XRD machine which would shift all peaks by the same amount but most shifts are due to differences in composition of the phases. Due to the heterogeneous nature of cement, the peaks were not adjusted to an expected 2θ value.

XRD curves are displayed in Figure 4.1-30 with the location of peaks for $Ca(OH)_2$, Aft and NaCl. These are the most distinct peaks present and represent hydration products that are definitely in the pastes. Friedel salt is also suspected to be in the 7.5 wt% Cl NaCl paste shown in Figure 4.1-30 and is denoted by an 'F'. Additional peaks may be the result of Afm, hydrocalumite, calcite, C-S-H, Friedel Salt or other compounds. Peaks for $Mg(OH)_2$, $CaCl_2$, $MgCl_2$ and oxychlorides were compared to the reference peaks and were not found to fit. The possible implications of the XRD scans are discussed in section 5.1.4. A detailed discussion of peaks that may or may not be possible matches to the experimental scans is provided in Appendix D. While some researchers have attributed peaks to C-S-H, it is a strongly amorphous or micro-crystalline phase which results in a very broad, shallow peak between 27° to 35° 2θ. Background noise due to low angle scattering was removed using dynamic beam optimization software built into the Bruker XRD system. In the uncorrected scan the hump for C-S-H was compared and no significant changes were observed (Appendix D).

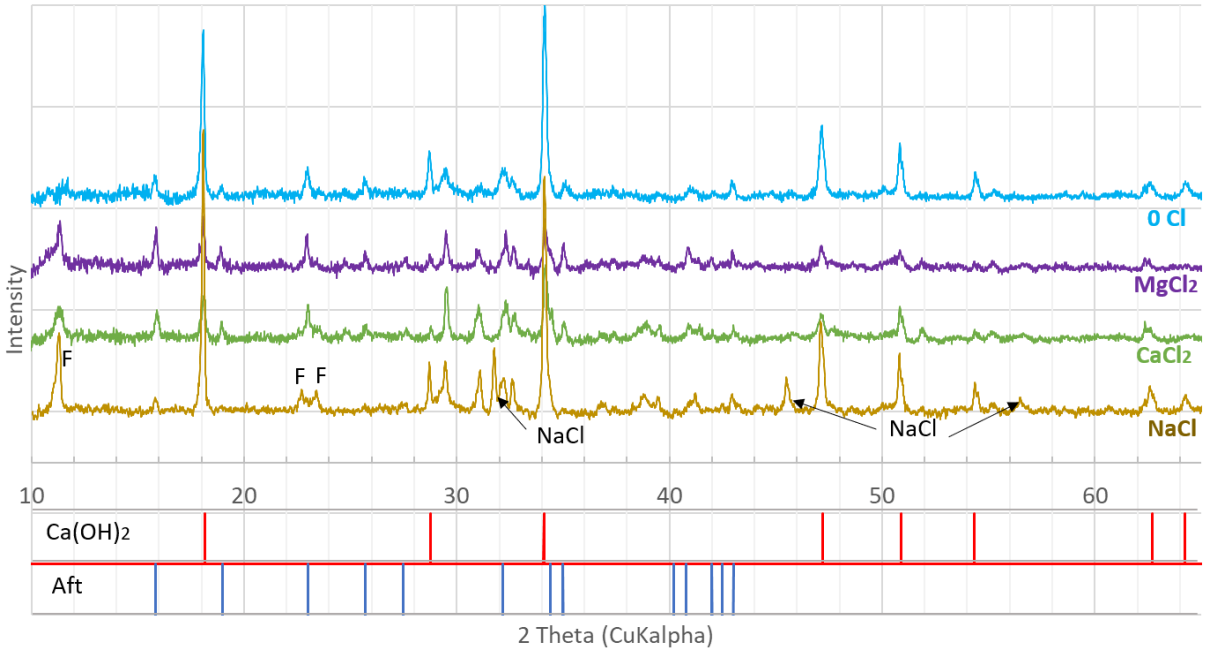

Figure 4.1-30: XRD scans of cement with 0 wt% Cl, 7.5 wt% Cl by weight of cement containing NaCl, $CaCl_2$ and $MgCl_2$ respectively where 'F' indicates Friedel's Salt, 'Aft' is ettringite and $Ca(OH)_2$ is portlandite.

4.2 Corrosion Tests in Synthetic Pore Solution

The corrosion tests were conducted in the different synthetic pore solution tests to investigate response of reinforcing bars to different environments and with chloride additions in the form of NaCl, $CaCl_2$ and $MgCl_2$. This section discusses the rebar specimens that were placed in synthetic pore solutions for a minimum of 17 weeks with salt being added each week to ensure the same chloride concentration increase in all solutions. The long duration of the tests resulted in issues with crevice corrosion under the lacquer at the ends of the bars, the extent of which varied between pore solution used. Some of the corrosion detected in electrochemical tests must then be attributed to the crevice corrosion, making the true corrosion behaviour difficult to determine for these specimens.

4.2.1 As Received Rebar

4.2.1.1 SEM Images

Samples from the two steel types were examined using SEM. It should be noted that the less conductive nature of the oxides which form mill scale can cause some distortion to the SEM image.

The surfaces of the two bars are irregular and rough, with type A being smoother. Both bars have sections of mill scale which have flaked off, as well as pin hole type openings in the remaining mill scale which are visible as dark spots in the SEM images. Note that the longitudinal rib has been included in the lower magnification images in Figure 4.2-1. A higher magnification of this rib was not possible due to the angle between this part of the sample and the secondary electron detector. The radial ribs were further investigated with locations being chosen on the top and the side of the ribs for higher magnification in Figure 4.2-2.

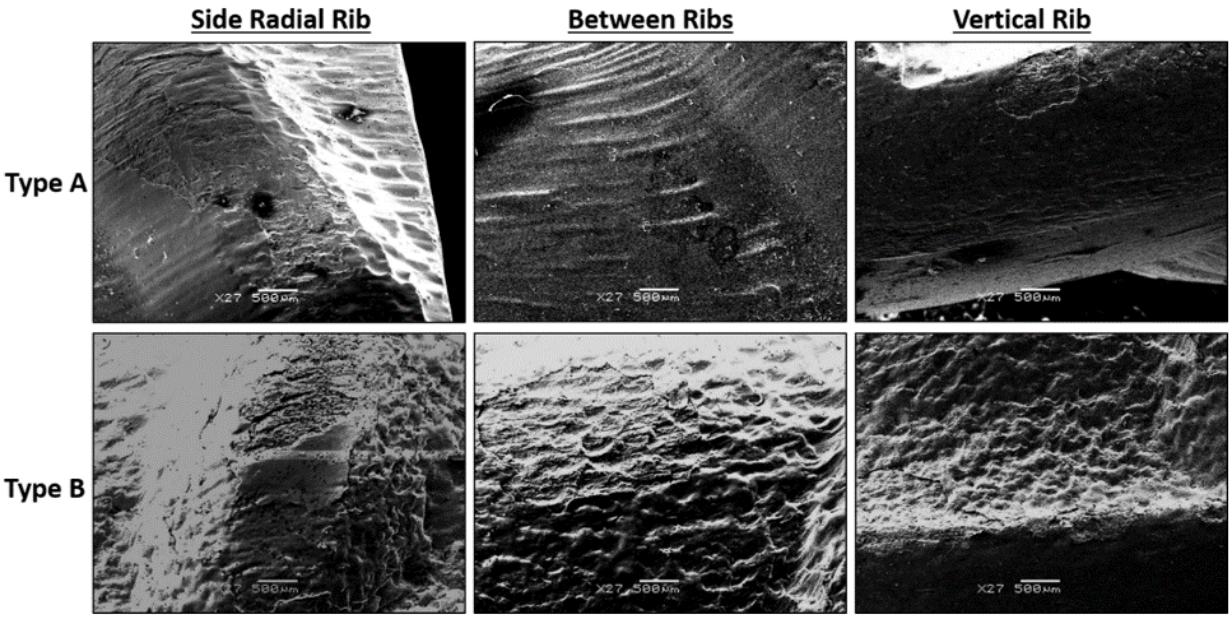

Figure 4.2-1: SEM images of rebar types A and B (lower magnification)

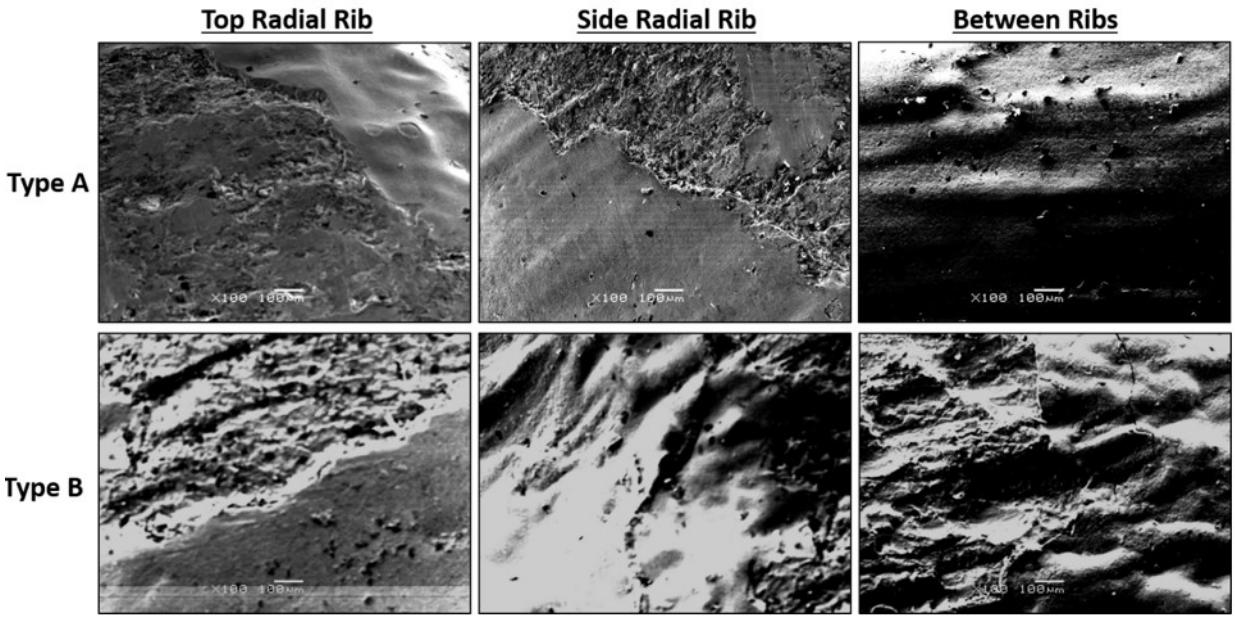

Figure 4.2-2: SEM images of rebar types A and B (higher magnification)

4.2.1.2 Rebar Microstructure

Microstructure was investigated in various locations near the longitudinal and radial ribs. There does not appear to be sufficient variation to explain differences in mill scale or corrosion performance at a given location or attribute differences to manufacturing. The microstructure of both Type A and Type B samples were internally consistent and appear to be quite similar as seen in Figure 4.2-3 where the light sections are composed of ferrite and the dark sections are pearlite.

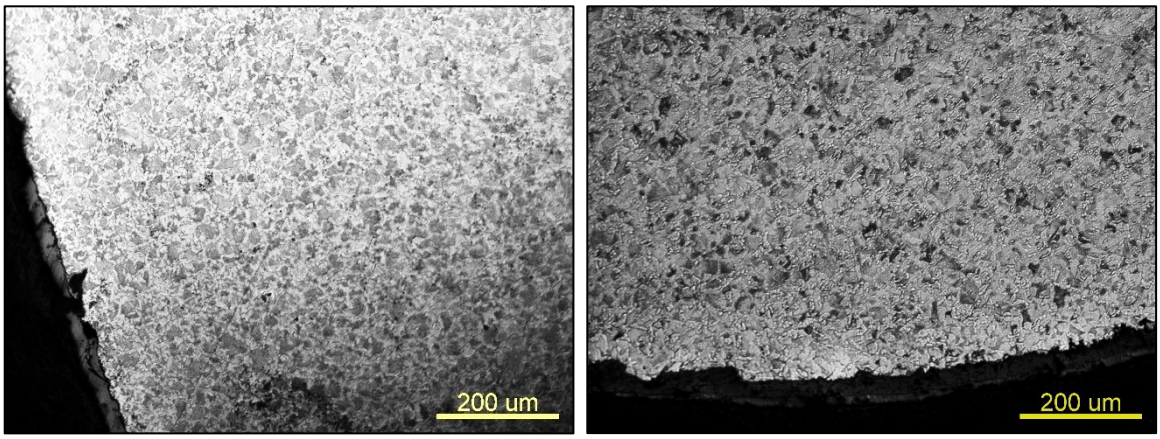

Figure 4.2-3: Microstructure of steel type A (left) and type B (right) at 100x magnification

Microscope images (Figure 4.2-4 and Figure 4.2-5) show the variation in mill scale quality and the presence of cracks which would allow solution to penetrate to the steel surface and initiate corrosion. These defects were also observed in the above SEM images.

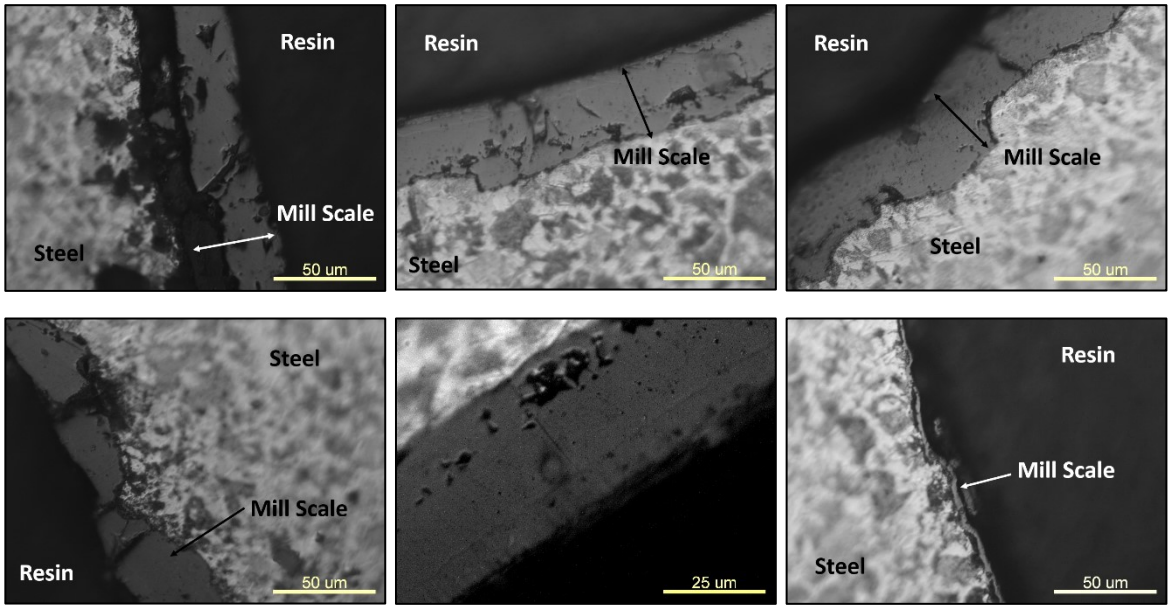

Figure 4.2-4: Mill scale observed at 500x magnification and 1000x magnification on steel type A

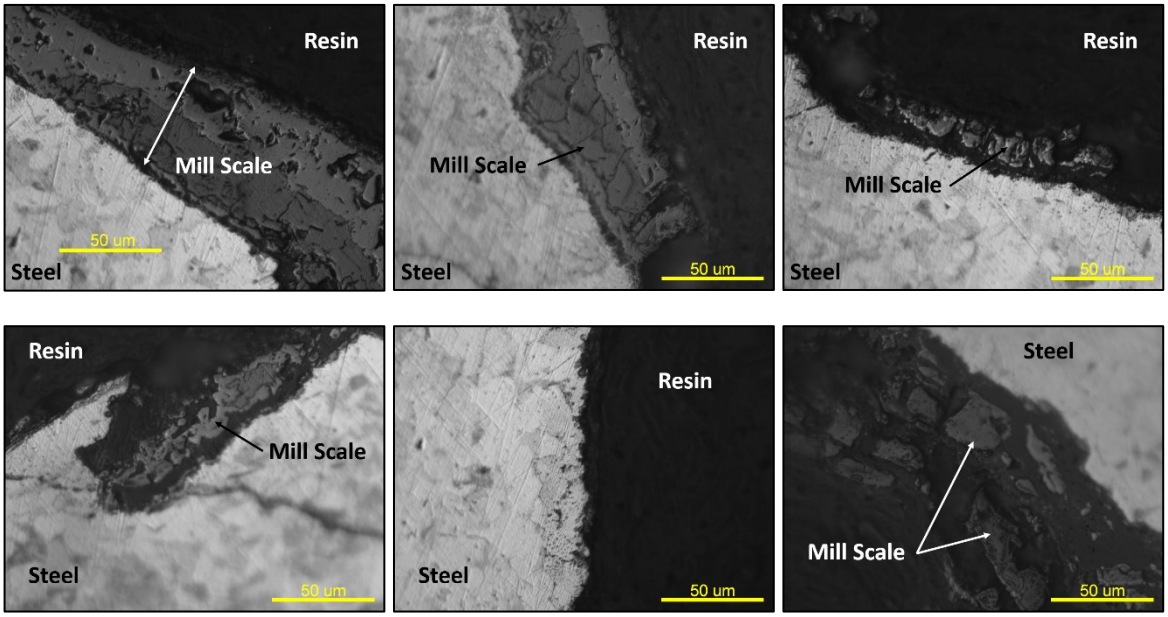

Figure 4.2-5: Mill scale observed at 500x magnification on steel type B

The mill scale for steel type B was found to be more discontinuous with cracking and porosity observed. Another interesting aspect is the two-toned coloring of the mill scale which indicates differences in composition.

4.2.2 Synthetic Pore Solution pH with Admixed Chloride

The addition of $CaCl_2$ or $MgCl_2$ salts to cement decrease the pH of expressed pore solutions. It is reasonable that a similar phenomenon would occur in synthetic pore solution (SPS) due to the formation of the precipitates $Ca(OH)_2$ and $Mg(OH)_2$. All SPS used in this section were made fresh and pH was sampled over several hours. This allowed for comparison between all SPS and synthetic expressed pore solution (SEPS) where calibration, potential carbonation from contact with air and temperature were controlled. The pH was checked using the same hand-held pH probe used to measure pH in expressed pore solution (section 4.1.1). The pH and temperature were recorded with salt equating to approximately 0.20 wt% Cl added incrementally every half hour until 1.00 wt% Cl by weight of solution was reached. NaCl was added to the $CaOH_2$, ASTM, and Tri-hydroxide solutions. To understand the effect of the salts, NaCl, $CaCl_2$ or $MgCl_2$ were added to SEPS along with corresponding amounts of $CaSO_4$. The solutions were allowed to settle for 30 minutes between the addition of salt and measuring of pH. Calibration of the pH meter with 4, 7 and 10 pH buffers was performed before each set of pH measurements. Synthetic pore solutions used are specified in Table 4.2-1 (next page) and the exact compositions are available in Table 3.3-1.

Table 4.2-1: Abbreviations for synthetic pore solutions

ASTM	ASTM A955 guideline for St.St Rebar, admixed NaCl Contains: *KOH, NaOH*
CH	Saturated Calcium Hydroxide, admixed NaCl Contains: $Ca(OH)_2$
TH	Tri-hydroxide Pore Solution, admixed NaCl Contains: $Ca(OH)_2$, *KOH, NaOH*
SEPS	Synthetic expressed pore solution based on 0.5 w/c GU Contains: $Ca(OH)_2$, *KOH, NaOH,* $CaSO_4$ *(corresponding to salt type used)*

The pH of synthetic pore solutions prior to the addition of chlorides can be calculated based on $[OH]^-$ of the components. These calculated pH values were compared with measured values which reveals an increasing discrepancy as the pH of solution increased suggesting clear pH drift as shown in Figure 4.2-6.

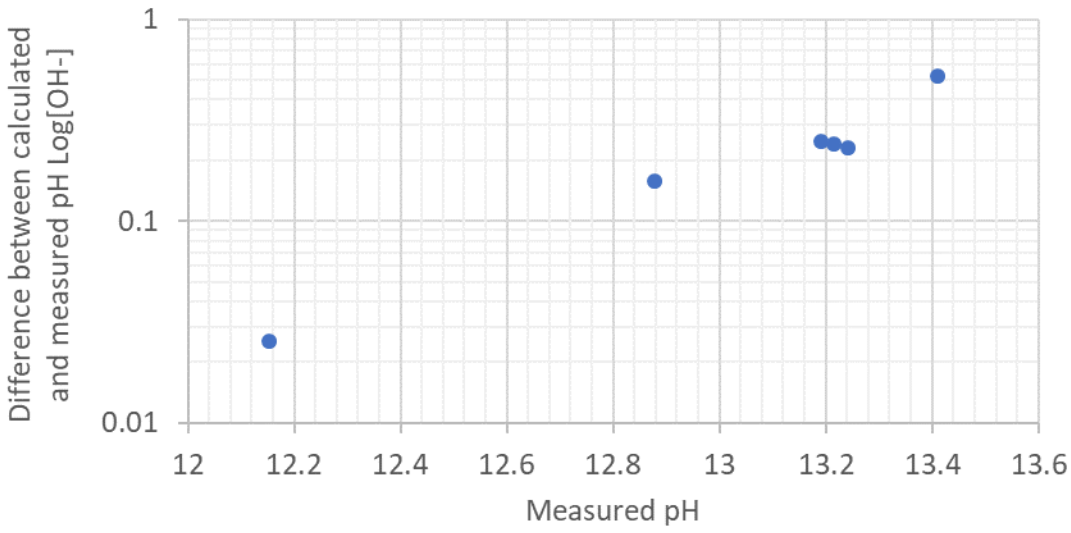

Figure 4.2-6: Difference between measured and calculated pH of synthetic pore solutions

An adjustment was made to all pH measurements by calculating the [OH^-] difference between the measured and calculated values of each chloride SPS and SEPS then adding this difference to all subsequence measurements in the respective solutions since the effect of the respective chlorides is unknown. Since the discrepancy between measured and calculated values is much larger in the higher pH solutions this method over corrects for the SEPS with admixed $CaCl_2$ and $MgCl_2$ salts since the measured pH decreases significantly with salt addition. The corrected pH measurements with admixed salt are shown in Figure 4.2-7 on the next page. Given the trends in the measured values it is expected that the SEPS with 0.80 wt% added Cl^- by weight of solution containing CaCl2 and MgCl2 would be closer to 13.4. Similarly using Figure 4.2-6 as a guideline the pH for these two solutions with 1.00 wt% Cl^- would be approximately 13.2.

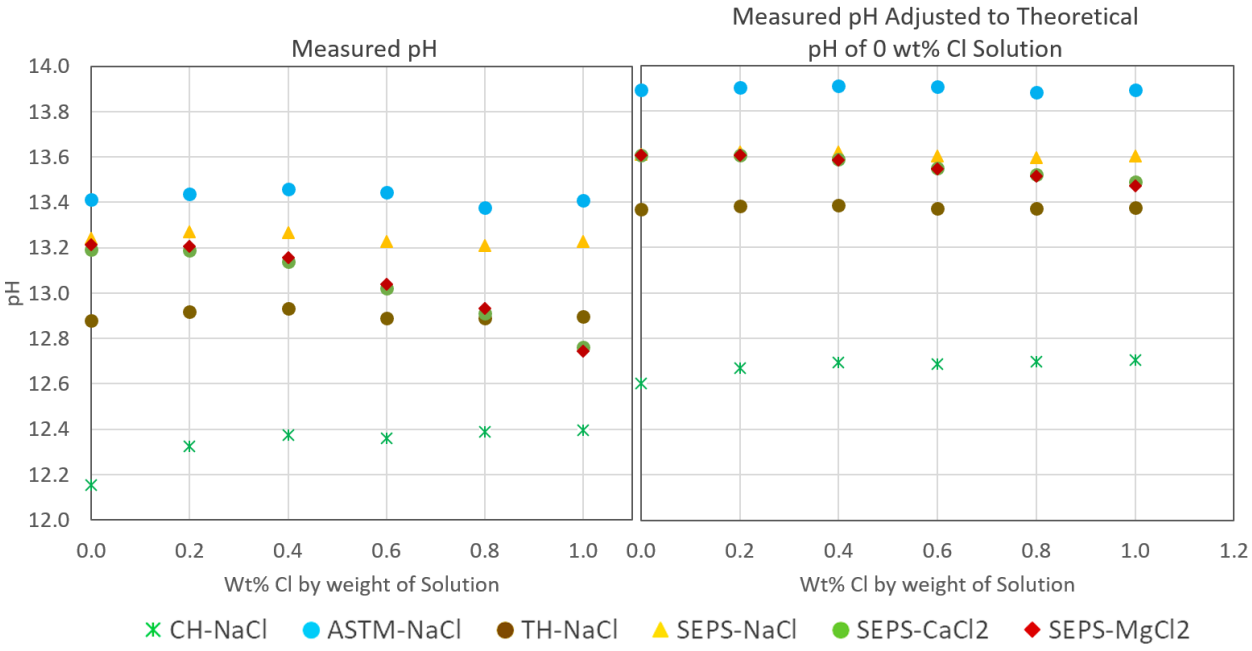

Figure 4.2-7: pH of synthetic pore solutions with admixed chloride as measured (left) and after correction (right)

4.2.3 Electrochemical Results

The electrochemical testing employed for this research can not identify the location or extent of individual corrosion pits. Instead tests indicate the average current or potential over the rebar surface.

This presents an issue when crevice corrosion, which is not representative of normal corrosion behaviour, occurs between the lacquer and a sample. The second set of pore solution specimen experienced extensive crevice corrosion such that only two specimens were completely unaffected. Due to the crevice corrosion experienced by specimens in the TH2 solution, as well as all SEPS with admixed NaCl, $CaCl_2$ or $MgCl_2$ there were insufficient unaffected specimen to be statistically significant. Due to difficulty viewing the entirety of specimens while in the pore solutions it is impossible to identify the chloride concentration where crevice corrosion became an issue for these specimens. The type B rebar (2 specimens in each container in the second set) was found to be initially more resistant to corrosion than type A (Figure 4.2-8).

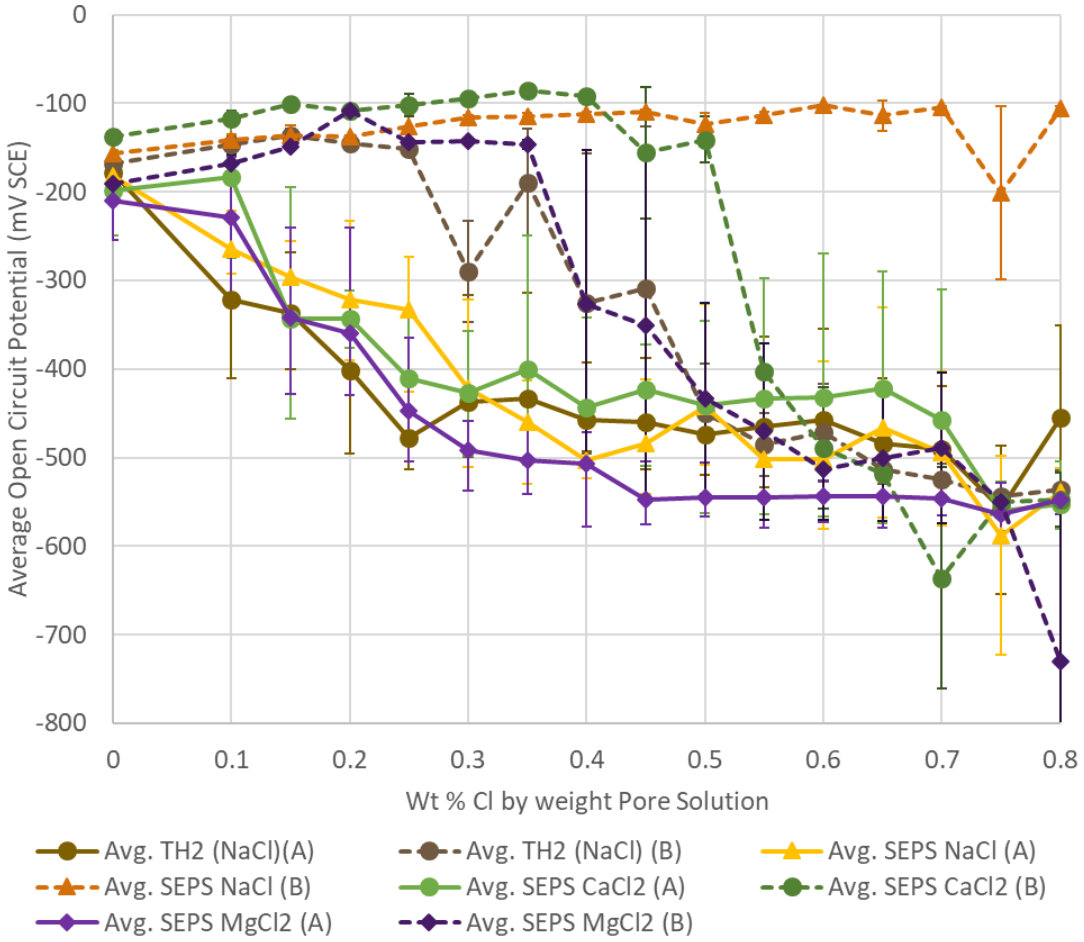

Figure 4.2-8: Half cell potential of rebar type A (3 replicates per solution) and type B (2 replicates per solution). The maximum and minimum values encountered are indicated by error bars.

Laboratory temperature is higher when winter heating is switched on. Since the experiments were conducted in different winters the Tri-hydroxide pore solution was used both times as a control. For the type A rebar (3 specimens in each container in the second set) the half cell potential of specimens was found to be very similar, while the type B rebar was found to be initially more resistant to corrosion (these have been shown in Figure 4.2-9 for clarity). However, as discussed in section 4.2.5, visual inspection ultimately revealed less corrosion on the rebar surface of specimens from the second set of Tri-hydroxide.

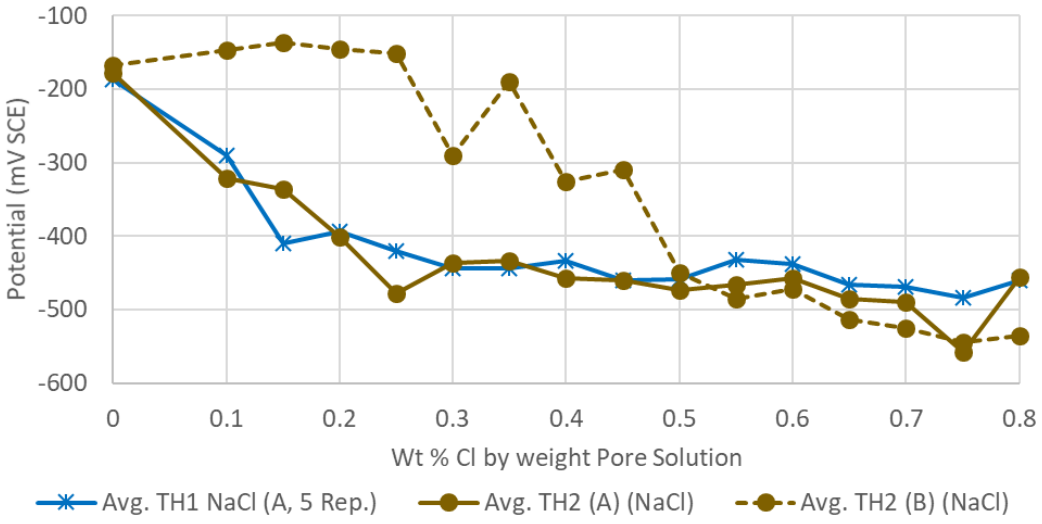

Figure 4.2-9: Half cell Potentials of Specimen in Tri-hydroxide Pore Solution exposed to NaCl

When corrosion occurs, the open circuit potential is expected to become more negative while the corrosion current density is expected to increase relative to initial values. This trend is generally observed in the experimental results but cannot be directly attributed to corrosion performance due to the inability of this measurement technique to track individual instances of corrosion on the surface. LPR and half cell Potential readings provide one value which is essentially an average of the electrochemical activity on the exposed surface of the rebar specimen. A bar that has general corrosion on most of its surface may have similar results to a specimen with a smaller area of pitting corrosion or crevice corrosion. The results in Figure 4.2-10 and Figure 4.2-11 indicate that the least corrosive environment is the ASTM synthetic pore solution which has the most positive OCP and lowest i_{corr} corroborated by visual inspection. The next best

synthetic pore solutions are the SEPS with added NaCl and $CaCl_2$. The tri-hydroxide solutions have the next lowest i_{corr} values but there is overlap with specimens in the saturated $Ca(OH)_2$ solution. The highest i_{corr} was consistently found in the SEPS $MgCl_2$ specimens despite higher OCP values compared to specimens in the first tri-hydroxide solution and the saturated $Ca(OH)_2$ solution however this may be the result of significant crevice corrosion on $MgCl_2$ specimens. As mentioned in section 4.2.6 crevice corrosion on specimens in the SEPS's and TH2 may affect the values in the figures below.

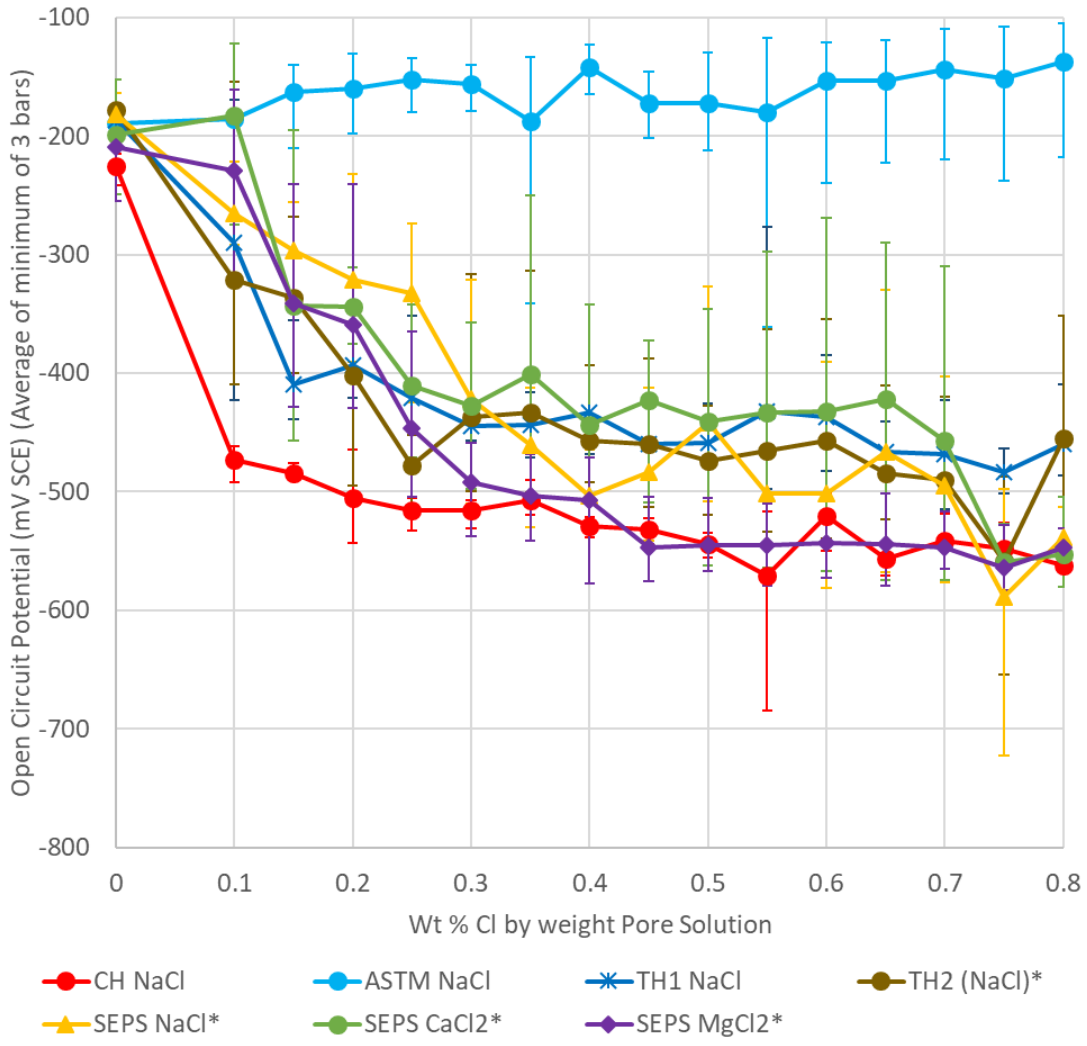

*Figure 4.2-10: Average Open Circuit Potential (OCP) of type A rebar in each solution, where * denotes the average of 3 rebar specimen while the CH, ASTM and TH1 are the average value of 5 rebar specimen. The maximum and minimum values encountered are indicated by error bars.*

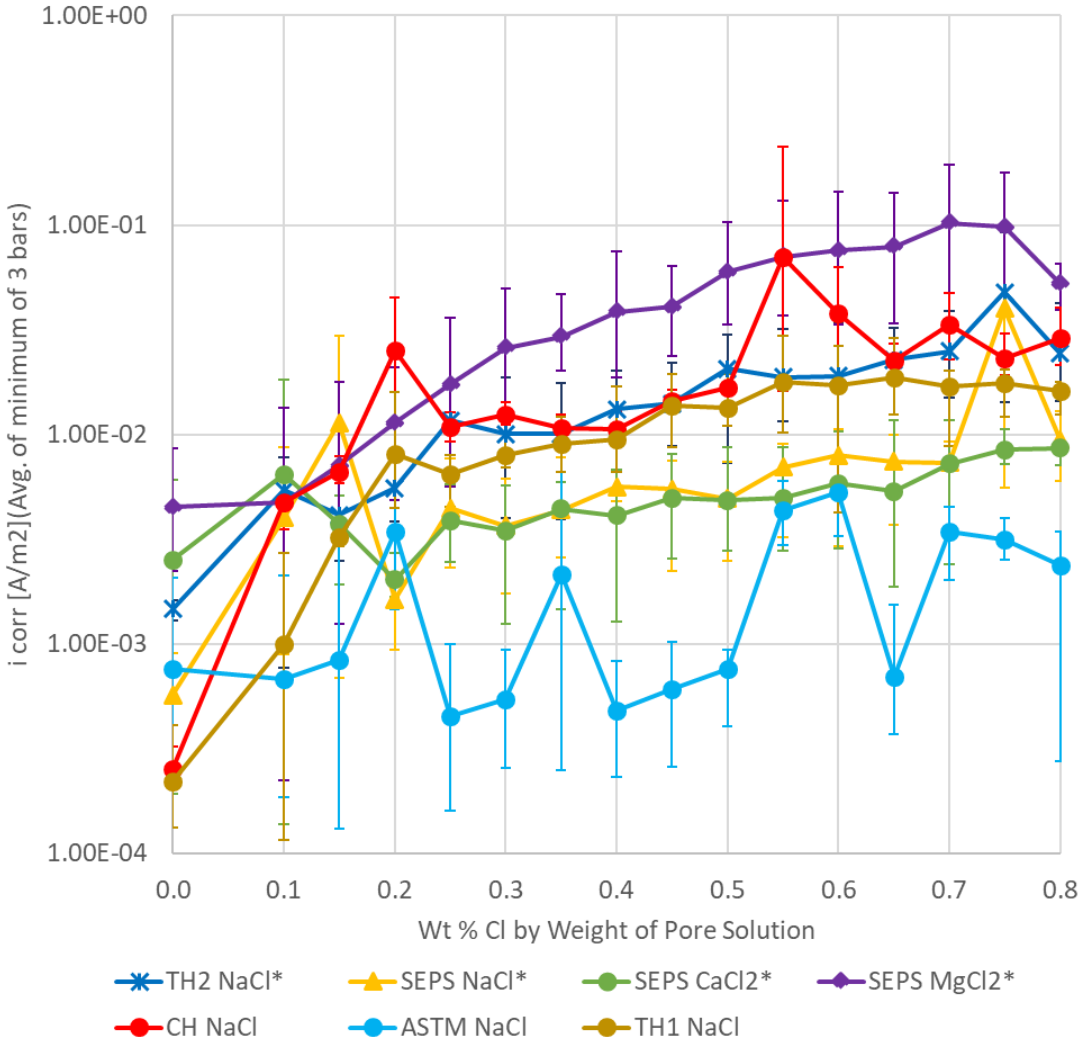

*Figure 4.2-11: Average Corrosion Current Density (i_{corr}) of type A rebar in each solution, where * denotes the average of 3 rebar specimen while the CH, ASTM and TH1 are the average value of 5 rebar specimen. The maximum and minimum values encountered are indicated by error bars.*

4.2.4 Mass loss

Mass loss was calculated using Faraday's law of electrolysis by calculating the area under the curves of icorr vs. time (Figure 4.2-11). All specimens have been included in Table 4.2-2 but, as discussed in the above section, specimens in the Tri-hydroxide solution (2), and SEPS with admixed NaCl, $CaCl_2$ and $MgCl_2$ were significantly impacted by crevice corrosion causing an over estimation of mass loss in the exposed bars. The mass loss has been plotted versus the initial pH of solutions in Figure 4.2-12.

Table 4.2-2: Calculated Mass Loss for Pore Solution specimens.

Sat'd $CaOH_2$			ASTM Std.			Tri-hydroxides (1)			Tri-hydroxides (2)		
ID	**Coulombs**	**Mass loss (g)**	**ID**	**Coulombs**	**Mass loss (g)**	**ID**	**Coulombs**	**Mass loss (g)**	**ID**	**Coulombs**	**Mass loss (g)**
06	194597	56.32‡	**03**	25163	7.28	**01**	99399	28.77	**11**	166291	48.12
10	145860	42.21‡	**05**	19679	5.69	**02**	111523	32.27	**24**	215134	62.26‡
13	216936	62.78‡	**17**	14654	4.24	**04**	117593	34.03	**28**	89100	25.79‡
15	141517	40.95‡	**19**	15024	4.35	**07**	100449	29.07	**30**	65189	18.87‡
16	285117	82.51‡	**20**	15696	4.54	**18**	92462	26.76	**32**	63671	18.43‡

SEPS-NaCl			SEPS-$CaCl_2$			SEPS-$MgCl_2$		
ID	**Coulombs**	**Mass loss (g)**	**ID**	**Coulombs**	**Mass loss (g)**	**ID**	**Coulombs**	**Mass loss (g)**
08	122778	35.53‡	**09**	78117	22.61‡	**14**	805242	233.03‡
22	74225	21.48‡	**12**	37440	10.83‡	**21**	244873	70.87‡
26	30529	8.83‡	**23**	29476	8.53‡	**25**	191998	55.56‡
27	8964	2.59	**31**	20430	5.91‡	**29**	732273	211.92‡
34	8833	2.56	**33**	13144	3.80‡	**35**	292944	84.78‡

‡ Specimen with crevice corrosion on at least one end

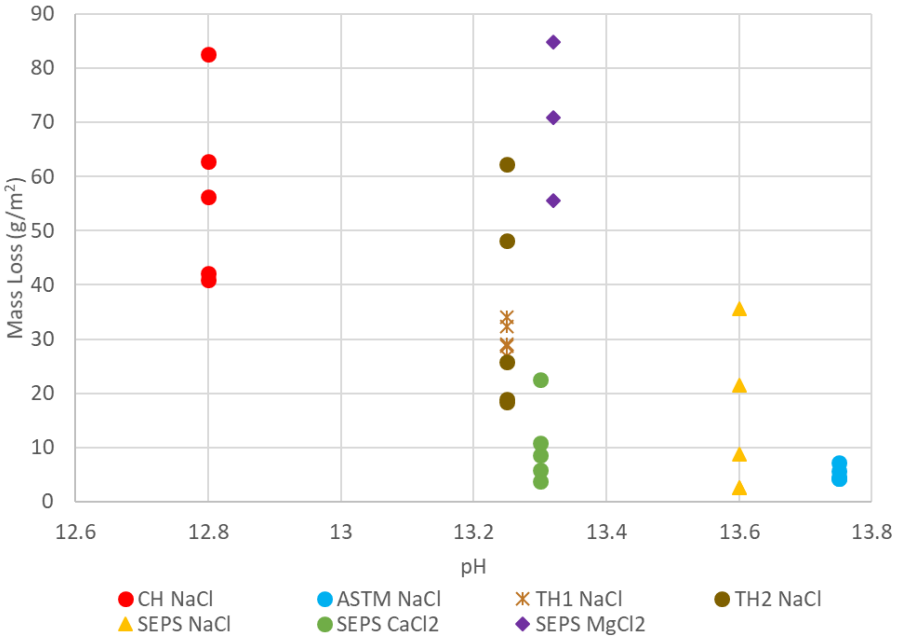

Figure 4.2-12: Calculated annual mass loss of rebar specimen in pore solution versus the pH of salt free solutions

Mass loss in the saturated calcium hydroxide solution was significantly higher, and less consistent between specimen, than the other solutions. This can be attributed to lower pH which produced the deep pits observed on the bars in the $CaOH_2$ solution and the fact that some specimens had no pits while other specimens may have had one or more. The high mass loss values for SEPS $MgCl_2$ specimens is likely due to the formation of large volumes of corrosion products due to crevice corrosion. These large volumes of corrosion were observed after removing the rebar samples from solution and would have contributed to the electrochemical measurements used to calculate the mass loss.

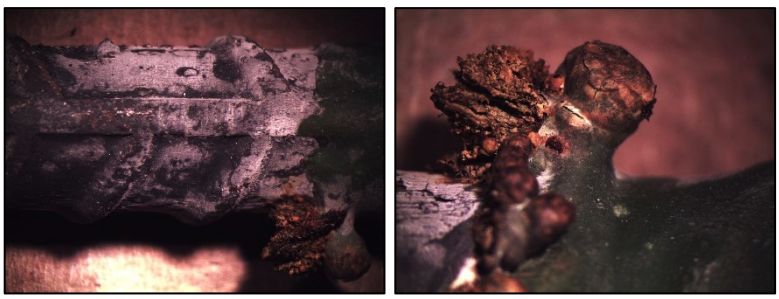

Figure 4.2-13: Crevice corrosion on Sample 21 after removal from SEPS (MgCl2) illustrating the large volume of corrosion products formed.

4.2.5 Visual Inspection of Corrosion

To verify the electrochemical results discussed in Sections 4.2.3 and 4.2.4, each rebar specimen was examined after removal from the respective SPS. Rebar specimens were visually examined and low magnification optical images were taken. Specimen were then pickled using a 30 vol% HCl solution to remove corrosion products and further optical images were taken.

Corrosion of the bars in the saturated $Ca(OH)_2$ solution resulted in deep pits located between ribs with corrosion products extending directly out from the surface. Additional areas with small pits were also observed, with corrosion concentrated between the ribs. While the pitting corrosion that occurred was severe, there were large sections of the exposed area of each specimen where no corrosion occurred. Corrosion may initiate at locations where the mill scale has cracks or similar types of irregularities however these irregularities are not visible to the naked eye as seen in Figure 4.2-14 where corrosion initiated in a seemingly continuous section of rebar. This would result in the surrounding area becoming cathodic accounting for the absence of corrosion in these locations.

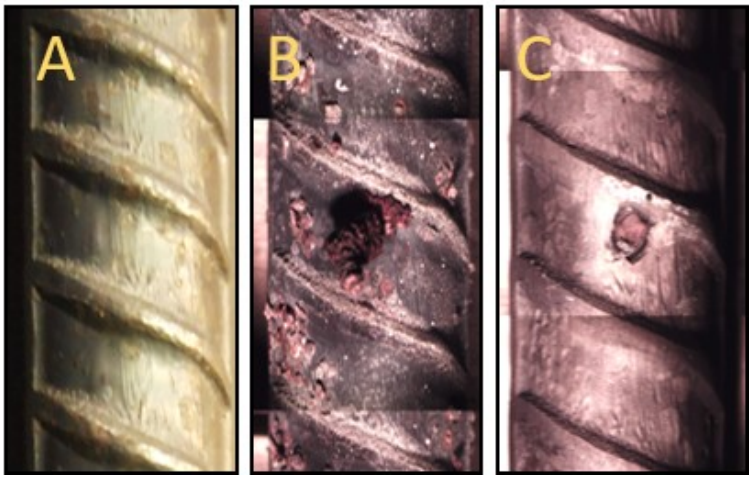

Figure 4.2-14: Specimen 06 a) prior to immersion in SPS, b) after removal from CH SPS, c) After pickling

Corrosion in the tri-hydroxide solution was focused in areas that had good mill scale coverage. In the first set of specimens, small pits were found on the majority of the specimen surface, with no

discrimination between ribs or inter-rib locations. Corrosion of the second set of tri-hydroxide pore solution specimens was found to be less prolific. However, the initial mill scale coverage was less complete than in earlier specimens and corrosion was found to occur at surfaces where mill scale was present rather than at the bare steel surface. Specimens 1 and 24 from the first and second sets of tests, respectively, show this trend in Figure 4.2-15. Corrosion on Specimen 24 occurred in areas with good mill scale coverage.

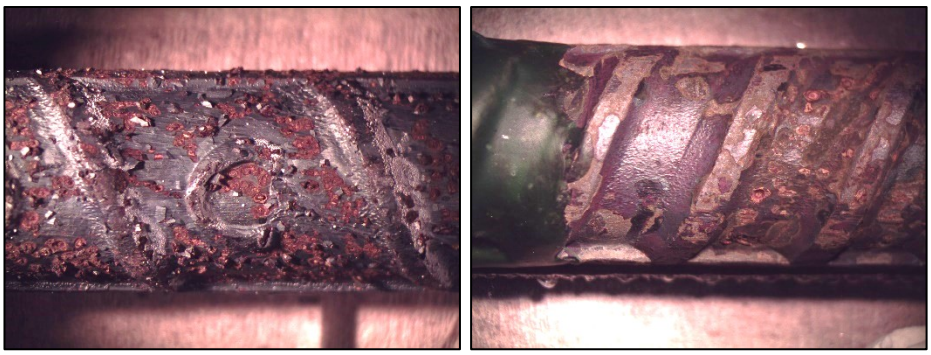

Figure 4.2-15: Corrosion of bars 01 (left) and 24 (right) after removal from tri-hydroxide synthetic pore solution with 0.80 wt% admixed Cl (NaCl) by weight solution

The least amount of corrosion was observed on specimens in the ASTM solution although the mill scale was observed to be much darker than the surface of other specimens as shown in Figure 4.1-15. Where corrosion occurred in all solutions, the mill scale was pushed up by corrosion and came away in small flakes.

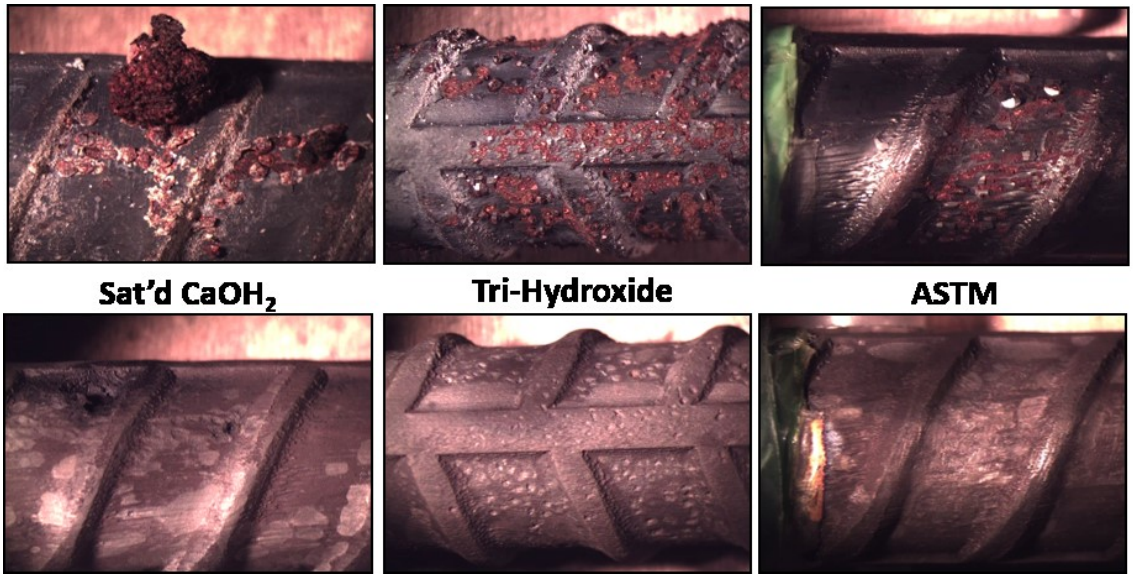

Figure 4.2-16: Rebar exposed to NaCl in Saturated $Ca(OH)_2$, Tri-hydroxide and ASTM solutions before (top) and after pickling (bottom)

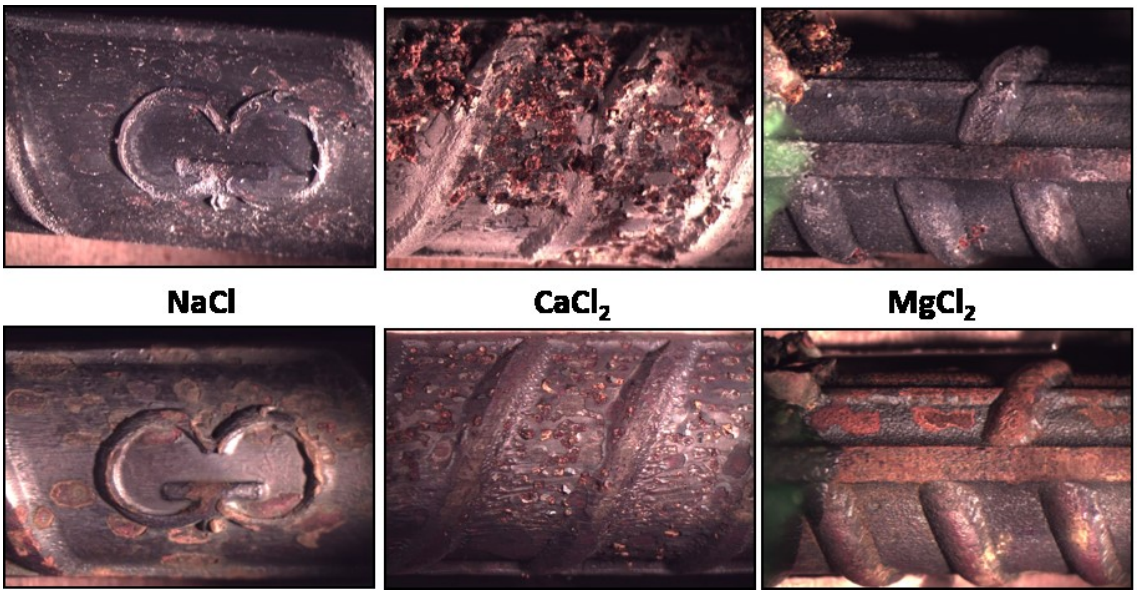

Figure 4.2-17: Rebar exposed to NaCl, $CaCl_2$ and $MgCl_2$ in Synthetic expressed pore solution (SEPS) before (top) and after pickling (bottom)

Bars tested in the synthetic expressed pore solutions (SEPS) based on the results of pore expression are shown in Figure 4.2-17 above. In the solution containing NaCl, only one specimen was found to have

significant amounts of corrosion on the exposed surface (shown in Figure 4.2-18 below) although crevice corrosion was observed for three of the five specimens, accounting for all type A rebar in. Pickling revealed some areas of discolouration which suggest localized environments formed between the mill scale and the steel surface. This is evident for the specimens exposed to NaCl and $MgCl_2$ in Figure 4.2-17 above.

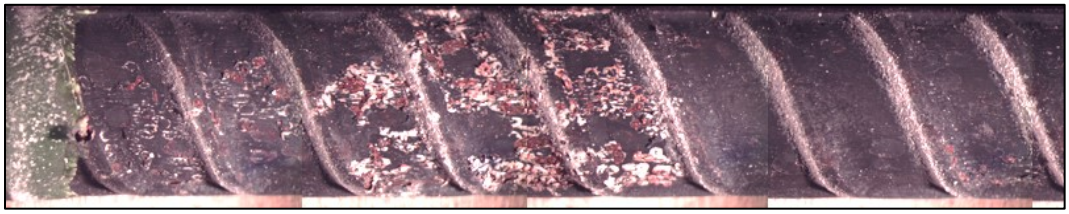

Figure 4.2-18: Example of corroded rebar on specimen 26 from NaCl SEPS

Corrosion of bars in solution with added $CaCl_2$ was found to be more severe than that of bars in the NaCl SEPS, but individual Specimens experienced very different levels of corrosion. The relatively severe corrosion shown in Figure 4.2-17 was only found on small portions of most bars, occurring between 2 or 3 ribs with the exception of specimen 23 which had corrosion on approximately 60% of the bar.

Corrosion of bars in the pore solution containing $MgCl_2$ was inconsistent between specimens making it difficult to compare to other specimen from other SPS. Specimen had varying amounts of small pitting corrosion and general corrosion as seen on pickled bars in Figure 4.2-19. The location of corrosion also varied with some specimens having the most corrosion near the top while other specimens had more corrosion near the bottom of the bar.

Crevice Corrosion was a significant issue for specimen in TH2 and the three SEPS as shown in Figure 4.2-19 and will be discussed further in Section 4.2.6. Expansive corrosion products were found under the lacquer with varying severity. Two specimens from the SEPS $MgCl_2$ solution are included due to the large variability between specimens. In some cases, the presence of crevice corrosion has resulted in much less corrosion on the exposed bar, However, as can be seen on SEPS $MgCl_2$ 25 this was not always the case.

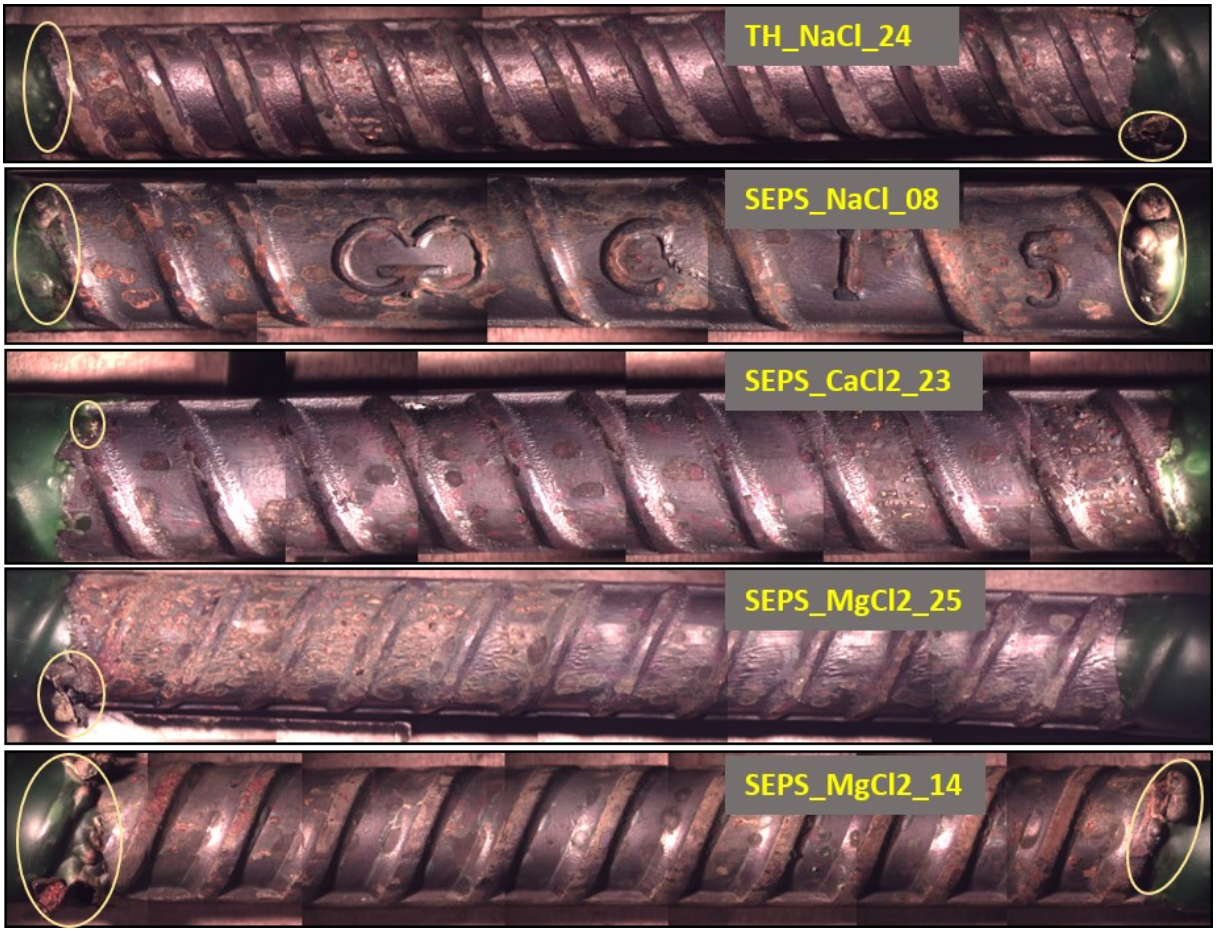

Figure 4.2-19: Specimen from the TH2 SPS and SEPS with added NaCl, $CaCl_2$, and $MgCl_2$. After pickling. Crevice corrosion is circled.

Corrosion of many specimens initiated under the mill scale and can be seen pushing mill scale away as the corrosion products propagated outwards as shown below. Flaking of mill scale around growing corrosion products occurs in all pore solutions with some examples shown in Figure 4.2-20 below.

Figure 4.2-20: Corrosion on specimens in (L to R) the tri-hydroxide(NaCl), SEPS with $CaCl_2$ and in the ASTM solution (NaCl) before pickling

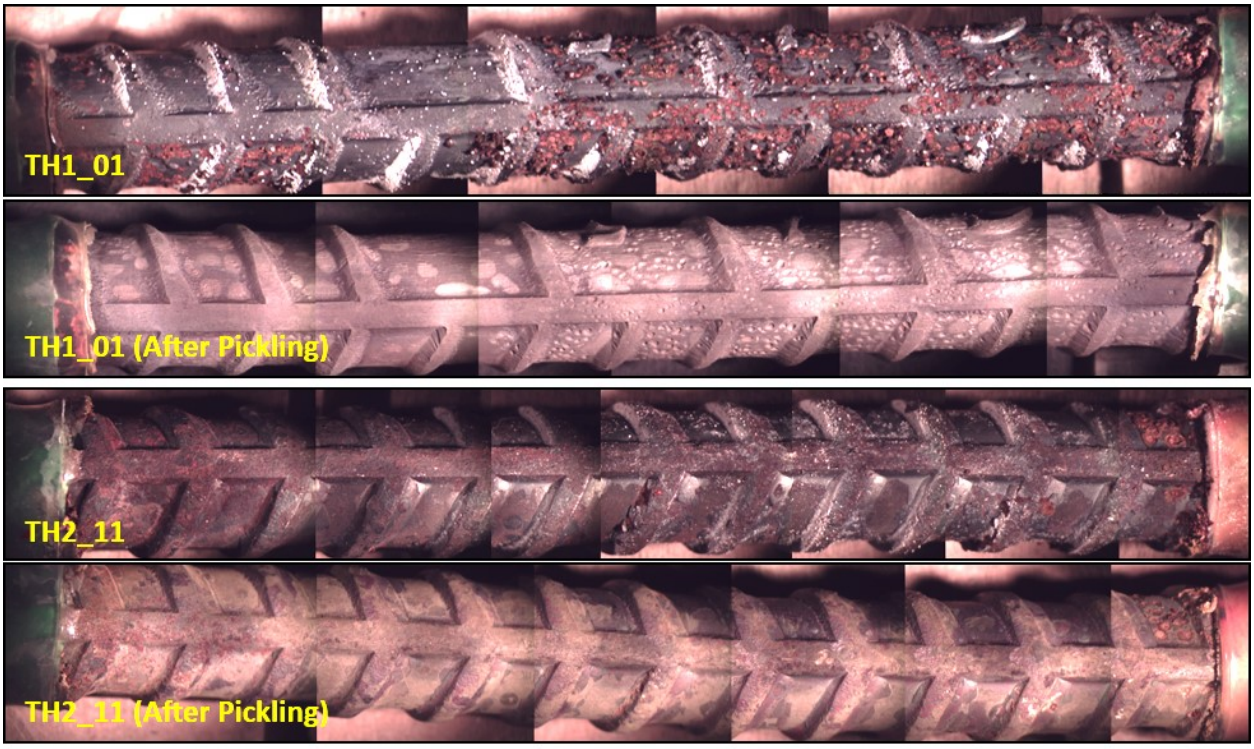

Figure 4.2-21: Comparison of Corrosion on specimens in TH1 SPS (top two) and TH2 SPS (bottom two)

This was especially apparent for specimen in the second TH SPS which was used as a control. Small pits that covered most of the surface of specimen in the first TH SPS were much less frequent on specimen in the second TH SPS as shown in Figure 4.2-21. However, the specimen in the second pore solution also had less mill scale coverage with more areas of bare steel which is thought to be a factor.

4.2.6 Crevice Corrosion

The application of the lacquer used to protect the ends of the specimen was insufficient to prevent crevice corrosion over the 17-week testing period. Two methods of application were undertaken. Initially three layers of lacquer were applied to each specimen. Heat shrink tubing was then used over the lacquer but corrosion occurred despite these measures. Imperfections at the edge of the lacquer were thought to contribute, in the second method lacquer was applied such that it followed along the diagonal and vertical ribs tightly and a 4th layer of lacquer was applied. Unfortunately, corrosion still initiated under the lacquer resulting in significant crevice corrosion, examples of which are shown in Figure 4.2-22 below where the

lacquer can be seen stretched over corrosion products. This has an impact on both the electrochemical results as well as the mass loss calculations since LPR values are an average from activity over the entire bar.

Crevice corrosion is a well-known issue for this type of testing. Examination of specimens show a clear trend of corrosion initiating under the lacquer then expanding and pushing mill scale and lacquer away as corrosion products form as in (Figure 4.2-22). Additionally, upon pickling, corrosion is found beneath the mill scale, usually visible as circles as seen for many of the specimens in Figure 4.2-16 and Figure 4.2-17. This indicates that pore solution can easily move through the loose sections of mill scale and travel in the space next to the steel surface which would not be blocked by the lacquer. To minimize crevice corrosion, it may be necessary to completely remove mill scale from the sections where lacquer is desired. While the entirety of mill scale at the end could be removed it is more likely that it is only necessary to remove enough mill scale to disrupt the transfer of liquid to the area under the lacquer.

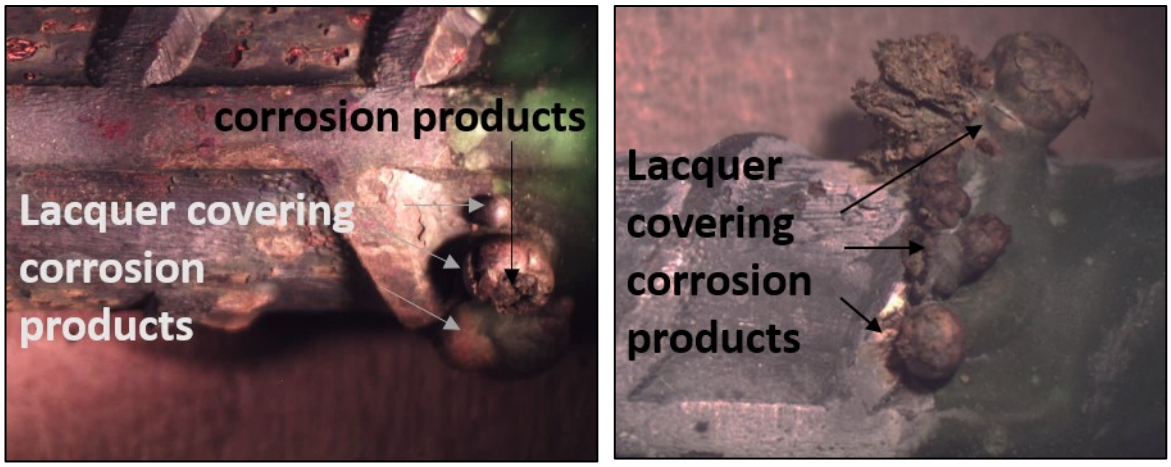

Figure 4.2-22: Crevice Corrosion on specimens 08 (NaCl SEPS) (left) and 25 ($MgCl_2$ SEPS) (right) where lacquer has been damaged

The lacquer was removed from bars with possible crevice corrosion to determine if the corrosion initiated outside the lacquer then moved into the lacquer or vice versa. Several examples are shown below in Figure 4.2-23.

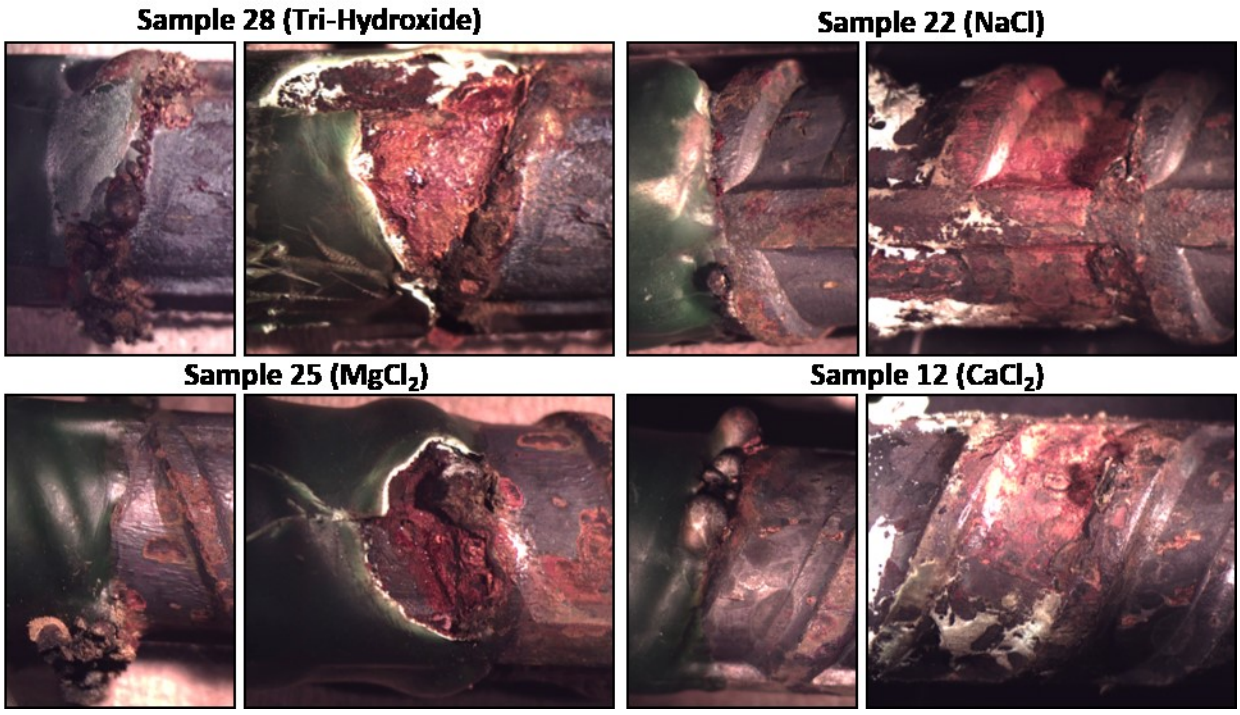

Figure 4.2-23: Examples of crevice corrosion on rebar specimen (before and after lacquer removal)

5 Discussion and Analysis

Data collected over the course of this thesis research indicates clearly that NaCl, $CaCl_2$ and $MgCl_2$ have unique impacts on both cement composition and rebar corrosion behaviour. In cement the changes in equilibrium between the pore solution and the solid hydration phases caused by salt addition can significantly alter both pore solution composition and the solid phases in cement. This supports the idea of a dynamic environment surrounding reinforcement bars which can change substantially over time as salt diffuses into cement. The ability of various synthetic pore solutions to recreate corrosion behaviour is also addressed.

This section seeks to shed more light on how the addition of different types of salts alters hydration products in general use cement paste and how these changes impact the cement pore solution resulting in potentially less protective pore solution. The effects of the sulphate in pore solution on rebar corrosion will be discussed as will the interdependencies of pH, chloride and salt cations.

5.1 Cement Paste and Pore Solutions with Admixed Salt

It has been widely established that the environment inside cement is initially conducive to the use of steel reinforcing bars due to the high pH which allows a protective passive film to be formed. Rebar corrosion is frequently observed after the ingress of surface contaminants, particularly de-icing salts which result in an environment favourable to corrosion initiation. In this research expressed pore solutions from pastes with admixed salts give some insight into how admixed salts alter the pH and composition of cement pore solution.

5.1.1 Changes in Hydration with Salt Addition

Moisture content is frequently used to determine how much free water is in a cement paste. The moisture content for samples used in this experiment are shown in Figure 4.1-2 where the weight change

on drying is calculated as a percentage of the sample weight prior to drying. A sample calculation is shown in Appendix B. This method suggests that the amount of water that is not evaporated at 105 °C varies from 0.19 to 0.26 g per g cement (Table 5.1-1). However, the act of grinding the sample prior to drying it at 105 °C may result in an under estimation of free water in the cement due to evaporation prior to the initial mass measurement.

Table 5.1-1: Chemically and Physically Bound Water Calculated from Moisture Content

Admixed Chlorides (wt% Cement)	g water per g dry cement		
	NaCl	**$CaCl_2$**	**$MgCl_2$**
0.00	*0.24*	*0.24*	*0.24*
0.25	*0.22*	*0.22*	*0.23*
0.50	*0.19*	*0.22*	*0.20*
0.75	*0.21*	*0.21*	*0.22*
1.00	*0.22*	*0.24*	*0.23*
2.50	*0.23*	*0.24*	*0.23*
5.00	*0.24*	*0.26*	*0.24*
7.50	*0.21*	*0.26*	*0.26*

Similar concentrations of calcium and magnesium were found in expressed pore solution from pastes with admixed $CaCl_2$ and $MgCl_2$ despite the addition of 1.41 mol/L calcium and magnesium respectively when 5 wt% Chloride was added in these salts. This may suggest that the maximum solubility of both elements was reached in these pore solutions resulting in precipitates such as $Mg(OH)_2$, $Ca(OH)_2$ and oxychloride. XRD peaks corresponding to $Mg(OH)_2$ and various forms of hydroxy chlorides were not visible in the 7.50 wt% Cl pastes, however this may simply be due to the relatively low weight percentage of

these compounds. Additionally, calcium and magnesium from admixed salts may interact with the hydrating cement to form other hydration products.

5.1.2 Bound Chloride and Bound Sulphates

The amount of chemically bound or physically trapped chlorides (Table 5.1-2) has been calculated by subtracting the amount of dissolved chlorides from the amount of admixed chlorides. The volume of expressed pore solution containing dissolved chlorides is calculated from the moisture content. The percentage of expressed and bound chlorides do not appear to indicate a plateau that would suggest NaCl saturation. However visual assessment of the demoulded cylinders indicate increasing amounts of crystalized salt in pastes with admixed NaCl for 2.50, 5.00 and 7.50 wt% admixed NaCl (Figure 4.1-3 and Figure 4.1-4) suggesting that a maximum concentration of NaCl is reached in these cylinders. It is of note that cylinders demoulded at 28 days for the purpose of pore solution expression (Figure 4.1-4) do not exhibit this visible salt formation.

The concentration of chloride in expressed pore solutions continues to increase as the amount of admixed chloride is increased for all salt types. For 2.50 and 5.00 wt% admixed chloride the NaCl pastes have over twice the amount of expressed chloride (mols Cl) compared to pastes with admixed $CaCl_2$ and $MgCl_2$ a trend that is expected to continue in the 7.5 wt% Cl^- pastes.

Sulphate, which is included in cement as $CaSO_4$ to prevent rapid set, is consumed in the formation of hydration products such as Aft and Afm. The cement mill certificate indicated that SO_3 constituted 3.40 wt% of the cement for a maximum expected sulphate content of 4.08 wt% by mass of cement. When considered relative to the mass of cement used (Table 5.1-3) there is very little change in bound sulphate when $CaCl_2$ or $MgCl_2$ were added. However, bound sulphate in pastes with admixed NaCl decreases significantly as the amount of admixed salt is increased.

Table 5.1-2: Bound and Expressed Cl (weight % of cement)

	NaCl		**$CaCl_2$**		**$MgCl_2$**	
Admixed Chlorides (wt. % Cement)	Bound Chlorides (wt. % Cement)	Expressed Cl (wt. % Cement)	Bound Chlorides (wt. % Cement)	Expressed Cl (wt. % Cement)	Bound Chlorides (wt. % Cement)	Expressed Cl (wt. % Cement)
0.00	0.00%	0.00%	0.00%	0.00%	0.00%	0.00%
0.25	0.23%	0.02%	0.24%	0.01%	0.24%	0.01%
0.50	0.40%	0.10%	0.45%	0.05%	0.46%	0.04%
0.75	0.52%	0.23%	0.63%	0.12%	0.65%	0.10%
1.00	0.67%	0.33%	0.83%	0.17%	0.85%	0.15%
2.50	1.01%	1.49%	1.85%	0.65%	1.90%	0.60%
5.00	1.80%	3.20%	3.72%	1.28%	3.79%	1.21%
7.50	2.67%	4.83%				

Table 5.1-3: Bound and Expressed SO_4 (weight % of cement)

	NaCl		**$CaCl_2$**		**$MgCl_2$**	
Admixed Cl (wt. % Cement)	Bound Sulphates (wt. % Cement)	Expressed SO_4(wt. % Cement)	Bound Sulphates (wt. % Cement)	Expressed SO_4(wt. % Cement)	Bound Sulphates (wt. % Cement)	Expressed SO_4(wt. % Cement)
0.00	4.068%	0.011%	4.068%	0.011%	4.068%	0.011%
0.25	4.061%	0.018%	4.069%	0.010%	4.072%	0.007%
0.50	4.035%	0.044%	4.068%	0.011%	4.071%	0.008%
0.75	4.017%	0.062%	4.067%	0.012%	4.071%	0.008%
1.00	4.005%	0.074%	4.073%	0.007%	4.072%	0.008%
2.50	3.877%	0.203%	4.076%	0.003%	4.075%	0.004%
5.00	3.465%	0.614%	4.078%	0.001%	4.077%	0.002%
7.50	3.014%	1.065%				

For admixed NaCl there is a trend of increasing sulphate as the admixed chloride is increased; for $CaCl_2$ and $MgCl_2$ the trend is opposite with decreasing expressed sulphate as admixed chloride concentration increases. For pastes with 5.00 wt % admixed Cl^- approximately 20 mol % less sulphate is bound in cement with admixed NaCl. The XRD scans of the 7.5 wt% Cl^- pastes (Figure 4.1-30) indicate peaks corresponding to Friedel's salt ($Ca_4Al_2Cl_2(OH)_{12} \cdot 4H_2O$) and decreased intensity of peaks attributed to ettringite ($Ca_6(Al,Fe)_2(SO_4)_3(OH)_{12} \cdot 26\ H_2O$) in the NaCl containing paste compared to other pastes. Since Aluminum availability limits the formation of these products the formation of more Friedel's salt would result in more sulphate dissolved in the pore solution. In pastes containing $CaCl_2$ and $MgCl_2$ the cations may precipitate to form $Ca(OH)_2$ and $Mg(OH)_2$ allowing more ettringite and ultimately Afm ($Ca_4Al_2(SO_4)(OH)_{12} \cdot 6\ H_2O$) to form which both utilize sulphate. Additionally, the decreased pH in the $CaCl_2$ and $MgCl_2$ pastes have been found to increase Ca^{2+} solubility as discussed in Section 2.1.4 resulting in the high concentrations detected in expressed pore solution at 5.0 Wt% Cl^-.

5.1.3 Implications of Cylinder Cracking

After demoulding and storage in the laboratory cylinders containing 2.50, 5.00 and 7.50 wt% Cl by weight of cement as $CaCl_2$ and $MgCl_2$ exhibited cracking. Cylinders with lower chloride contents stored in the same location did not exhibit cracking. This indicates that the high concentrations of admixed salts result in a more significant volume change compared to cylinders with less admixed chloride. This may be the result of more extensive hydration, or a shift in the proportions of hydration products formed. The relatively small cylinders used for this experiment made volume change difficult to measure.

Shrinkage was observed anecdotally when a cylinder containing paste with 7.5 wt% Cl (as $CaCl_2$) by weight of cement was unable to be demoulded when the storage cylinder was damaged. This cylinder was stored at room temperature in the plastic cylinder with the lid removed so the top of the cylinder was in contact with the air and moisture could evaporate. Several unsuccessful attempts were made to remove

the cylinder in the first two months. After approximately 4.5 months the cylinder was found to have shrunk sufficiently to be removed simply by inverting the cylinder.

Demoulded cylinders were stored exposed to air in a laboratory room at approximately 23 °C. This allows moisture to evaporate from the cylinder and is not necessarily representative of bulk concrete, that is not near the surface in a large structure. The formation of deep cracks at the surface of large structures exposed to salt solutions, such as anti-icing brines, may allow provide an access point for increased chloride penetration.

5.1.3.1 Cylinders with Admixed NaCl

Cylinders containing admixed NaCl experienced cracking only in the 2.50 wt% admixed Cl cylinders but these cracks became less pronounced over time (Figure 4.1-3). Increased surface roughness was observed in the 5.00 wt% admixed chloride and ultimately salt crystals became visible on the 7.5 wt% admixed chloride paste. Crystallization on the 7.5 wt% admixed chloride became more apparent after the cylinder had been demoulded for several weeks.

5.1.3.2 Cylinders with Admixed $CaCl_2$ and $MgCl_2$

Several cylinders with either admixed $CaCl_2$ or $MgCl_2$ exhibited deep cracks which continued through both the top or bottom surface as well as the vertical face. These cracks are probably associated with the formation of oxychlorides. While low temperatures allow more rapid formation of oxychlorides, significant damage was seen in mortar samples at 23 °C as discussed in section 2.1.2.1. Cracking in the small cylinders is not as extensive as in the larger samples used by Betancourt and Hooton[36]. However, peaks identified for oxychlorides in the reviewed literature[35,36] were not observed by XRD of freshly demoulded cylinders with 7.50 wt% Cl; indicating that any oxychlorides present represented a very small percentage of the overall sample or are formed after evaporation after demoulding. The conditions of this experiment are significantly different from Betancourt and Hooton. In this experiment salt was admixed

at the point of mixing rather than being introduced externally after 28 days of hydration and specimen were stored in a dry environment rather than being immersed in a high concentration salt brine. Betancourt and Hooton identified oxychlorides which formed from the interaction of $Ca(OH)_2$ which leached from mortar specimens and highly concentrated $CaCl_2$ brine solution. This allowed the oxychloride to be isolated for XRD and subjected to common laboratory preparation techniques. Further investigation on specimen that have been demoulded for a longer period of time prior to XRD investigation may provide different results.

Cylinders with admixed $CaCl_2$ and $MgCl_2$ exhibited cracking shortly after demoulding but more cracks became visible over time. Cracking appears to have lessened in the 5.00 wt% admixed Cl in both cylinders. Cracking then increased in the 7.50 wt% admixed chloride $MgCl_2$ cylinder but minimal cracking was observed in the $CaCl_2$ cylinder with the same chloride content (Figure 4.1-6 and Figure 4.1-8). Since cracking became more extensive in the days after demoulding. While in the mold specimen have very limited evaporation and are constrained. This combination of no longer being constrained, being in an environment with less than 100% humidity coupled with ongoing reactions likely contribute to cracking.

5.1.4 XRD Analysis of Cement Paste Composition

There was insufficient pore solution from pastes with 7.5 wt% chloride ($CaCl_2$ and $MgCl_2$) by weight cement. The use of XRD gives more insight to the solid phases present in these specimens however it is challenging because there are many phases present. This section addresses interpretation of the XRD scans from Figure 4.1-30. XRD scans were conducted on newly demoulded cylinders containing 7.5 wt% admixed Cl by weight of cement. As mentioned earlier in the discussion section this is representative of the cement subjected to pore solution expression but can not be directly related to cracking observed in the specimen demoulded after 24 hours discussed in Section 5.1.3. For brevity in this section samples will be described as ‘admixed NaCl’, ‘admixed $CaCl_2$’ and ‘admixed $MgCl_2$’. Because cement is a composite

material and can contain many hydration products the XRD peaks for many possible compounds were compared to the experimental peaks, these comparisons are available in Appendix C.

The XRD scan for the admixed NaCl cylinder indicates clear peaks corresponding to NaCl. This was not the case for $CaCl_2$ and $MgCl_2$ in their respective admixed pastes suggesting that these salts have dissolved and/or reacted to form different compounds. $Mg(OH)_2$ and $Ca(OH)_2$ are common precipitates in cement following the reactions outlined in Section 2.1.2.1.

5.1.4.1 Ettringite (Aft)

The peak intensity of Aft ($Ca_6(Al,Fe)_2(SO_4)_3(OH)_{12} \cdot 26\ H_2O$) is approximately 80% that of chloride free cement for admixed NaCl while the admixed $CaCl_2$ and $MgCl_2$ pastes have approximately the same intensity. Some peaks are a slightly higher intensity possibly due to overlap with other compounds.

5.1.4.2 Portlandite ($Ca(OH)_2$)

The intensity of Portlandite peaks vary significantly for the different admixed salts. Peaks were approximately twenty percent more intense in the paste with admixed NaCl than in the chloride free paste. In pastes with admixed $CaCl_2$ and $MgCl_2$ peaks were approximately two thirds of the intensity of the chloride free paste. This is discussed further in Section 5.1.5.1.

Reference peaks for $Ca(OH)_2$ often had different intensities with the maximum intensity peak being located at different 2θ locations. This was also the case in these experimental peaks, when compared to the intensity of peaks in the chloride free paste there was some variation in the ratio of peak intensity. For examples, the intensity of the peak at 18 2θ is 1.5x higher in the admixed NaCl paste than in the salt free paste but exactly the same intensity at 28.8 2θ. This could be due to overlap between peaks for different compounds or could simply be due to noise in the data.

Even at 7.50 wt% Cl^- there is no discernable difference between the peak intensity of pastes with admixed $MgCl_2$ and $CaCl_2$ suggesting an additional mechanism beyond the formation of Ca(OH)2 precipitates when the calcium solubility is reached in pore solution.

5.1.4.3 Chloride Containing Compounds

The addition of chlorides results in a strong peak around 11.3° for all three admixed salts that is not present in the chloride free version. This initial peak is close to that of Friedel Salt ($Ca_4Al_2(Cl_2)(OH)_{12}\cdot 4H_2O$)[27,108] however subsequent expected peaks at 22.6° and 23.2° only appear for the admixed NaCl paste. The formation of Friedel salt in admixed NaCl specimen agrees with the increase in sulphate concentration in expressed pore solution corresponding to an increase in the amount of admixed Chloride as discussed in Section 5.1.2.

Identification of the peak at 11.3° in specimen with admixed $CaCl_2$ and $MgCl_2$ is more complicated. The Afm phase, which may have a varied composition, has a strong peak in the region 10.7° – 11.5° depending on whether SO_4^{2-} has been replaced by OH^-, Cl^- or CO_3^{2-} and to which extent. Other possible compounds include Kuzel salt ($Ca_4Al_2(SO_4)_{0.5}(Cl)(OH)_{12}\cdot 6H_2O$) and hydrotalcite ($Mg_{1-x}(Al,Fe)_x(OH)_2 \cdot [Cl^-]_{x/n} \cdot mH_2O$) where again the Cl- can be replaced by SO_4^{2-}, OH^- or CO_3^2. Peaks from literature are compared to experimental results in Appendix D.

Results of the XRD scans did not match peaks identified for oxychlorides in literature[35,36]. Since a variety of conditions were investigated in these papers, including how peak positions and intensities change as the salts dehydrate with temperature, comparison to the peaks from literature is included in Appendix D. Both papers used CuKα radiation, as was used in the present work. Since there was no visible crystal or precipitate to isolate it is possible that some oxychloride has formed but it is not in a sufficiently large amount to be detected in the XRD scan. It is also possible that oxychloride crystals were destroyed

during preparation of the powdered sample or that they form more readily when a specimen is unconstrained for a longer period of time prior to testing.

5.1.5 Relationship Between Expressed Pore Solution and Cement Microstructure

As the amount of admixed chloride was increased the concentration of individual elements in pore solution changed. Differences between solution from pastes with admixed NaCl and solution from pastes with admixed $CaCl_2$ or $MgCl_2$ became more evident as the amount of admixed chloride increased. This section aims to connect trends identified in expressed pore solution to possible changes in hydration products with the three admixed salts as the amount of admixed chloride increased.

5.1.5.1 Calcium Depletion and Chloride Binding

The concentration of calcium in the expressed pore solution from pastes with both admixed $CaCl_2$ and $MgCl_2$ was found to increase with an especially steep increase between 2.50 and 5.00 wt% Cl by weight cement (Figure 4.1-11). The calcium concentration in expressed pore solution is expected to increase following this trend for the pastes with 7.50 wt% Cl by weight cement, this was not tested because there was insufficient expressed pore solution.

Calcium solubility increases in solution as the pH decreases, $Ca(OH)_2$ is typically accepted as the precipitate formed once this limit is reached. XRD testing indicated lower intensity peaks for $Ca(OH)_2$ (portlandite) in the 7.5 wt% Cl by weight cement pastes with admixed $CaCl_2$ and $MgCl_2$ although the peak intensities are similar for the two salts. Despite the extra calcium added through $CaCl_2$, the amount of calcium in expressed pore solution from the two salts is very similar to that in pore solution from admixed $MgCl_2$, especially when considered relative to the pH. Excess calcium introduced by $CaCl_2$ may explain the increased intensity of the XRD peak at 29.5° which is often attributed to C-S-H[27,58,109,110] or calcite[39,56,111].

Calcium in expressed pore solution from pastes with admixed NaCl actually decreases slightly with increasing chlorides (Figure 4.1-12) mirroring changes in pH (Figure 4.1-1). This further suggests that

calcium solubility is dependant on pH. However, the pH of the 7.5 wt% Cl by weight cement paste with admixed NaCl used for XRD is lower than the pH found for the chloride free paste, so extra precipitation due to a higher pH. It is more likely that for admixed NaCl a shift from ettringite to Friedel salt or Afm would result in excess calcium which would then precipitate in the form of $Ca(OH)_2$.

Major phases affected by changes in calcium solubility in the pore solution are $Ca(OH)_2$ and C-S-H with calcium leaching resulting in dissolution of $Ca(OH)_2$ and a shift to a more dense structure for C-S-H. While leaching can occur due to external contaminants, like contact with acidic liquids, the low pH that occurs as a result of high concentrations of $CaCl_2$ and $MgCl_2$ salts can also deplete $Ca(OH)_2$ and cause changes to C-S-H morphology. Work by De Weerdt et al 2019 suggested that calcium availability was critical for the understanding of C-S-H morphology and by extension chloride binding on C-S-H[26]. Several researchers have linked chloride adsorption in C-S-H to the pH with higher adsorption at lower pH due to increased binding sites[23,41]. In this research the concentration of calcium in pore solution increased as the amount of $CaCl_2$ and $MgCl_2$ was increased while less chloride was expressed compared to the NaCl paste. Since no strong XRD peaks have been identified corresponding to crystalline materials which would chemically or physically bind chloride, like Friedel or Kuzels salts, C-S-H must be considered as a significant source of chloride binding.

Chloride in expressed pore solutions increases in proportion with the amounts of chloride added with no apparent saturation limit for chloride in expressed pore solution (Figure 4.1-14). However crystalized NaCl detected by XRD and by visual observation, confirms that the solubility limit for NaCl was reached in the NaCl pastewith 7.50 wt% admixed Cl by weight cement. Pastes with 2.50 and 5.00 wt% Cl (NaCl) by weight cement have increased surface roughness compared to the 1.00 wt% cylinder suggesting that the solubility limit for NaCl was reached prior to 2.50 wt% admixed Cl. The measured pH for NaCl pastes decreased from an average of 13.26 at 2.50 wt% Cl to an average of 13.16 at 7.50 wt% Cl which may have

increased NaCl solubility allowing the amount of chloride in expressed pore solution to continue increasing.

Bound chlorides in NaCl containing pastes are likely in the form of Friedel's salt ($Ca_4Al_2(Cl_2)(OH)_{12}\cdot 4H_2O$). This would be limited by aluminum availability. The concentration of Aluminum is seen to decrease in expressed pore solution with increasing admixed salt (Figure 4.1-9). Lower intensity Aft peaks in XRD and peaks corresponding to Friedels salt indicate that a shift from Aft to Friedel salt likely took place at 7.5 wt% admixed Cl (NaCl) by weight cement. The concentration of aluminum in expressed pore solution decreases below the concentration in the chloride free paste between 1.00 and 2.50 wt% admixed Cl by weight cement. Likewise a decrease of iron in expressed pore solution with 7.5 wt% admixed Cl may indicate the formation of Fe-Friedel salt[29] with Fe instead of aluminum.

Increased Chloride binding occurs for pastes with admixed $CaCl_2$ and $MgCl_2$ compared to NaCl with the same chloride content. XRD scans did not indicate Friedel's salt or oxychloride compounds although other chloride binding compounds are possible. Several researchers have linked chloride adsorption in C-S-H to the pH with higher adsorption at lower pH due to increased binding sites[23,41].

5.2 The Use of Synthetic Pore Solutions to Test Rebar Corrosion

Synthetic pore solutions allow researchers to rapidly assess corrosion on different rebar types. This is especially valuable for comparison between different materials such as stainless-steel types and coated steels. However, the synthetic pore solutions used by researchers vary, making comparison of different results difficult. Pore solution expression from pastes with up to 7.5 wt% Cl of admixed salts by mass of cement indicates large variation in pore solution composition. Variations were observed both between the type of admixed salt as well as between high and low admixed salt compositions. For stainless steels in a high chloride environment, the chemical composition of the pore solution in contact with the reinforcement will be drastically different than that in a lower chloride solution.

When salt diffuses into hydrated cement rather than being directly mixed at casting, differences in pore solution composition between different salt types are expected to be less pronounced. As discussed in Section 2.1.2, studies of chloride ingress have found that Cl^- penetrates into cement more rapidly than its associated cations, especially Mg^{2+}. For example, in a real structure exposed to $MgCl_2$, chloride would reach the surface of the rebar prior to decreased pH as a result of $Ca(OH)_2$ and $Mg(OH)_2$ formation. Additionally, the increased chloride binding that occurs with $MgCl_2$ and CaCl2 may reduce the rate of chloride diffusion. As a result, testing in synthetic pore solutions with the same amount of chloride but different cations may represent the pore solution in a concrete structure with very different salt exposure at the surface. Synthetic Pore Solution tests are useful for comparing different rebar materials and the damage that can` be expected given a certain chloride concentration and pH but can not be directly related to a timeline for structure durability.

5.2.1 Cl^-/OH^- Ratio Compared to Expressed Pore Solution

A Cl^-/OH^- ratio provides a method to quantify the conditions under which corrosion initiates and relates them to the cement service environment. In particular it takes into account the impact of lower pH which may be caused by carbonation or the presence of $CaCl_2$ or $MgCl_2$ salts. As discussed in Section 2.4.1, lower pH has been associated with poorer passive film performance. Although it is difficult to test pH in real structures it is important to be aware that in lower pH environments less chloride may be required to initiate corrosion. This ratio has been chosen for evaluating experimental results because it can relate the conditions where corrosion initiated in synthetic pore solution compared to the conditions in the actual cement pore solution. In this section, Cl^-/OH^- ratio is discussed for the bulk solution rather than in the context of pitting or crevice corrosion.

In all cases the rebar in synthetic pore solution tests was immersed in solution for 17 weeks with salt added weekly up to 0.80 wt% Cl by weight solution. It was not always possible to visually identify corrosion

at a given admixed chloride concentration so the electrochemical results in Figure 4.2-10 and Figure 4.2-11 must be considered along with the corrosion observed after the specimen was removed from solution. Crevice corrosion was the most difficult to observe and it is unclear when this corrosion initiated. To standardize this approach, a threshold value was chosen for average corrosion current density over the exposed area of the specimen. An i_{corr} value of 1.0 x 10^{-3} A/m^2 has been used as an active corrosion threshold by some researchers[74,81,112] and so this value was chosen. Active corrosion was considered to have happened when an i_{corr} value greater than 1.0 x 10^{-3} A/m^2 had occurred for a minimum of two consecutive weeks. Once that criteria was met the chloride concentration at which the i_{corr} value initially exceeded the threshold. The hydroxyl concentration was calculated from the measured pH (Figure 4.2-7) and the Cl^-/OH^- ratio was calculated for each individual specimen at the point where i_{corr} exceeded each threshold. It should be noted that these i_{corr} thresholds are not a definitive indication of corrosion, especially considering crevice corrosion. Since the extent of damage to bars after exposure to 0.80 wt% Cl by weight solution was the desired outcome specimen were not removed after this threshold was reached for observation.

The Cl^-/OH^- for the six synthetic pore solutions at the threshold is shown in Figure 5.2-1. To compare with the actual environment that would exist in cement exposed to chloride the Cl^-/OH^- of expressed pore solution from the admixed NaCl, $CaCl_2$ and $MgCl_2$ specimen was calculated using the pH and expressed chloride content (Figure 4.1-1 and Figure 4.1-14). These are shown by the yellow, green and purple lines in Figure 5.2-1 and the square points indicate the admixed chloride content (0.00, 0.25, 0.50, 0.75 and 1.00 wt% admixed chloride) where expressed chloride content was measured. Presenting the data in this way emphasizes the relationship between admixed and expressed chloride in cement to the chloride content in synthetic pore solutions. Less chloride binding in admixed NaCl pastes results in a faster increase in chloride content in the pore solution and ultimately faster initiation of active corrosion.

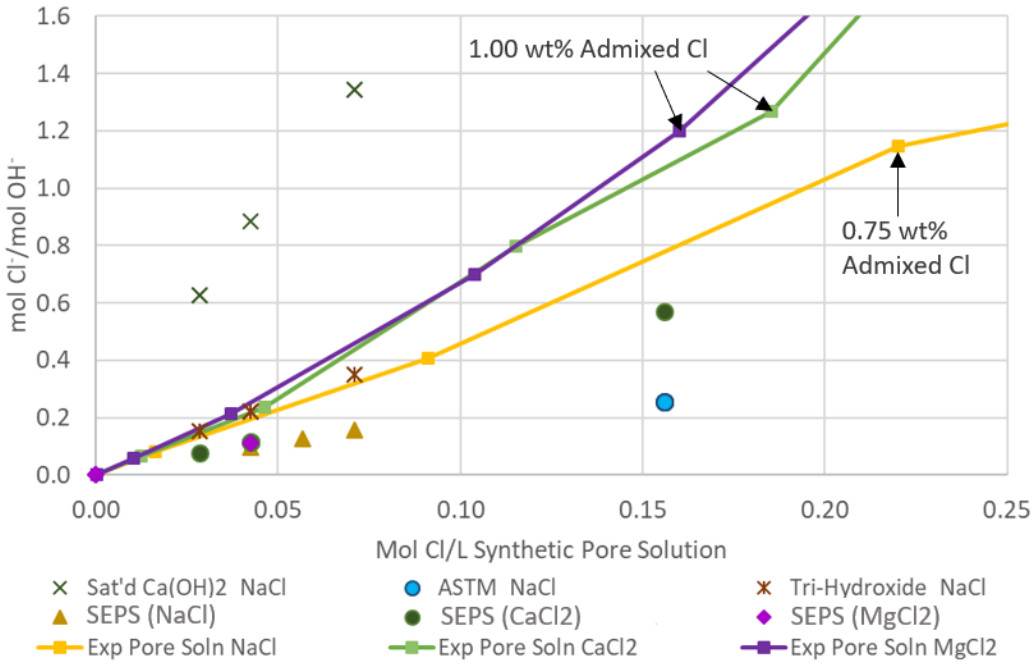

Figure 5.2-1: Cl^-/OH^- ratios of rebar specimens exceeding icorr = 1.0 x10^{-3} A/m2 vs. mol Cl/ L synthetic pore solution (points) compared to Cl/OH ratio of expressed pore solutions with different admixed salts (lines)

In Figure 5.2-1 the area under the lines for expressed Cl from admixed NaCl, $CaCl_2$ and $MgCl_2$ respective indicates the Cl^-/OH^- ratios which could occur indicating that these SPS are realistic in that the Cl^-/OH^- ratios could reasonably be expected to occur in cement. In real structures salts typically diffuses into the cement rather than being admixed so using the data from expressed pore solution is a conservative estimate. It follows that the saturated $Ca(OH)_2$ solution is unrealistic for cement exposed to these salts as corrosion would not occur at this chloride concentration unless carbonation had also occurred decreasing the pH. The position of the tri-hydroxide SPS in Figure 5.2-1, which has admixed NaCl, suggests that the composition of pore solution itself, in addition to the pH contributes to corrosion behaviour.

SEPS are intended to closely replicate the expressed pore solutions. However, it was felt that three unique solution compositions would make corrosion behaviour difficult to compare resulting in the same

amount of Ca(OH)2, NaOH and KOH being used with only the amount of sulphate used and salt type being varied. This may explain why these points do not occur closer to their respective lines.

Ultimately arranging data in terms of Cl^-/OH^- ratio has provided a convenient way to link the results of SPS corrosion testing to the environment inside cement as well as the corresponding admixed chloride contents where these would occur. However, given the spread in this data, a Cl^-/OH^- ratio is not sufficient to indicate whether corrosion will initiate in cement under certain conditions.

5.2.2 Rebar Corrosion in Synthetic Pore Solution

Both type A and type B rebar have imperfections in the mill scale which allow the formation of localized acidic regions causing corrosion[71,90,91,113]. In both types of rebar, mill scale thicknesses ranged from zero to nearly 100 µm. Mill scale imperfections included voids, crevices and sections detached from the steel surface examples of which are shown in Figure 4.2-2, Figure 4.2-4 and Figure 4.2-5.

5.2.2.1 Rebar Passivation

All rebar specimen were submerged in chloride-free SPS for one week prior to chloride addition. The half cell potentials became less negative over this time, starting around an average value of -360 mV SCE and rising to -170 mV SCE. While type B rebar appeared more resistant to corrosion after salt addition, the pre-chloride half cell potentials were similar to the type A rebar in the same SPS. Rebar in the saturated $Ca(OH)_2$ solution reached the least positive half cell potentials after one week of passivation. An average half cell potential of approximately -220 mV SCE was reached. This is of interest because some researchers have suggested that although a stable passive film can form at pH as low as 11.5[75] the stability and protectiveness of the passive film is better in higher pH environments and can be less effective the film is formed in the presence of aggressive ions or if rebar has millscale[75].

Mill scale on rebar introduces significant variability in corrosion initiation but this is less evident during passivation. The agrees with the assertion by Ahlström et al[87] that mill scale acts as a cathode with any exposed steel acting as an anode increasing chloride movement towards the steel surface.

5.2.2.2 Corrosion of Rebar in Pore Solutions with Added NaCl

Overall electrochemical measurements indicate a linear trend of decreased mass loss with increasing pH of the solution. Significant scatter can be observed in Figure 4.2-12 with the exception of bars in the high pH ASTM solution which remained passive at all Cl^- levels. Visual inspections of rebar after removal from the solutions revealed that, in most cases, corrosion initiated underneath the mill scale and pushed upwards. Pitting corrosion occurred predominantly in areas with nearly-continuous mill scale coverage as the cathode effect was likely magnified for the small cracks and pin holes that were visible in both the SEM images of the surface (Figure 4.2-1 and Figure 4.2-2) and in the microscope images of steel cross sections (Figure 4.2-4 and Figure 4.2-5). The incidence of corrosion in nearly-continuous mill scale covered areas was especially clear for the two sets of TH SPS specimen. The second set of type A bars had more sections of exposed steel and ultimately less small pitting corrosion despite being subject to the same pore solution and salt concentration. Ultimately the presence of sulphates in the SEPS NaCl solution does not appear to have significantly altered corrosion performance in these tests while the pH had a significant influence.

Rebar in the saturated $Ca(OH)_2$ solution (CH) experienced at least one deep pit on each specimen along with some smaller pits. In corrosion initiated by chloride the passive film can be repaired by OH- in the pore solution from sources such as $Ca(OH)_2$ as discussed in Section 2.4. Although $Ca(OH)_2$ is present in excess in the CH SPS the solubility of calcium limits the ability of this precipitate to dissolve into solution. Once initiated, reactions following Equation 2.1-1 would propagate to form a larger pit. Once a large pit is established more of the surface area needs to act as a cathode as Fe^{2+} is formed. Oxygen availability for the cathodic reaction (Equation 2.4-2) results in the need for a larger cathodic area and limits further

pitting. The half cell potential of these specimen was more negative than specimen in other synthetic pore solutions after one-week passivation and further decreased by approximately 260 mV after initial salt addition (Figure 4.2-10). This illustrates the variability in electrochemical data which makes the use of an i_{corr} threshold difficult.

In the tri-hydroxide (TH) SPS, corrosion observed visually and electrochemically, was found to be more varied for the second set of specimens. All rebar in TH2 solution experienced some form of crevice corrosion however the mean mass losses (Table 4.2-2) for specimens from both solutions were within ±5 g/m^3 which is closer than expected given the different corrosion performance. In addition to issues with crevice corrosion, scatter in the corrosion behaviour of bars in the TH2 solution may be due to a less continuous mill scale coverage on specimens as seen in Figure 4.2-21. The small pits observed on large portions of rebar in the TH1 SPS (Figure 4.2-15, left image) were also observed on rebar from the TH2 SPS however they were less widespread (Figure 4.2-15, right image). Small pits were observed primarily in areas where mill scale was present in a continuous layer rather than at locations where mill scale had flaked off. Since this solution has a higher pH than CH SPS and contains KOH and NaOH there is more hydroxides to buffer the Fe^{2+} reaction with Cl^-, and calcium solubility no longer limiting.

Minimal corrosion was observed on specimens in the ASTM solution although all of the mill scale on the exposed surface became visibly darker. Since no corrosion was observed on 4/5 specimen in this solution and minimal corrosion was seen on the fifth specimen this discolouration was likely due to the equilibrium reached between the hematite layer and the SPS. Hematite is stable in equilibrium with air[85] and in a Fe-H_2O system[114] differences in pH between the different SPS's should not be sufficient to change this equilibrium. However, interactions between hematite and the K^+, Na^+ and Cl- ions may result in reduction from hematite to magnetite or even wustite[93]. Oxygen availability or substitutions by chloride ions may also play a role. Mill scale on specimen in other SPS was observed however it was more noticeable in specimens from the ASTM SPS.

In the SEPS with added NaCl, sulphate was added, in concentrations corresponding to those measured in the expressed pore solutions to the synthetic pore solution. Sulphate did not appear to influence the passive film protectiveness: the half cell potential of rebar in the SEPS-NaCl solution is similar to those of specimens in the other pore solutions and less negative than those of bars in the saturated $Ca(OH)_2$ solution. Two specimens in the SEPS-NaCl solution were type B rebar, these specimens remained passive throughout the test which was observed electrochemically and confirmed visually after removing them from solution. Crevice corrosion occurred on all type A rebar. The half cell potential of type A rebar in this solution became more negative as soon as salt was added, this may indicate decreased effectiveness of the mill scale and passive film or initiation of crevice corrosion. After removal from the SPS only one of these type A specimens, number 26, had significant corrosion on the exposed surface in addition to crevice corrosion. Crevice corrosion occurred under the lacquer on both ends of these specimens except on the end where corrosion occurred on the exposed surface of specimen 26 (Figure 4.2-18). The half cell potential values for the individual specimen are available in appendix B.

The colour of corrosion products was mentioned by Wimpenny and Slater[55] with dark powdery corrosion products being observed in pits when sulphate and chloride were present although the powder was not identified. After removing the top corrosion products using a knife, a dark powdery substance was also found in deeper pits in the CH SPS (Figure 5.2-2). Corrosion products were found to be a variety of colours from bright red to black. This is likely more a function of the location in actively corroding pit which would impact the pH, oxygen availability and availability of elements such as Cl^-, than the SPS especially since there is no sulphate in the CH SPS.

The corrosion products formed on rebar specimen in all pore solutions consisted of several types as evidenced by different colours and textures. It would be expected that as pitting corrosion proceeds the pit would be less alkaline due to the formation of H^+ and less oxygen which would be limited by its diffusion into the pit. Lighter red corrosion products typically indicate more oxidation[115]. Especially where deep pits

occur the corrosion products observed formed a hard dome like structure with the interior pit being occupied by less rigid, often powdery, corrosion products as shown in Figure 5.2-2.

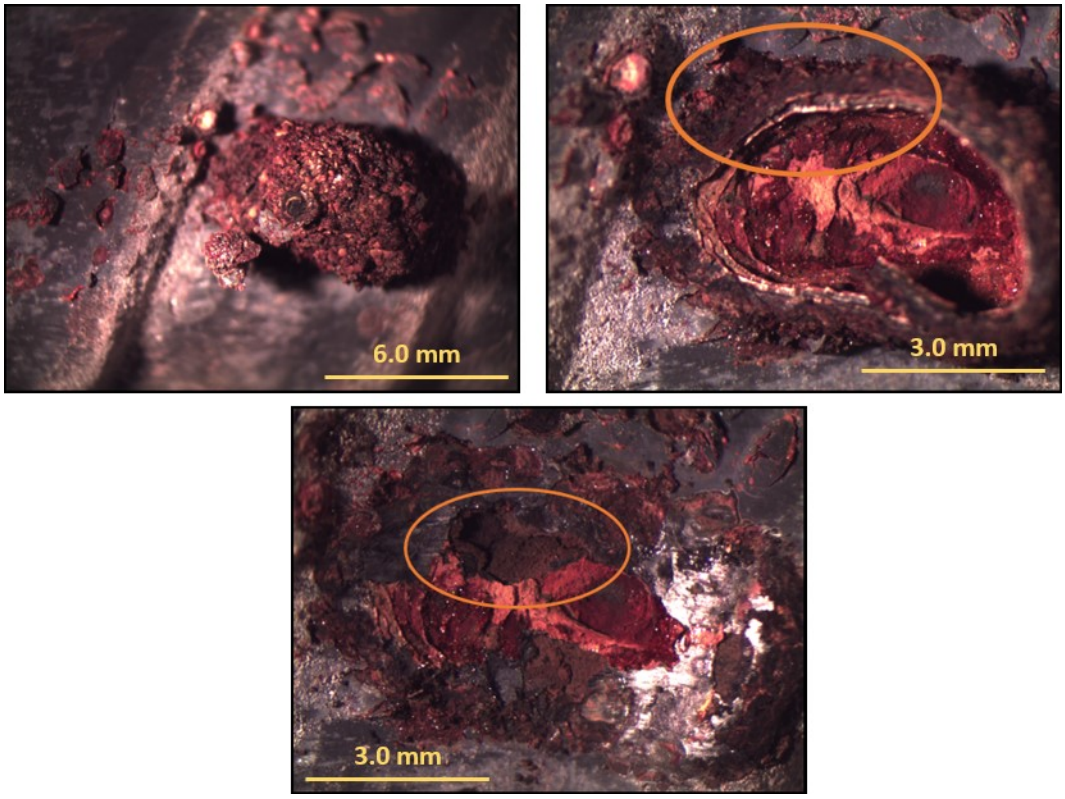

Figure 5.2-2: Closer look at corrosion products as pit is exposed on rebar in CH SPS with NaCl, Orange circles identify the location that was revealed after more corrosion products were removed.

5.2.2.3 SEPS with Admixed NaCl, $CaCl_2$ and $MgCl_2$

Corrosion on specimen immersed in SEPS with $CaCl_2$ and $MgCl_2$ were also investigated electrochemically which suggests that specimen in SEPS with $CaCl_2$ would have less severe corrosion than specimen in SEPS with $MgCl_2$. However, all specimen had evidence of crevice corrosion. This means that electrochemical data was not representative of true rebar corrosion. Crevice corrosion in these specimens resulted in similar behaviour to specimens in saturated $Ca(OH)_2$ solution (Section 5.3.2.2), where much of the rebar surface acted as a cathode for deep pits. High volumes of corrosion products were formed under the lacquer at the edges, stretching the lacquer as shown in Figure 4.2-19. Due to poor visibility into the

containers, the extent of crevice corrosion was not fully understood until the end of the 17-week period and the time where this crevice corrosion became dominant electrochemically is not known. Since many specimens have severe crevice corrosion and minimal corrosion on the exposed area it must be assumed that crevice corrosion initiated relatively early in most cases.

For the SEPS with NaCl, $CaCl_2$ and $MgCl_2$, the amount of sulphate added was different for each solution. This was to reflect the equivalent amount of sulphate that was found in expressed pore solution (Figure 4.1-26 and Figure 4.1-27). Sulphate in synthetic pore solution did not impact the passivation potentials prior to salt addition.

Once salts and the corresponding sulphates were added to these SPS the type A rebar specimens (3 replicates in each solution) performed similarly for all SEPS (Figure 4.2-8) with the potentials decreasing with increasing salt content eventually reaching a steady state of ~ -475 mV SCE at an admixed chloride content of approximately 0.30 wt% Cl by weight of solution. The individual performance of each specimen was used to create Figure 5.2-1.

The corrosion performance of type B rebar (two replicates per solution) was more varied and suggests that sulphate has a corrosion inhibiting effect, as has been observed previously in literature[100]. Type B rebar in SEPS with admixed $MgCl_2$, which has the least sulphate in solution, had a poor electrochemical performance (Figure 4.2-8). A rapid decrease in potential of Type B bars in the SEPS with admixed $CaCl_2$ was observed after 0.5 wt% admixed chloride by weight of solution was reached, shown in Figure 4.2-8, indicated the onset of active corrosion in these bars. The type B rebar in the SEPS NaCl solution, which had the highest sulphate content, performed the best electrochemically and had no visible corrosion.

5.2.2.4 Crevice Corrosion Under Lacquer

As can be seen in Figure 4.2-23, corrosion products were formed under the lacquer for up to several cm. Crevice corrosion under lacquer appeared to mainly occur in the space between radial ribs, this may

be because mill scale is often flaked off the ribs during transport and storage while the space between ribs maintains a more continuous mill scale covering on the macro level. Where the lacquer is in contact with the base metal it is able to seal more completely. Capillary suction between the lacquer and rebar surface may also contribute to crevice corrosion initiation. Removal of mill scale and or removal of ribs at the locations where lacquer will be applied may be necessary to reduce crevice corrosion for these tests.

6 Summary, Conclusions and Recommendations

This section presents conclusions and recommendations summarized from the research presented and discussed in previous sections. For clarity, conclusions are presented in two sections addressing the most significant findings for cement interactions with salts (section 6.1) and corrosion behaviours in synthetic pore solutions (section 6.2). Recommendations for future research is also addressed (section 6.3).

6.1 Summary and Conclusions: Cement Hydration with Admixed Salts

The type of salt used impacts cement differently. When $CaCl_2$ or $MgCl_2$ are admixed to cement they have similar behaviour but it differs significantly from admixed NaCl. Differences between the salts increase as the amount of admixed chlorides is increased.

Expressed pore solutions were found to differ in the following ways:

- Pore solutions with admixed NaCl have more chloride and sulphate than when an equivalent amount of chloride as admixed $CaCl_2$ or $MgCl_2$ are used.
- Sodium from admixed NaCl remains primarily in the pore solution however this was not the case for pastes with admixed $CaCl_2$ and $MgCl_2$ which did not result in significant increases of calcium and magnesium respectively.
- Pore solutions with admixed NaCl have less calcium than when an equivalent amount of chloride as admixed $CaCl_2$ or $MgCl_2$ are used.
- The pH of pore solutions from pastes with admixed $CaCl_2$ or $MgCl_2$ decrease as the amount of admixed salt increases.

The above noted changes will impact the ability of rebar imbedded in cements exposed to these salts to maintain a protective passive film. There are detriments to exposure to both salt types. Admixed NaCl

results in a pore solution which maintains a high pH as the amount of chloride is increased which will help maintain the passive film. However, the amount of chloride in pore solution increases more quickly which creates a less protective environment and increases the probability of pitting rather than general corrosion. The concentration of sulphate increases with increasing admixed chloride which is especially significant at high admixed chloride concentrations so this is of particular interest for creating synthetic pore solutions used for testing stainless steel.

Admixed $CaCl_2$ and $MgCl_2$ result in pore solutions which decrease in pH as the amount of admixed chloride is increased going from approximately 13.3 in cement without admixed chloride to approximately 12.3 when 5.00 wt% admixed Cl^- is used. Since pH is on a log scale this decrease is significant for maintaining a protective passive film. The concentration of chloride increases more slowly from pastes with admixed $CaCl_2$ and $MgCl_2$ indicating that more chloride remains bound in the solid phase leaving chloride in solution to attack the passive film. Another trend was that of increasing calcium in pore solution which is a function of the pH of the solution.

The amount of pore solution that could be expressed from pastes with admixed $CaCl_2$ and $MgCl_2$ decreased as the amount of admixed salt increased and ultimately insufficient pore solution could be expressed at 7.50 wt% admixed Cl^-. This was not the case for pastes with admixed NaCl. This indicates that sufficient changes occurred to the type or quantity of hydration products to either chemically bind more water or to block pores during pore expression testing. $CaCl_2$ in particular is known to cause cement to set rapidly which may increase overall hydration.

Changes to the elemental composition of the expressed pore solutions with increasing admixed chlorides are a direct result of changes to the solid phases. Understanding what products are formed for these pastes at w/c ratio 0.5 may help better understand why certain products may be formed at other w/c ratios in cements exposed to these salts. When a w/c ratio is used that is insufficient to completely

hydrate cement there is less liquid in the form of pore solution. Less free liquid in the paste means the concentration of elements like chloride and sulphate would increase more rapidly. For example, the chloride concentration in pore solution from a 0.5 w/c paste with 0.5 wt% Cl as NaCl might be equivalent to a 0.4 w/c paste with less admixed chlorides as NaCl. However, this would only be true if the mechanism ruling the concentration of an element in pore solution is independent of solubility and the stability of solid phases. The large range of admixed chlorides investigated in this thesis allows general trends to be identified.

XRD scans of pastes with 7.50 wt% Cl^- as admixed $CaCl_2$ and $MgCl_2$ had stronger peaks for ettringite compared to pastes with admixed NaCl or paste with no admixed chlorides. Ettringite chemically binds more water than monosulphate (Afm) which would form in paste without exposure to chloride or Friedel's salt which is frequently found after exposure to NaCl. The paste with admixed NaCl did have peaks corresponding to Friedel's salt, which binds chloride instead of sulphate. This explains the higher concentration of sulphate in expressed pore solution because Friedel salt forms preferentially over ettringite and monosulphate.

The amount of calcium in pore solution is typically attributed to Ca^{2+} and OH^- ions that are in equilibrium with $Ca(OH)_2$. However, as the pH decreases, the solubility of calcium increases significantly. If all the $Ca(OH)_2$ is consumed 'calcium leaching' may occur causing calcium to enter solution from other sources like C-S-H. XRD scans indicate that $Ca(OH)_2$ is present in all 7.5 wt% Cl pastes scanned, however pastes with admixed $CaCl_2$ and $MgCl_2$ had lower intensity peaks than the pastes with admixed NaCl and no admixed salt.

Despite significantly more calcium introduced to pastes with admixed $CaCl_2$, the calcium expressed in pore solution from pastes with admixed $CaCl_2$ were similar to the concentrations of calcium from pastes with equivalent amounts of admixed $MgCl_2$. For some admixed chloride contents pore solution from

pastes with admixed $CaCl_2$ appear to have more calcium in solution than pastes with an equivalent amount of chloride as $MgCl_2$. However when calcium concentration is plotted against the pH of the expressed pore solution it becomes clear that these differences are the result of calcium solubility at that pH. When the 7.5 wt% Cl pastes were investigated with XRD, the peak intensity for portlandite was approximately the same for admixed $CaCl_2$ and $MgCl_2$. This suggests that the calcium from $CaCl_2$ chloride did not simply precipitate out as $Ca(OH)_2$. This further points to the formation of other products like calcium oxychloride.

Additional Mg^{2+} introduced in admixed $MgCl_2$ did not result in increased concentrations of this element in expressed pore solution from $MgCl_2$ pastes. Investigation with XRD did not detect brucite ($Mg(OH)_2$) or other probable magnesium containing compounds. Conversely the amount of Na^+ in pore solution was found to increase corresponding to higher concentrations of admixed NaCl.

Chloride binding was more significant for pastes with admixed $CaCl_2$ and $MgCl_2$ than for those with NaCl. Since oxychlorides, oxychloride hydrates and Friedel salts are not observed in XRD scans for pastes with $CaCl_2$ and $MgCl_2$, the source of chloride binding is unclear. These phases may have been present in quantities or crystal sizes too small to be detected by XRD or, as suggested in Ref. 35, be unstable and have decomposed during preparation of the powdered pastes. Physical and chemical binding of Cl^- into the C-S-H gel, which can not be reliably identified by XRD due to its amorphous structure, may explain chloride binding.

Cracking was observed in paste cylinders with 2.5, 5.0 and 7.5 wt% Cl by weight of cement admixed $CaCl_2$ and $MgCl_2$. Cracking occurred in cylinders after demoulding and was most severe in the 2.50 wt% Cl $CaCl_2$ paste and the 7.5 wt% Cl $MgCl_2$ paste. Since XRD testing was performed on freshly demoulded cylinders to replicate pore solution expression conditions salts like oxychlorides and hydroxychlorides may appear if testing is performed on pastes which have been demoulded for a longer period of time.

Cracking was only observed in the 2.5 wt% Cl by weight of cement cylinders with admixed NaCl. However, cracking became less noticeable over time. Surface roughness on cylinders with 5.0 and 7.5 wt% admixed Cl by weight cement was significant with salt crystals visible on the cylinder surface.

6.2 Summary and Conclusions: Steel Rebar Corrosion in Synthetic Pore Solutions

Analysis of expressed pore solutions indicate significantly different compositions in pore solution depending on the amount of admixed salt and the cation of that salt. An understanding of these effects can influence the decision of which form and composition of de-icing or anti-icing agent to use and under what climate conditions.

For laboratory testing, the corrosion tests showed clearly that the use of saturated calcium hydroxide will give very conservative results, while the KOH + NaOH mix recommended by ASTM A955 may overestimate the rebar's resistance to corrosion in concrete. These differences can significantly affect service life predictions for reinforced concrete.

The significant influence on pH of solutions with added $CaCl_2$ and $MgCl_2$, will have even greater implications for service life models, which are generally based on the influence of NaCl.

Variability between rebar manufacturers results in different corrosion behaviour. This was seen with the type A and type B rebars used in this study. In electrochemical testing the type A rebar initiated active corrosion quickly while type B rebar initiated active corrosion more slowly as seen in the tri-hydroxide synthetic pore solution. Differences in surface roughness and mill scale coverage are thought to have contributed to these different corrosion initiation behaviours. To control for variability due to surface finish concurrent testing of rebar samples with the mill scale removed and as received rebar samples may be instructive to gauge expected surface life where rebar may be used from many manufacturers.

6.3 Recommendations for Future Research

The mechanism of chloride binding from Ca and Mg salts remains unclear and warrants further research.

Due to crevice corrosion on rebar specimen in synthetic pore solutions containing sulphate the effects of sulphate were not conclusively evaluated. It would be of value to repeat these tests using a different technique to seal the ends of specimen. Further variation of the sulphate content in these solutions would also be of interest since the two type B bars that did not experience any corrosion were in the SEPS NaCl solution which had the highest sulphate content.

Since pore solution expression indicated large variations in expressed sulphate depending on salt cation, the amount of sulphate should be chosen with consideration to the type of salt used, especially if investigating high chloride environments. If sulphate it not included in the synthetic pore solution the equilibrium of the solution should be considered since concentrations of the anion SO_4^{2-} must be balanced by cations.

Rebar preparation to avoid crevice corrosion may require the milling of the ends of specimens to remove both mill scale and ribs prior to application of coatings to isolate an active area. This measure is expected to be sufficient to reduce liquid transfer to the area under the lacquer. Because corrosion is suspected to initiate in these localized environments caused by discontinuous contact between the mill scale and the steel, bare metal is expected to exhibit a higher chloride threshold than areas covered by mill scale. These areas of discontinuous mill scale contact were observed in microscope images of as received bars and areas of discolouration observed after pickling.

A Cl-/OH- ratio can be useful to relate rebar corrosion in synthetic pore solution to the environment in cement. However, the use of a specific threshold may not be reliable because of the stochastic nature of corrosion. Removal of rebar from the synthetic pore solution and visual inspection after the chosen

threshold has been reached is recommended to ensure that corrosion has initiated on the exposed surface.

Cracking observed in pastes demoulded after 24 hours and stored in a laboratory suggest was not observed when cylinders were demoulded at 28 days for pore expression testing. The nature of this cracking may not be accurately captured by the composition of pore solution expressed from recently demoulded cylinders. Additionally, had these pastes with admixed salts been demoulded and stored in more controlled environments, for example where temperature, moisture content and/or carbonation can be controlled different behaviour may be observed.

The use of a vibration table is recommended to allow better consolidation of pastes when preparing pastes with high concentrations of admixed $CaCl_2$ and $MgCl_2$. Consolidations issues were encountered for pastes containing 5.0 and 7.5 wt% Cl by weight cement due to a rapid set.

7 Copyright Permission

Dec 20, 2019

This Agreement between Leah CL Kristufek ("You") and Elsevier ("Elsevier") consists of your license details and the terms and conditions provided by Elsevier and Copyright Clearance Center.

License Number	4710280027830
License date	Nov 15, 2019
Licensed Content Publisher	Elsevier
Licensed Content Publication	Cement and Concrete Research
Licensed Content Title	Chloride concentration in the pore solution of Portland cement paste and Portland cement concrete
Licensed Content Author	Kyle A. Anders,Bradley P. Bergsma,Carolyn M. Hansson
Licensed Content Date	Sep 1, 2014
Licensed Content Volume	63
Licensed Content Issue	n/a
Licensed Content Pages	3
Start Page	35
End Page	37
Type of Use	reuse in a thesis/dissertation
Portion	figures/tables/illustrations
Number of figures/tables/illustrations	1
Format	both print and electronic
Are you the author of this Elsevier article?	No
Will you be translating?	No
Title	The Effect of De-Icing Saltsonthe Chemistry of the Pore Solution in Cement Pastes and their Influence on Rebar Corrosion
Institution name	University of Waterloo
Expected presentation date	Dec 2019
Portions	Fig. 1 (a) Schematic diagram from [1]; (b) photograph of the assembly at the University of Waterloo. [I have requested permission for the schematic separately]

Dec 20, 2019

This Agreement between Leah CL Kristufek ("You") and Elsevier ("Elsevier") consists of your license details and the terms and conditions provided by Elsevier and Copyright Clearance Center.

License Number	4710270812649
License date	Nov 15, 2019
Licensed Content Publisher	Elsevier
Licensed Content Publication	Cement and Concrete Research
Licensed Content Title	Expression and analysis of pore fluids from hardened cement pastes and mortars
Licensed Content Author	R.S. Barneyback,Sidney Diamond
Licensed Content Date	Mar 1, 1981
Licensed Content Volume	11
Licensed Content Issue	2
Licensed Content Pages	7
Start Page	279
End Page	285
Type of Use	reuse in a thesis/dissertation
Portion	figures/tables/illustrations
Number of figures/tables/illustrations	1
Format	both print and electronic
Are you the author of this Elsevier article?	No
Will you be translating?	No
Title	The Effect of De-Icing Saltsonthe Chemistry of the Pore Solution in Cement Pastes and their Influence on Rebar Corrosion
Institution name	University of Waterloo
Expected presentation date	Dec 2019
Portions	Fig. 1: Isometric half section of pore fluid expression device

Dec 20, 2019

This Agreement between Leah CL Kristufek ("You") and John Wiley and Sons ("John Wiley and Sons") consists of your license details and the terms and conditions provided by John Wiley and Sons and Copyright Clearance Center.

License Number	4733210115509
License date	Dec 20, 2019
Licensed Content Publisher	John Wiley and Sons
Licensed Content Publication	Materials and Corrosion
Licensed Content Title	Pore solution of concrete: The equilibrium of bound and free chloride
Licensed Content Author	J. Tritthart
Licensed Content Date	Aug 21, 2009
Licensed Content Volume	60
Licensed Content Issue	8
Licensed Content Pages	7
Type of Use	Dissertation/Thesis
Requestor type	University/Academic
Format	Print and electronic
Portion	Figure/table
Number of figures/tables	1
Original Wiley figure/table number(s)	Figure 9
Will you be translating?	No
Title of your thesis / dissertation	The Effect of De-Icing Saltsonthe Chemistry of the Pore Solution in Cement Pastes and their Influence on Rebar Corrosion
Expected completion date	Dec 2019
Expected size (number of pages)	170

Dec 20, 2019

This Agreement between Leah CL Kristufek ("You") and Elsevier ("Elsevier") consists of your license details and the terms and conditions provided by Elsevier and Copyright Clearance Center.

License Number	4733210227924
License date	Dec 20, 2019
Licensed Content Publisher	Elsevier
Licensed Content Publication	Cement and Concrete Research
Licensed Content Title	Comparing chloride ingress from seawater and NaCl solution in Portland cement mortar
Licensed Content Author	K. De Weerdt,B. Lothenbach,M.R. Geiker
Licensed Content Date	Jan 1, 2019
Licensed Content Volume	115
Licensed Content Issue	n/a
Licensed Content Pages	10
Start Page	80
End Page	89
Type of Use	reuse in a thesis/dissertation
Portion	figures/tables/illustrations
Number of figures/tables/illustrations	1
Format	both print and electronic
Are you the author of this Elsevier article?	No
Will you be translating?	No
Title	The Effect of De-Icing Saltsonthe Chemistry of the Pore Solution in Cement Pastes and their Influence on Rebar Corrosion
Institution name	University of Waterloo
Expected presentation date	Dec 2019
Portions	Figure 10

Bibliography

1. Riebe, N. Edmonton ditches calcium chloride as anit-icing agent for this winter at least. *CBC News* (2019).

2. Canada, G. of. *Population estimates, July 1, by census metropolitan area and census agglomeration, 2016 boundaries*. *Stats Canada* **91**-**214**–**X**, (2018).

3. City of Edmonton. Anti-icing Pilot. (2019). Available at: www.edmonton.ca/transportation/on_your_streets/anti-icing-pilot-program.aspx. (Accessed: 14th May 2019)

4. Mermigas, K. K. Evolution of Bridge Practices in Ontario , Canada. in *Transport Association of Canada* 1–18 (2018).

5. CSA Group. Canadian Highway Bridge Design Code S6-14. (2014).

6. Justnes, H. A Review of Chloride Binding in Cementitious Systems, Cement and concrete. *Nord. Concr. Res.* **21**, 1–6 (1997).

7. Lothenbach, B. & Winnefeld, F. Thermodynamic modelling of the hydration of Portland cement. *Cem. Concr. Res.* **36**, 209–226 (2006).

8. Lothenbach, B., Damidot, D., Matschei, T. & Marchand, J. Thermodynamic modelling: state of knowledge and challenges. *Adv. Cem. Res.* **22**, 211–223 (2010).

9. Gégout, P., Revertégat, E. & Moine, G. Action of chloride ions on hydrated cement pastes: Influence of the cement type and long time effect of the concentration of chlorides. *Cem. Concr. Res.* **22**, 451–457 (1992).

10. Okoronkwo, M. U. & Glasser, F. P. Compatibility of hydrogarnet, Ca3Al2(SiO4)x(OH)4(3 -X),with

sulfate and carbonate-bearing cement phases: 5-85 °c. *Cem. Concr. Res.* **83**, 86–96 (2016).

11. Dhir, R. K. & Yap, A. W. F. Superplasticizing flowing concrete: strength and deformation properties. *Mag. Concr. Res.* **36**, 203–215 (1984).

12. Morrison, J., Jauffret, G., Galvez-Martos, J. L. & Glasser, F. P. Magnesium-based cements for CO2capture and utilisation. *Cem. Concr. Res.* **85**, 183–191 (2016).

13. Quennoz, A. Hydration of C3A with Calcium Sulfate Alone and in the Presence of Calcium Silicate. **5035**, (École Polytechnique Fédérale de Lausanne, 2011).

14. Damidot, D., Lothenbach, B., Herfort, D. & Glasser, F. P. Thermodynamics and cement science. *Cem. Concr. Res.* **41**, 679–695 (2011).

15. Glasser, F. P., Marchand, J. & Samson, E. Durability of concrete - Degradation phenomena involving detrimental chemical reactions. *Cem. Concr. Res.* **38**, 226–246 (2008).

16. Lothenbach, B., Kulik, D. A., Matschei, T., Balonis, M., Baquerizo, L., Dilnesa, B. Z., Miron, G. D. & Myers, R. J. Cemdata18: A chemical thermodynamic database for hydrated Portland cements and alkali-activated materials. *Cem. Concr. Res.* **115**, 472–506 (2019).

17. Berner, U., Kulik, D. A. & Kosakowski, G. Geochemical impact of a low-pH cement liner on the near field of a repository for spent fuel and high-level radioactive waste. *Phys. Chem. Earth* **64**, 46–56 (2013).

18. Thien, B. M. J., Kulik, D. A. & Curti, E. A unified approach to model uptake kinetics of trace elements in complex aqueous - Solid solution systems. *Appl. Geochemistry* **41**, 135–150 (2014).

19. Hansson, C. M., Poursaee, A. & Jaffer, S. J. Corrosion of Reinforcing Bars in Concrete. *The Masterbuilder* **15**, (2012).

20. Williamson, J. & Isgor, O. B. The effect of simulated concrete pore solution composition and chlorides on the electronic properties of passive films on carbon steel rebar. *Corros. Sci.* **106**, 82–95 (2016).

21. Abrams, D. A. Proportioning concrete mixtures. *J. Proc.* **18**, 174–181 (1922).

22. Neville, A. M. *Properties of Concrete*. (Longman Scientific & Technical, 1981).

23. Tritthart, J. Pore solution of concrete : The equilibrium of bound and free chloride. *Mater. Corros.* **60**, 579–585 (2009).

24. Galan, I., Perron, L. & Glasser, F. P. Impact of chloride-rich environments on cement paste mineralogy. *Cem. Concr. Res.* **68**, 174–183 (2015).

25. Bernard, E., Lothenbach, B., Le Goff, F., Pochard, I. & Dauzères, A. Effect of magnesium on calcium silicate hydrate (C-S-H). *Cem. Concr. Res.* **97**, 61–72 (2017).

26. Weerdt, K. De, Lothenbach, B. & Geiker, M. R. Comparing chloride ingress from seawater and NaCl solution in Portland cement mortar. *Cem. Concr. Res.* **115**, 80–89 (2019).

27. Shi, Z., Geiker, M. R., Lothenbach, B., De Weerdt, K., Garzón, S. F., Enemark-Rasmussen, K. & Skibsted, J. Friedel's salt profiles from thermogravimetric analysis and thermodynamic modelling of Portland cement-based mortars exposed to sodium chloride solution. *Cem. Concr. Compos.* **78**, 73–83 (2017).

28. Loser, R., Lothenbach, B., Leemann, A. & Tuchschmid, M. Chloride resistance of concrete and its binding capacity - Comparison between experimental results and thermodynamic modeling. *Cem. Concr. Compos.* **32**, 34–42 (2010).

29. Balonis, M. & Glasser, F. P. The density of cement phases. *Cem. Concr. Res.* **39**, 733–739 (2009).

30. Enevoldsen, J. N., Hansson, C. M. & Hope, B. B. Binding of chloride in mortar containing admixed or penetrated chlorides. *Cem. Concr. Res.* **24**, 1525–1533 (1994).

31. El-Gamal, S. M. A., Al-Nowaiser, F. M. & Al-Baity, A. O. Effect of superplasticizers on the hydration kinetic and mechanical properties of Portland cement pastes. *J. Adv. Res.* **3**, 119–124 (2012).

32. Balonis, M., Lothenbach, B., Le Saout, G. & Glasser, F. P. Impact of chloride on the mineralogy of hydrated Portland cement systems. *Cem. Concr. Res.* **40**, 1009–1022 (2010).

33. Jiang, L., Liu, R., Mo, L., Xu, J. & Yang, H. Influence of chloride salt type on critical chloride content of reinforcement corrosion in concrete. *Mag. Concr. Res.* **65**, 1–13 (2013).

34. Arya, C., Buenfeld, N. R. & Newman, J. B. Factors influencing chloride-binding in concrete. *Cem. Concr. Res.* **20**, 291–300 (1990).

35. Peterson, K., Julio-betancourt, G., Sutter, L., Hooton, R. D. & Johnston, D. Cement and Concrete Research Observations of chloride ingress and calcium oxychloride formation in laboratory concrete and mortar at 5 ° C. *Cem. Concr. Res.* **45**, 79–90 (2013).

36. Julio-Betancourt, G. A. & Hooton, R. D. Calcium and Magnesium Chloride attack on cement based materials: Formation, stability, and effects of oxychlorides. in *2nd International RILEM Workshop on Concrete Durability and Service Life Planning* 432–439 (2009).

37. Hunt, M. J. & Hansson, C. M. The Influence of the Cations in Anti-Icing Brines on the Corrosion of Reinforcing Steel in Synthetic Concrete Pore Solution. *Corrosion* **71**, 749–758 (2015).

38. Rayment, D. L. & Majumdar, A. J. The composition of the C-S-H phases in portland cement pastes. *Cem. Concr. Res.* **12**, 753–764 (1982).

39. Kunther, W., Lothenbach, B. & Skibsted, J. Influence of the Ca/Si ratio of the C-S-H phase on the

interaction with sulfate ions and its impact on the ettringite crystallization pressure. *Cem. Concr. Res.* **69**, 37–49 (2015).

40. Suryavanshi, A. K., Scantlebury, J. D. & Lyon, S. B. Pore Size Distribution of OPC & SRPC Mortars in Presence of Chlorides. *Cem. Concr. Res.* **25**, 980–988 (1995).

41. De Weerdt, K., Colombo, A., Coppola, L., Justnes, H. & Geiker, M. R. Impact of the associated cation on chloride binding of Portland cement paste. *Cem. Concr. Res.* **68**, 196–202 (2015).

42. Chatterji, S. Mechanism of the CaCl2 attack on portland cement concrete. *Cem. Concr. Res.* **8**, 461–467 (1978).

43. Hansson, C. M., Frølund, T. & Markussen, J. B. The effect of chloride cation type on the corposion of steel in concrete by chloride salts. *Cem. Concr. Res.* **15**, 65–73 (1985).

44. Rahman, M. M. & Bassuoni, M. T. Thaumasite sulfate attack on concrete: Mechanisms, influential factors and mitigation. *Constr. Build. Mater.* **73**, 652–662 (2014).

45. Suryavanshi, A. K., Scantlebury, J. D. & Lyon, S. B. The binding of chloride ions by sulphate resistant Portland cement. *Cem. Concr. Res.* **25**, 581–592 (1995).

46. Jiang, L., Huang, G., Xu, J., Zhu, Y. & Mo, L. Influence of chloride salt type on threshold level of reinforcement corrosion in simulated concrete pore solutions. *Constr. Build. Mater.* **30**, 516–521 (2012).

47. De Weerdt, K., Orsáková, D. & Geiker, M. R. The impact of sulphate and magnesium on chloride binding in Portland cement paste. *Cem. Concr. Res.* **65**, 30–40 (2014).

48. Mittermayr, F., Baldermann, A., Kurta, C., Rinder, T., Klammer, D., Leis, A., Tritthart, J. & Dietzel, M. Evaporation — a key mechanism for the thaumasite form of sulfate attack. *Cem. Concr. Res.* **49**,

55–64 (2013).

49. Al-Amoudi, O. S. B. Attack on plain and blended cements exposed to aggressive sulfate environments. *Cem. Concr. Compos.* **24**, 305–316 (2002).

50. Tishmack, J., Olek, J. & Diamond, S. Characterization of High-Calcium Fly Ashes and Their Potential Influence on Ettringite Formation in Cementitious Systems. *Cem. Concr. Aggregates* **21**, 82–92 (1999).

51. Thomas, M. D. A., Rogers, C. A. & Bleszynski, R. F. Occurrences of thaumasite in laboratory and field concrete. *Cem. Concr. Compos.* **25**, 1045–1050 (2003).

52. Taylor, H. F. W. Determination of the quantitative phase composition of alite and belite in portland cement clinker by microphotometry. *Cem. Concr. Res.* **29**, 1173–1179 (1999).

53. Gartner, E. M., Tang, F. J. & Weiss, S. J. Saturation Factors for Calcium Hydroxide and Calcium Sulfates in Fresh Portland Cement Pastes. *J. Am. Ceram. Soc.* **68**, 667–673 (1985).

54. Crammond, N. The occurrence of thaumasite in modern construction – a review. *Cem. Concr. Compos.* **24**, 393–402 (2002).

55. Wimpenny, D. & Slater, D. Evidence from the highways agency thaumasite investigation in Gloucestershire to support or contradict postulated mechanisms of thaumasite formation (TF) and thaumasite sulfate attack (TSA). *Cem. Concr. Compos.* **25**, 879–888 (2003).

56. Sotiriadis, K., Nikolopoulou, E. & Tsivilis, S. Cement & Concrete Composites Sulfate resistance of limestone cement concrete exposed to combined chloride and sulfate environment at low temperature. *Cem. Concr. Compos.* **34**, 903–910 (2012).

57. Lothenbach, B. Thermodynamic equilibrium calculations in cementitious systems. *Mater. Struct.*

Constr. **43**, 1413–1433 (2010).

58. Baston, G. M. N., Clacher, A. P., Heath, T. G., Hunter, F. M. I., Smith, V. & Swanton, S. W. Calcium silicate hydrate (C-S-H) gel dissolution and pH buffering in a cementitious near field. *Mineral. Mag.* **76**, 3045–3053 (2012).

59. Bensted, J. A discussion of the review paper '' Sulphate attack research — whither. *Cem. Concr. Res.* **32**, 995–1000 (2002).

60. Byfors, K., Hansson, C. M. & Tritthart, J. Pore solution expression as a method to determine the influence of mineral additives on chloride binding. *Cem. Concr. Res.* **16**, 760–770 (1986).

61. Barneyback, R. S. & Diamond, S. Expression and Analysis of Pore Fluids from Hardened Cement Pastes and Mortars. *Cem. Concr. Res.* **11**, 279–285 (1981).

62. Vollpracht, A., Lothenbach, B., Snellings, R. & Haufe, J. The pore solution of blended cements: a review. *Mater. Struct.* **49**, 3341–3367 (2016).

63. Tritthart, J. & Ha, F. Pore solution analysis of cement pastes and nanostructural investigations of hydrated C 3 S. **33**, 1063–1070 (2003).

64. Van Niejenhuis, C. B., Ogunsanya, I. G. & Hansson, C. M. Analysis of pore solution expressed from Portland cement pastes with and without supplementary cementitious materials and admixed chlorides. (2018).

65. Jin, Z., Zhao, X., Zhao, T., Hou, B. & Liu, Y. Effect of Ca(OH)2, NaCl, and Na2SO4 on the corrosion and electrochemical behavior of rebar*. **35**, 681–692 (2017).

66. Mahmoud, H., Sánchez, M. & Alonso, M. C. Ageing of the spontaneous passive state of 2304 duplex stainless steel in high-alkaline conditions with the presence of chloride. *J. Solid State Electrochem.*

19, 2961–2972 (2015).

67. Yang, L., Chiang, K., Yu, H., Pabalan, R. T., Dasgupta, B. & Ibarra, L. Threshold Chloride Levels for Localized Carbon Steel Corrosion in Simulated Concrete Pore Solutions Using Coupled Multielectrode Array Sensors. *Corros. Sci.* **70**, 850–857 (2014).

68. Poursaee, A. Corrosion of steel bars in saturated Ca(OH)2 and concrete pore solution. *Concr. Res. Lett.* **1**, 90–97 (2010).

69. Ghods, P., Isgor, O. B., McRae, G. & Miller, T. The effect of concrete pore solution composition on the quality of passive oxide films on black steel reinforcement. *Cem. Concr. Compos.* **31**, 2–11 (2009).

70. Vigneshwaran, K. K., Permeh, S., Echeverría, M., Lau, K. & Lasa, I. Corrosion of Post-Tensioned Tendons with Deficient Grout, Part 1: Electrochemical Behavior of Steel in Alkaline Sulfate Solutions. *Corrosion* **74**, 362–371 (2017).

71. Ghods, P., Isgor, O. B., McRae, G. A., Li, J. & Gu, G. P. Microscopic investigation of mill scale and its proposed effect on the variability of chloride-induced depassivation of carbon steel rebar. *Corros. Sci.* **53**, 946–954 (2011).

72. Wang, X. & Melchers, R. E. Journal of Loss Prevention in the Process Industries Corrosion of carbon steel in presence of mixed deposits under stagnant seawater conditions. *J. Loss Prev. Process Ind.* **45**, 29–42 (2017).

73. Bergsma, B. P. & Hansson, C. M. The Formation and Stability of the Protective Passive Films formed on the New Generation of Stainless Steel Rebar Alloys. (2012).

74. Scott, A. & Alexander, M. G. Effect of supplementary cementitious materials (binder type) on the pore solution chemistry and the corrosion of steel in alkaline environments. *Cem. Concr. Res.* **89**,

45–55 (2016).

75. Gouda, V. K. Corrosion and Corrosion Inhibition of Reinforcing Steel I. Immersed in Alkaline Solutions. *Br. Corros. J.* **5**, 198–203 (1970).

76. Hunt, M. J. Effects of De-icing and Anti-icing Chemicals on the Durability of Reinforcing Steel in Concrete. (University of Waterloo, 2013).

77. Duchesne, J. & Bérubé, M. A. Evaluation of the Validity of the Pore Solution Expression Method from Hardened Cement Pastes and Mortars. *Cem. Concr. Res.* **24**, 456–462 (1994).

78. Tritthart, J. Chloride Binding in Cement I Investigations to Determine the Composition of Pore Water in Hardened Cement. *Cem. Concr. Res.* **19**, 586–594 (1989).

79. Aitcin, P. C. Durable Concrete - Current Practice and future trends. in *Concrete technology past, present, and future proceedings of V. Mohan Malhotra Symposium* 85–104 (1994).

80. Tang, S. W., Yao, Y., Andrade, C. & Li, Z. J. Recent durability studies on concrete structure. *Cem. Concr. Res.* **78**, 143–154 (2015).

81. Alonso, C., Andrade, C., Castellote, M. & Castro, P. Chloride threshold values to depassivate reinforcing bars embedded in a standardized OPC mortar. *Cem. Concr. Res.* **30**, 1047–1055 (2000).

82. Gonzalez, J. A., Algaba, S. & Andrade, C. Corrosion of Reinforcing Bars in Carbonated Concrete. *Br. Corros. J.* **15**, 135–139 (1980).

83. Andrade, C. Propagation of reinforcement corrosion: principles, testing and modelling. *Mater. Struct. Constr.* **52**, 1–26 (2019).

84. Jones, D. A. *Principles and Prevention of Corrosion*. (Prentice-Hall Inc., 1996).

85. Cook, D. C. Spectroscopic identification of protective and non-protective corrosion coatings on

steel structures in marine environments. *Corros. Sci.* **47**, 2550–2570 (2005).

86. Jaffer, S. J. & Hansson, C. M. Chloride-induced corrosion products of steel in cracked-concrete subjected to different loading conditions. *Cem. Concr. Res.* **39**, 116–125 (2009).

87. Ahlström, J., Tidblad, J., Tang, L., Sederholm, B. & Leijonmarck, S. Electrochemical Properties of Oxide Scale on Steel Exposed in Saturated Calcium Hydroxide Solutions with or without Chlorides. *Int. J. Corros.* 1–10 (2018). doi:10.1155/2018/5623504

88. Ding, L. & Poursaee, A. The impact of sandblasting as a surface modification method on the corrosion behavior of steels in simulated concrete pore solution. *Constr. Build. Mater.* **157**, 591–599 (2017).

89. Gouda, V. K. Anodic polarisation measurements of corrosion and corrosion inhibition of Steel in concrete. *Br. Corros. J.* **1**, 138–142 (1966).

90. Ming, J., Shi, J. & Sun, W. Effect of mill scale on the long-term corrosion resistance of a low-alloy reinforcing steel in concrete subjected to chloride solution. *Constr. Build. Mater.* **163**, 508–517 (2018).

91. Karadakis, K., Azad, V. J., Ghods, P. & Isgor, O. B. Numerical Investigation of the Role of Mill Scale Crevices on the Corrosion Initiation of Carbon Steel Reinforcement in Concrete. *J. Electrochem. Soc.* **163**, C306–C315 (2016).

92. Gouda, V. K. & Mourad, H. M. Galvanic Cells Encountered in the Corrosion of Steel Reinforcement - III. Differential Surface Condition Cells. *Corros. Sci.* **15**, 317–328 (1975).

93. NAKAGAWA, H. & ONO, Y. Effects of potassium chloride on the reduction of iron oxides. *Trans. Iron Steel Inst. Japan* **25**, 1021–1024 (1985).

94. Gouda, V. K. & Halaka, W. Y. Corrosion and Corrosion Inhibition of Reinforcing Steel II. Embedded in Concrete. *Br. Corros. J.* **5**, 204–208 (1970).

95. Gouda, V. K. & Mourad, H. M. Galvanic Cells Encountered in the corrosion of steel reinforcement - II. Differential Salt Concentration cells. *Corros. Sci.* **15**, 307–315 (1975).

96. Gouda, V. K., Azim, A. A. A. & Sayed, H. A. El. Some Aspects of Reinforcement Corrosion in Egyptian Structures. *Br. Corros. J.* **3**, 185–189 (1974).

97. Tritthart, J. Changes in Pore Water Composition and in Total Chloride Content at Different Levels of Cement Paste Plates Under Different Storage Conditions. *Cem. Concr. Res.* **22**, 129–138 (1992).

98. Hausmann, D. A. Steel corrosion in concrete - How does it occur? *Mater. Prot.* **6**, 19–23 (1967).

99. Goñi, S. & Andrade, C. Synthetic concrete pore solution chemistry and rebar. *Cem. Concr. Res.* **20**, 525–539 (1990).

100. Ogunsanya, I. G. & Hansson, C. M. Detection of critical chloride threshold of carbon steel rebar in synthetic concrete pore solutions. *RILEM Tech. Lett.* **3**, 75–83 (2018).

101. Williams, G., Dafydd, H. A. L. & Mcmurray, H. N. Chloride Ion Concentration Effects on Passivity Breakdown in Magnesium. *224th ECS Meet.* **73**, 2013 (2017).

102. Bragg, W. H. & Bragg, W. L. The reflection of X-rays by crystals. *Proc. R. Soc. Lond.* **88**, 428–438 (1913).

103. ARMICRON. Bragg Diffraction. Available at: https://commons.wikimedia.org/wiki/File:Bragg_diffraction.svg.

104. ASTM. G59 - 97 Standard test method for Conducting Potentiodynamic Polarization Resistance Measurements. *ASTM International* (2014). doi:10.1520/G0059-97R14.2

105. Stern, M. & Geary, A. L. Electrochemical polarization. *J. Electrochem. Soc.* **104**, 56–63 (1957).

106. Anders, K. A., Bergsma, B. P. & Hansson, C. M. Chloride concentration in the pore solution of Portland cement paste and Portland cement concrete. *Cem. Concr. Res.* **63**, 35–37 (2014).

107. Randstrom, S., Almen, M., Pettersson, R. & Adair, M. Reproducibility of critical chloride threshold levels for stainless steel reinforcement. *Struct. Faults* (2010).

108. Renaudin, G., Kubel, F., Rivera, J. P. & Francois, M. Structural phase transition and high temperature phase structure of Friedels salt, 3CaO · Al2O3 · CaCl2 · 10H2O. *Cem. Concr. Res.* **29**, 1937–1942 (1999).

109. Walling, S. A., Bernal, S. A., Gardner, L. J., Kinoshita, H. & Provis, J. Blast furnace slag-Mg(OH) 2 cements activated by sodium carbonate. *RSC Adv.* **8**, 23101–23118 (2018).

110. Lothenbach, B., Le Saout, G., Ben Haha, M., Figi, R. & Wieland, E. Hydration of a low-alkali CEM III/B-SiO 2 cement (LAC). *Cem. Concr. Res.* **42**, 410–423 (2012).

111. Ramezanianpour, A. M. & Hooton, R. D. Thaumasite sulfate attack in Portland and Portland-limestone cement mortars exposed to sulfate solution. *Constr. Build. Mater.* **40**, 162–173 (2013).

112. González, J. A., Andrade, C., Alonso, C. & Feliu, S. Comparison of rates of general corrosion and maximum pitting penetration on concrete embedded steel reinforcement. *Cem. Concr. Res.* **25**, 257–264 (1995).

113. Shi, J. jie & Ming, J. Influence of mill scale and rust layer on the corrosion resistance of low-alloy steel in simulated concrete pore solution. *Int. J. Miner. Metall. Mater.* **24**, 64–74 (2017).

114. Pourbaix, M. *Atlas of Electrochemical Equilibria in Aqueous Solutions*. (National Associaton of Corrosion Engineers, 1966).

115. Pan, T. & Lu, Y. Quantum-Chemistry Based Studying of Rebar Passivation in Alkaline Concrete Environment. **6**, 4967–4983 (2011).

116. Powers, T. C. Absorption of Water by Portland Cement Paste during the Hardening Process. *Ind. Eng. Chem.* **27**, 790–794 (1935).

117. Lafuente, B., Downs, R. T., Yang, H. & Stone, N. The power of databases: The RRUFF project. in *Highlights in Mineralogical Crystallography* (eds. Armbruster, T. & Danisi, R. M.) 1–30 (W. De Gruyter, 2015). doi:10.1515/9783110417104-003

118. Mesbah, A., François, M., Cau-Dit-Coumes, C., Frizon, F., Filinchuk, Y., Leroux, F., Ravaux, J. & Renaudin, G. Crystal structure of Kuzel's salt 3CaO•Al2O 3•1/2CaSO4•1/2CaCl2•11H 2O determined by synchrotron powder diffraction. *Cem. Concr. Res.* **41**, 504–509 (2011).

119. Markgraf S A, R. R. J. High-temperature structure refinements of calcite and magnesite. *Am. Mineral.* **70**, 590–600 (1985).

120. Allmann, R. & Jepsen, H. P. Die struktur des hydrotalkits. *Neues Jahrb. fur Mineral.* 544–551 (1969).

121. Yoon, S., Ha, J., Chae, S. R., Kilcoyne, D. A., Jun, Y., Oh, J. E. & Monteiro, P. J. M. Phase changes of monosulfoaluminate in NaCl aqueous solution. *Materials (Basel).* **9**, (2016).

Appendix A: Expressed Pore Solution Experimental Data

A 1: Comparison of moisture content and volume of pore solution expressed

	Average Measured pH	Average Moist content (wt %)	Expressed Pore Soln (mL)	Max. applied load (KN)
0 wt% Cl	**13.32** ± 0.02	**17.60% ± 0.30%**	**6.5 ± 1.0**	**500**
0.25 wt% Cl - NaCl	13.34 ± 0.07	18.80% ± 0.18%	5.8 ± 1.5	500
0.50 wt% Cl - NaCl	13.35 ± 0.02	20.90% ± 0.68%	7.0 ± 0.5	500
0.75 wt% Cl - NaCl	13.28 ± 0.03	19.39% ± 0.01%	5.5 ± 1.0	500
1.00 wt% Cl - NaCl	13.37 ± 0.01	18.80% ± 0.03%	7.2 ± 0.8	500
2.50 wt% Cl - NaCl	13.26 ± 0.18‡	17.96% ± 0.07%	6.2 ± 1.3	500
5.00 wt% Cl - NaCl	13.19 ± 0.03	17.11% ± 0.06%	6.3 ± 0.5	500
7.50 wt% Cl - NaCl	13.16 ± 0.03	19.63% ± 0.05%	7.2 ± 0.8	500
0.25 wt% Cl - $CaCl_2$	13.28 ± 0.03	18.67% ± 0.16%	7.5 ± 0.0	500
0.50 wt% Cl - $CaCl_2$	13.29 ± 0.03	18.64% ± 0.08%	7.2 ± 1.8	500
0.75 wt% Cl - $CaCl_2$	13.16 ± 0.02	19.51% ± 0.33%	7.0 ± 0.5	500
1.00 wt% Cl - $CaCl_2$	13.17 ± 0.05	17.51% ± 0.02%	6.7 ± 1.0	500
2.50 wt% Cl - $CaCl_2$	12.92 ± 0.05	17.49% ± 0.08%	5.2 ± 0.3	700
5.00 wt% Cl - $CaCl_2$	12.35 ± 0.04	15.83% ± 0.27%	4.5 ± 0.5	700
7.50 wt% Cl - $CaCl_2$	NA	16.05% ± 0.18%	0.3*	800
0.25 wt% Cl - $MgCl_2$	13.25 ± 0.04	18.23% ± 0.14%	7.2 ± 0.8	500
0.50 wt% Cl - $MgCl_2$	13.24 ± 0.03	19.75% ± 0.06%	8.7 ± 1.0	500
0.75 wt% Cl - $MgCl_2$	13.18 ± 0.06	18.73% ± 0.02%	8.2 ± 0.5	500
1.00 wt% Cl - $MgCl_2$	13.13 ± 0.05	18.10% ± 0.06%	6.0 ± 0.5	500
2.50 wt% Cl - $MgCl_2$	12.98 ± 0.02	18.06% ± 0.13%	5.7 ± 0.3	700
5.00 wt% Cl - $MgCl_2$	12.31 ± 0.02	17.65% ± 0.06%	3.8 ± 0.8	900
7.50 wt% Cl - $MgCl_2$	NA	16.14% ± 0.42%	0.25*	800

‡ An outlier (13.04) resulted in accuracy ± 0.18

*Only one sample

Appendix B: Electrochemical Results for Rebar Specimen

B1) Saturated $Ca(OH)_2$ Solution (NaCl)

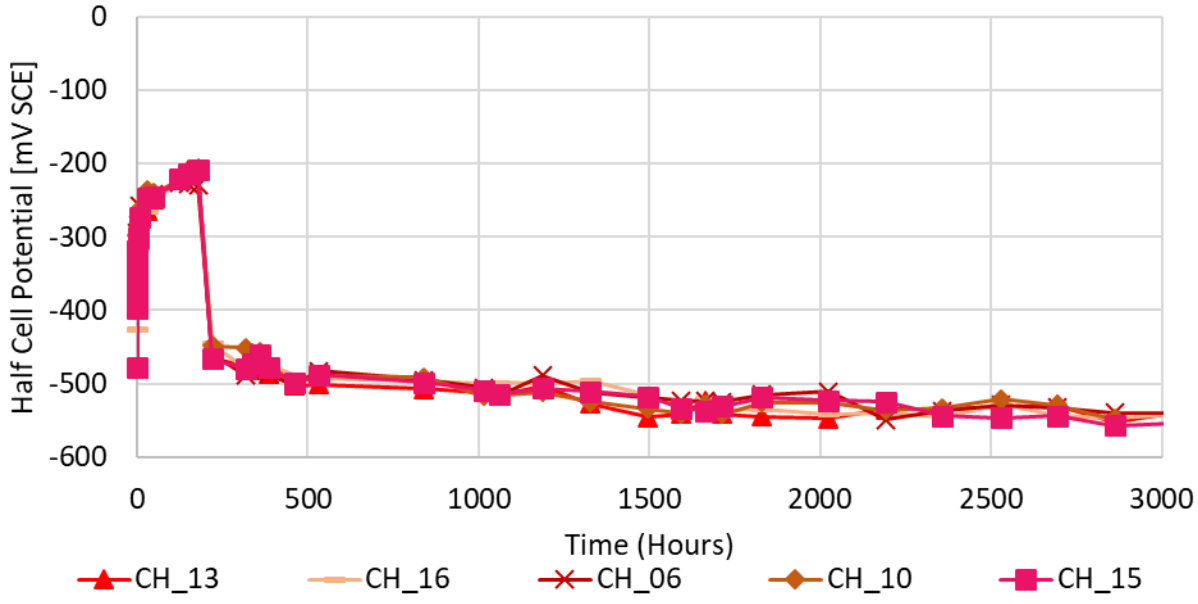

Figure B 1: Half cell potential of individual specimen in Saturated $Ca(OH)_2$ solution

B2) ASTM SPS (NaCl)

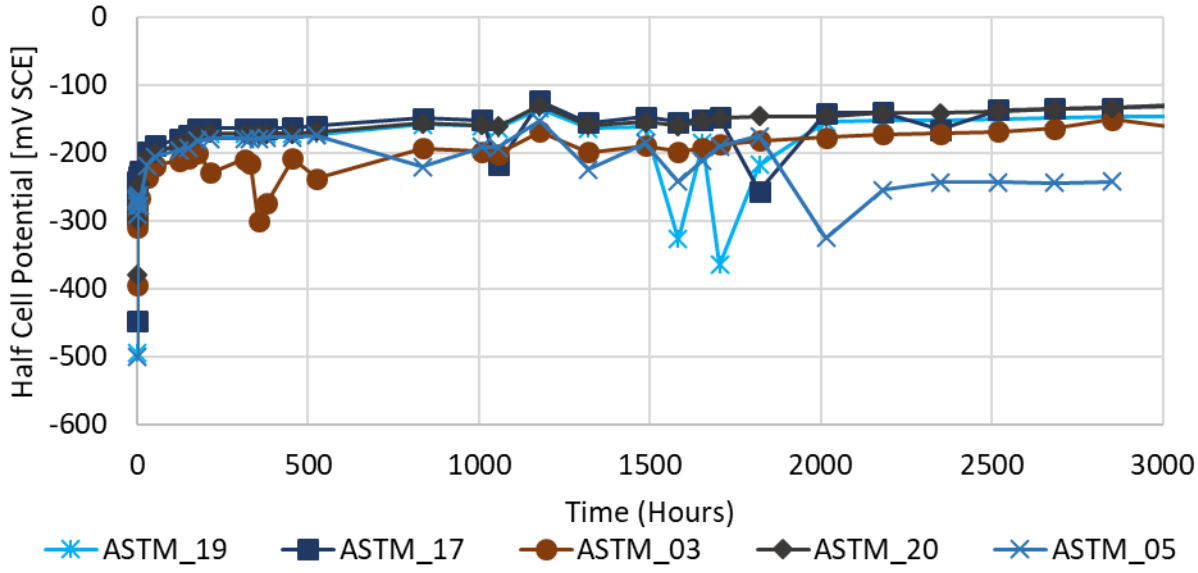

Figure B 2: Half cell potential of individual specimen in ASTM SPS

B3) Tri- Hydroxide Solution

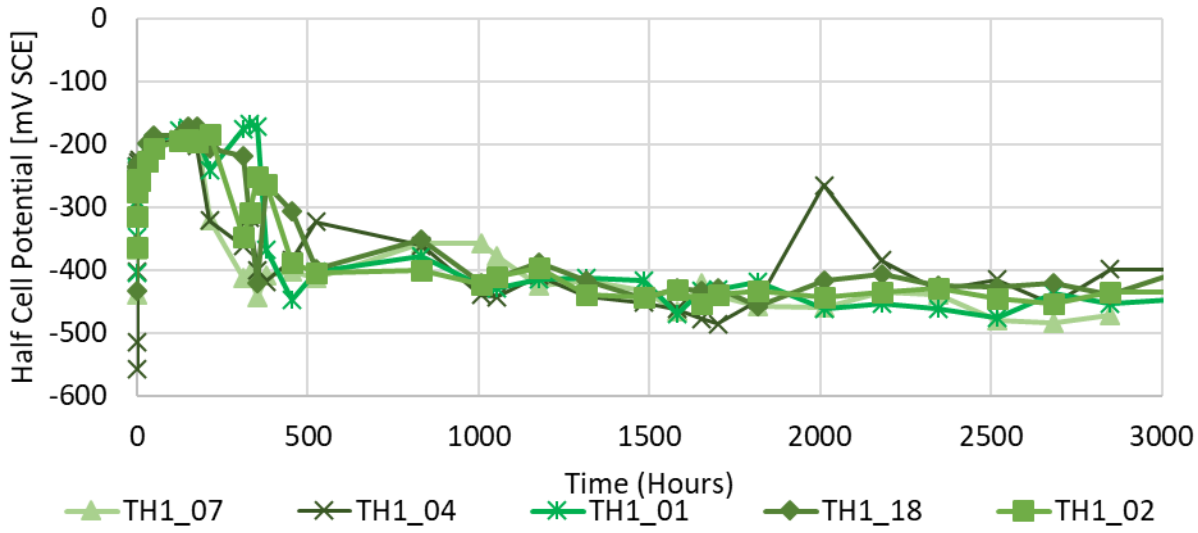

Figure B 3: Half cell potential of individual specimen in TH1 SPS

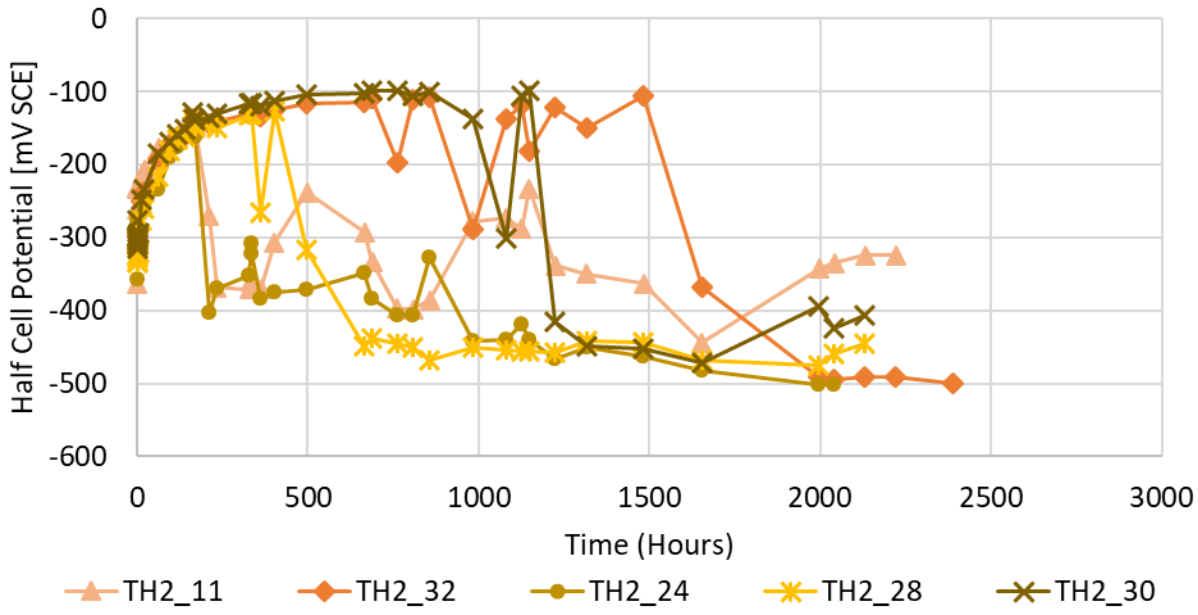

Figure B 4: Half cell potential of individual specimen in TH2 SPS

B4) SEPS - NaCl

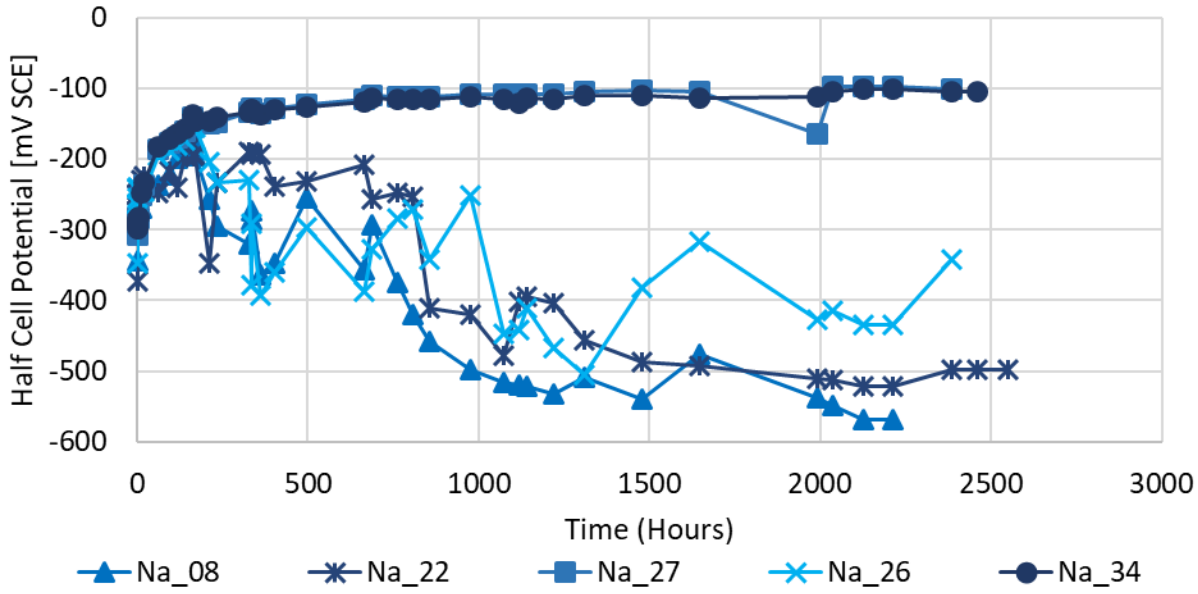

Figure B 5: Half cell potential of individual specimen in SEPS (NaCl)

B5) SEPS – $CaCl_2$

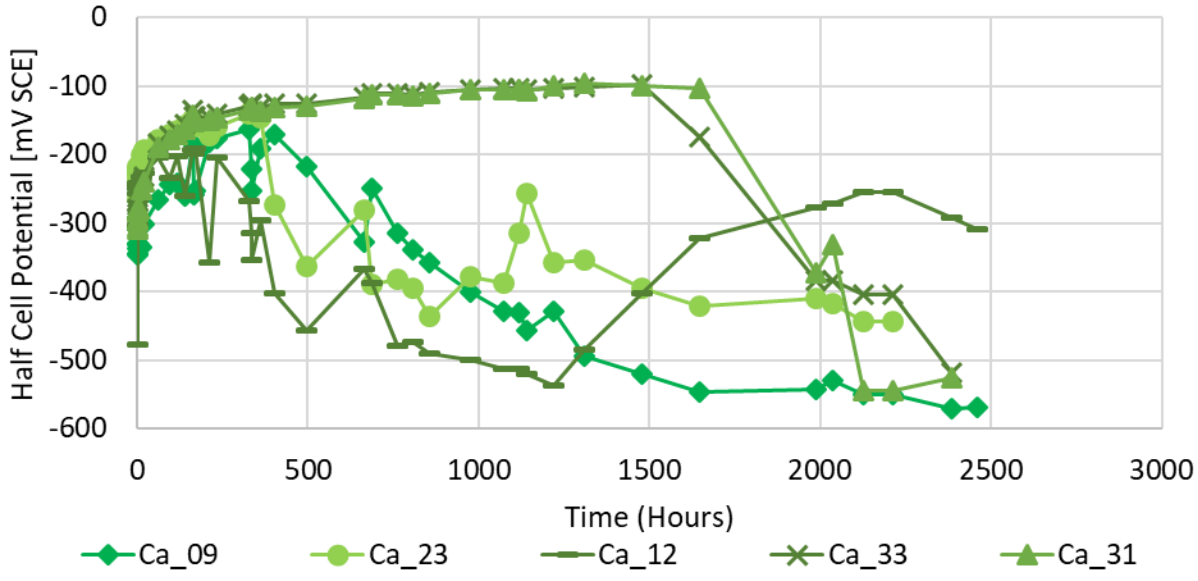

Figure B 6: Half cell potential of individual specimen in SEPS ($CaCl_2$)

B6) SEPS - $MgCl_2$

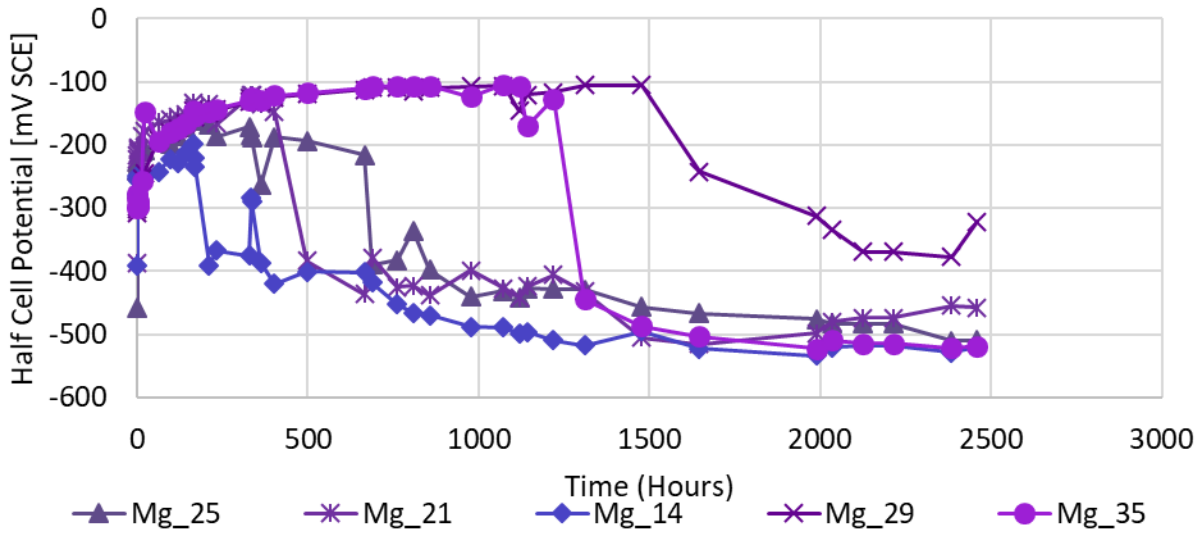

Figure B 7: Half cell potential of individual specimen in SEPS ($MgCl_2$)

Appendix C: Bound Chlorides and Sulphates

C1) Sample Calculation of g Non-Evapourated Water per g Cement from Moisture Content

It is assumed that:

- All water remains in the paste between mixing on day one and demoulding on day 28. Sample preparation at 28 days for moisture content sample is assumed to result in negligible evapouration.
- Powdered samples used for moisture content measurements (two samples, 10g each) are representative of that batch of cement.

Calculation:

Original 'Damp' cement: 1000g H_2O, 2000 g cement (Amounts used for each batch, salt was added in addition to cement).

Dried Cement: 2000g cement, (1000g – X) H_2O where X is the weight change after drying.

Water remaining in cement: 1000g – (3000*X)

w/c for chemically and physically bound water: w/c = (1000 – (3000*X))g H_2O/2000g cement

C2) Calculation of g water Required for Minimum hydration from Powers

In the 1935 publication "Absorption of Water by Cement Paste during the Hardening Process"[116] T.C. Powers investigated the water absorption of C3S, C2S, C3A and C4AF with various gypsum concentrations over the first 28 days of hydration. Using this figure, the minimum water requirements can be calculated using the equation below.

Equation 0-1: Water Requirement of Cement from Known Composition

$$A = aC3S + bC2S + cC3A + dC4AF$$

Where:

A is the percentage of water required by weight of cement

a,b,c,d are co-efficients determined for the cement compound and hydration time

C3S, C2S, C3A, C4AF are the percentages of these compounds in the cement mix

Powers suggests co-efficient based on a study of 22 cements which gives an A value of 0.135 while an approximation of co-efficient corresponding to the gypsum content used in the GU cement in this thesis results in an A value of 0.2517 as shown in the table below.

	Co-efficients Calculated by Powers from study of 22 cements	Co-efficients estimated from Powers Figure 5 for ~ 5.8 wt% CaSO4
a	0.0481	0.05
b	0.0202	0.01
c	0.1091	0.17
d	0.0247	0.11
C3S	0.52	0.52
C2S	0.17	0.17
C3A	0.80	0.80
C4AF	0.80	0.80
A	**0.135486**	**0.2517**

Appendix D: Comparison of XRD Peaks

Peak overlap and background noise must be considered when evaluating xrd scans. The maximum peaks are not in the same location for each sample although the highest intensity peaks are all peaks connected to ($Ca(OH)_2$ so normalizing to the highest intensity peak skews the results. Background noise has been removed using Dynamic Beam optimization which controls for slight differences in sample preparation including how the samples were packed into the sample holder.

The intensity of peaks from samples with admixed NaCl, $CaCl_2$ and $MgCl_2$ are compared with either the intensity of peaks for the chloride free sample or to example peaks obtained from the RRUFF database[117]. Because the cement samples are composed of many different hydration products many peaks are not distinguishable due to a decreased intensity when compared to a pure, single compound sample.

Reference peaks from literature are shown normalized to the largest peak. All literature values were recorded using CuKα radiation.

D1) Aft (Ettringite)

Table D 1: Aft peak intensities for admixed salt samples

	Maximum Peak Intensities					Peak height relative to 0 Cl		
2 Theta	**0Cl**	**NaCl**	**$CaCl_2$**	**$MgCl_2$**		**NaCl**	**$CaCl_2$**	**$MgCl_2$**
15.8	*720*	*637*	*774*	*900*		*0.88*	*1.08*	***1.25***
18.9	*633*	*543*	*678*	*709*		*0.86*	*1.07*	*1.12*
22.9	*800*	*623*	*843*	*843*		*0.78*	*1.05*	*1.05*
25.6	*700*	*567*	*700*	*700*		*0.81*	*1.00*	*1.00*
32.3	*773*	*813*	*900*	*900*		*1.05*	*1.16*	*1.16*
35.0	*638*	*539*	*684*	*745*		*0.84*	*1.07*	*1.17*
40.8	*597*	*597*	*667*	*700*		*1.00*	*1.12*	*1.17*

The location of Aft peaks is well established since Aft is present in many hydrated cements. Aft peaks are slightly less intense for NaCl and only slightly more intense for $CaCl_2$ and $MgCl_2$. At 15.8° the sample with admixed $MgCl_2$ is an outlier with an especially high intensity. Peaks do not align exactly at this location (±0.08°) so the increased intensity may result from substitutions which alter the D-spacing in this crystal orientation or overlap with another compound.

D2) Afm (Monosulphoaluminate)

The Afm phase has the general formula ($Ca_4Al_2(SO_4)(OH)_{12} \cdot 6\ H_2O$) however substitutions can occur resulting in varying compositions of aluminate phases all of which have slightly different bond lengths and peak locations. This made it challenging to identify any peaks as specifically Afm.

Several researchers have characterized different forms of Afm including Balonis et al. 2010 who synthesized Friedel salts, Kuzel salts and Afm phases and solid solutions of these. Mesbah et al. 2011 synthesizes Afm phases containing differing amounts of Cl and sulphate while studying the structure of Kuzel salt. Several of the experimental peaks identified in these papers have been identified in Figure D 1 below and are normalized to the highest peak.

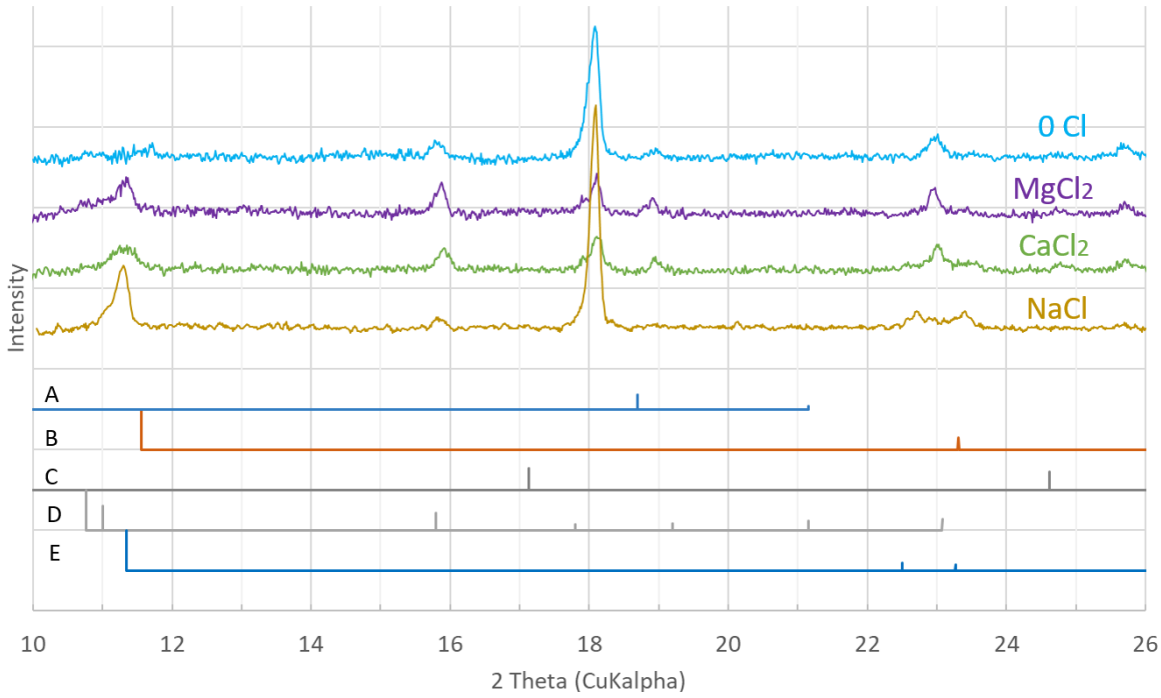

Figure D 1: Afm type phases identified by Balonis et al. 2010[32] and Mesbah et al. 2011[118] A) is SO4-Afm[32] B) is CO_3-Afm[32] C) is OH-Afm prior to drying[32] D) is Afm-($Cl_{0.25}SO4_{3/8}$) [118] E) is Afm-($Cl_{0.75}SO4_{1/8}$) [118]

D3) $Ca(OH)_2$ (Portlandite)

Table D 2: $Ca(OH)_2$ Peak intensities for admixed salt samples

	Maximum Peak Intensities					Peak height relative to 0 Cl		
2 Theta	**0Cl**	**NaCl**	**$CaCl_2$**	**$MgCl_2$**		**NaCl**	**$CaCl_2$**	**$MgCl_2$**
18	2155	3234	877	1026		1.50	0.41	0.48
28.8	975	975	610	610		1.00	0.63	0.63
34.1	2415	2811	1206	972		1.16	0.50	0.40
47.2	1192	1375	718	718		1.15	0.60	0.60
50.9	1043	1043	772	670		1.00	0.74	0.64
54.35	756	756	577	577		1.00	0.76	0.76
56.2	568	558	560	505		0.98	0.99	0.89
62.6	655	730	637	585		1.11	0.97	0.89
64.4	631	650	551	544		1.03	0.87	0.86

71.8	591	607	536	540		1.03	0.91	0.91
84.8	613	594	534	547		0.97	0.87	0.89

The crystal structure and associated xrd peaks of $Ca(OH)_2$ are well understood. Peaks for $Ca(OH)_2$ in samples with admixed salts vary in intensity relative to the chloride free sample although the variation decreases as peaks become less intense at higher angles. Some peaks may overlap with peaks for other compounds causing this variability.

D4) $CaCO_3$ (Calcite)

Table D 3: $CaCO_3$ peak intensities for admixed salt samples

	Maximum Peak Intensities					Peak height relative to 0 Cl		
2 Theta	**0Cl**	**NaCl**	**$CaCl_2$**	**$MgCl_2$**		**NaCl**	**$CaCl_2$**	**$MgCl_2$**
23.1	812	553	850	833		0.68	1.05	1.03
24.9	589	496	629	614		0.84	1.07	1.04
26.6	561	558	558	514		1.00	1.00	0.92
29.4	784	996	997	860		**1.27**	**1.27**	**1.10**
31.5	571	513	530	588		0.90	0.93	1.03
36.0	551	524	562	565		0.95	1.02	1.03
39.5	556	643	643	602		1.16	1.16	1.08
43.2	510	573	573	578		1.12	1.12	1.13
47.6	565	569	615	592		1.01	1.09	1.05
48.6	557	546	579	552		0.98	1.04	0.99

Calcite has a high intensity peak at 29.4° which significantly exceeds the intensity of other peaks, as such only the one location is expected to be detected in the scans of cement samples[119]. This makes identification of calcite inconclusive. When compared to the chloride free cement sample only the peak

at 29.4° varies significantly with a 27% increase in intensity for admixed NaCl and $CaCl_2$. This peak has also been identified as C-S-H by several researchers[27,58,109,110].

D5) C-S-H

C-S-H has a gel structure resulting in a broad low intensity hump over the range 27° to 35°. Many researchers attribute a peak at 29.5° to C-S-H[27,58,109,110]. The experimental scans prior to background removal are shown in Figure D 2 below.

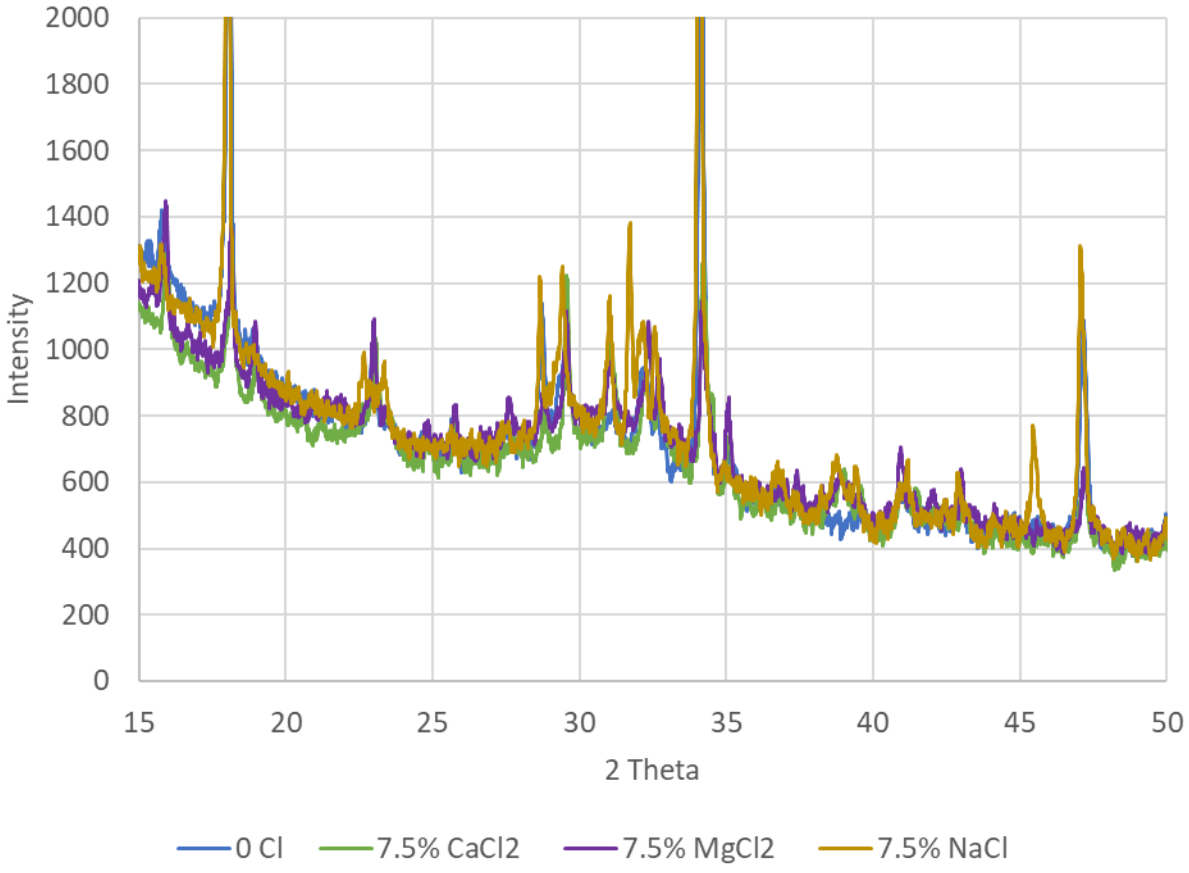

Figure D 2: Scans of pastes with 7.5 wt% Cl with admixed NaCl, $CaCl_2$ and $MgCl_2$ and paste without chloride prior to removal of background noise showing amorphous hump for C-S-H.

D6) Friedel Salt

Table D 4: Friedel's Salt peak intensities for admixed salt samples

	Maximum Peak Intensities					Peak height relative to 0 Cl		
2 Theta	**0Cl**	**NaCl**	**$CaCl_2$**	**$MgCl_2$**		**NaCl**	**$CaCl_2$**	**$MgCl_2$**
11.3	637	1260	806	968		**1.98**	1.27	1.52
22.6	510	615	582	536		**1.21**	1.14	1.05
22.8	570	612	589	617		1.07	1.03	1.08
23.4	547	709	600	568		**1.30**	1.10	1.04
23.5	556	609	608	529		1.10	1.09	0.95
31	610	828	840	661		**1.36**	**1.38**	1.08

Friedel salt ($Ca_4Al_2Cl_2(OH)_{12} \cdot 4H_2O$) has a similar composition to Afm where the SO_4^{2-} has been replaced by Cl^-. The initial peak occurs around 11.25° with subsequent peaks occurring at 22.6°, 23.15° (Line A). Heating Friedel salts was investigated by Renaudin et al[108] and a shift between 30 °C and 40 °C was detected with peaks at 40 °C being located at 11.35°, 22.8° and 23.5° (line B). Work by Balonis et al[32] investigating solid solutions of Afm investigated the transition of Cl-Afm (identified as Friedel salt) to OH-Afm. At 0.7 Cl/(Cl+OH) similar intensity double peaks occur at 22.6° and 23.4° (Line C).

Comparison of peaks to the 0 Cl sample is complicated by the wide base of the Afm peak at 23°. The sample with admixed NaCl has higher intensity peaks than the other samples at 11.3°, 22.6° and 23.4°. When visually assessed peak locations for the admixed NaCl sample align better with line B than Line A. Friction during sample preparation may have heated Friedel salt.

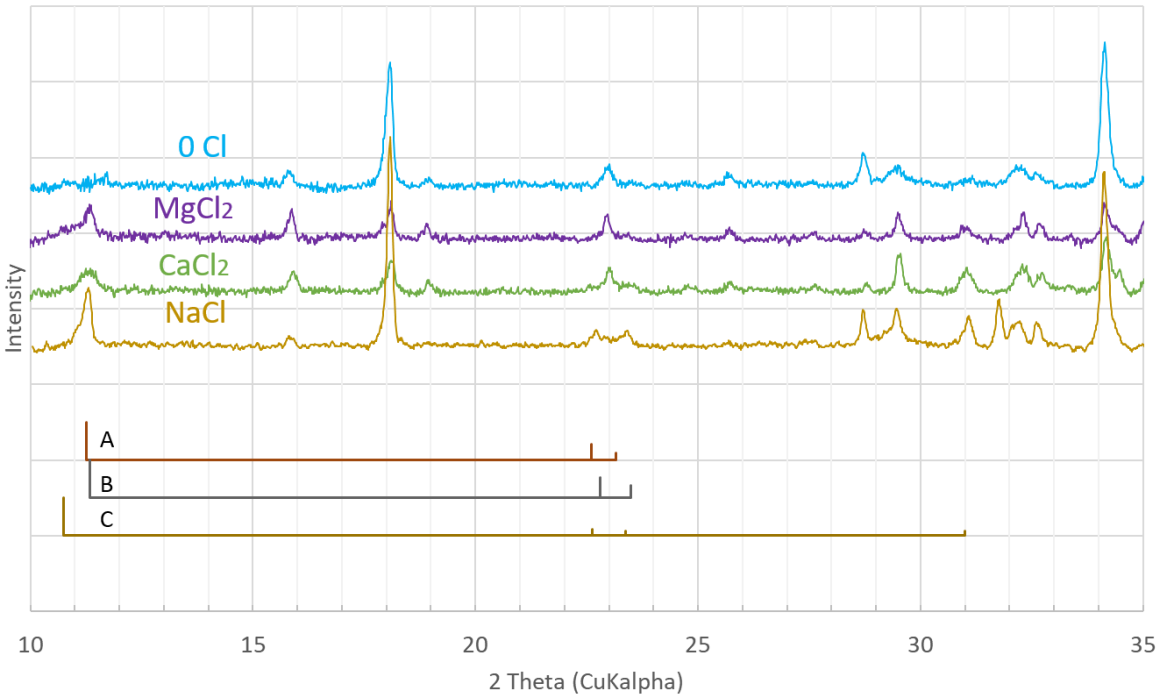

Figure D 3: Identified Friedel Peaks from Literature. A) Friedel salt at 20 °C[108] B) Friedel salt at 40 °C[108] C) Friedel salt in solid solution with OH-Afm at 0.7 Cl/(Cl+OH) at 25 °C [32]

D7) Hydrocalumite

Table D 5: Hydrocalumite peak intensities for admixed salt samples

	Approximate Peaks					Peak height relative to 0 Cl		
2 Theta	**0Cl**	**NaCl**	**$CaCl_2$**	**$MgCl_2$**		**NaCl**	**CaCl2**	**MgCl2**
11.3	601	1260	784	869		**2.10**	1.30	1.45
22.8	610	636	636	617		1.04	1.04	1.01
23.4	530	665	601	613		1.25	1.13	1.16
26.0	548	517	554	597		0.94	1.01	1.09
31.0	610	770	840	661		1.26	1.38	1.08
38.7	528	654	623	616		1.24	1.18	1.17
39.3	520	590	566	600		1.13	1.09	1.15

Hydrocalumite ($[Ca_2Al(OH)_6]OH \cdot nH2O$) was identified as a possibility for the admixed NaCl and $MgCl_2$ samples by the XRD software with the NaCl sample having the best fit.

D8) Hydrotalcite

Table D 6: Hydrotalcite peak intensities for admixed salt samples relative to reference scan

		Maximum Peak Intensities					Peak height relative to Reference Peaks			
2 Theta	Hydrotalcite Peaks[120]	**0Cl**	**NaCl**	**$CaCl_2$**	**$MgCl_2$**		**0Cl**	**NaCl**	**$CaCl_2$**	**$MgCl_2$**
11.3	1500	686	1262	816	937		0.46	0.84	0.54	0.62
22.7	692	641	692	627	610		0.93	1.00	0.91	0.88
23.24	139	563	662	592	597		4.05	4.76	4.26	4.29
34.7	89.5	550	570	632	608		6.15	6.37	7.06	6.79
38.9	83	545	645	615	630		6.57	7.77	7.41	7.59
46.2	50.7	505	530	568	570		9.96	10.45	11.20	11.24

The peaks for Hydrotalcite has the general formula ($Mg_{1-x}(Al,Fe)_x(OH)_2 \cdot [A^{n-}]_{x/n} \cdot mH_2O$) depend on the composition since substitutions are very common in the mineral which may include the cations: Mn, Mg, Ni, Zn, Al, Fe and may include the interlayer anions: OH-, Cl-, CO_3^{2-} and SO_4^{2-}. The hydrotalcite used for comparison had the measured composition $Mg_{6.0}(Al_{1.6}, Fe^{3+}_{0.4})\ (CO_{3.0})(OH)_{16} \cdot 4\ H_2O$.

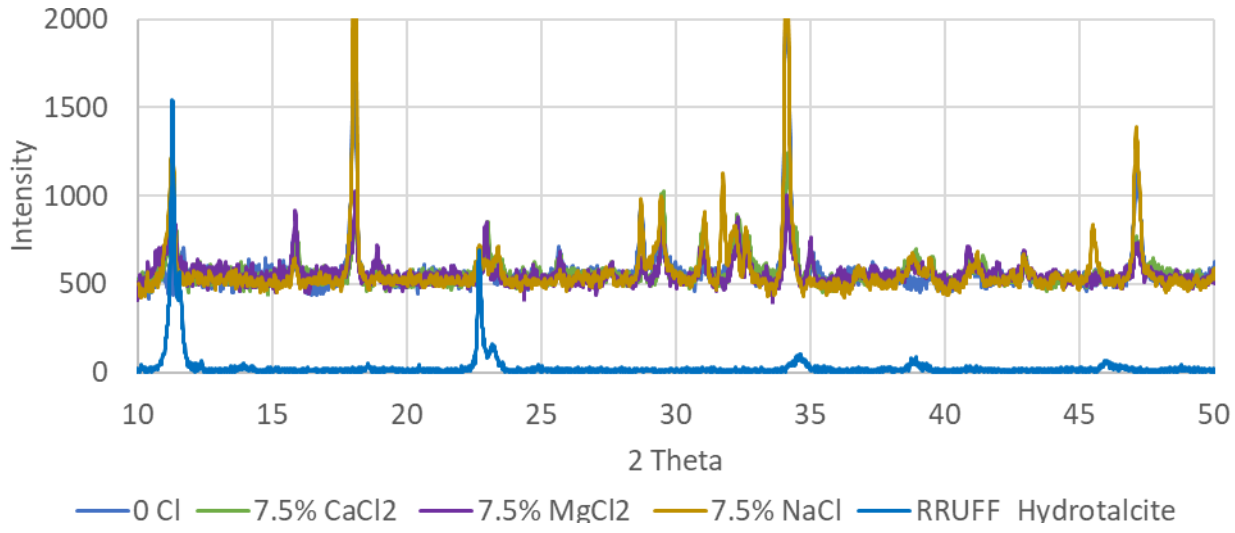

Figure D 4: Comparison of experimental xrd scans with hydrotalcite peaks from the RRUF database

D9) Kuzel's Salt

Kuzel's salt ($Ca_4Al_2Cl(SO_4)_{0.5}(OH)_{12} \cdot 6H_2O$) is frequently identified by the first peak which occurs around 10.8°. The formation of kuzel's salt was investigated by Yoon et al 2016[121] by suspending monosulphoaluminate in NaCl solution. Kuzel's salt was found to occur between 0.1 M NaCl and 3.0 M NaCl and was fully converted to Friedel's salt at 5 M NaCl. All experimental peaks occurred between 11.0 and 11.3 so no Kuzel's salt is thought to be present at 7.5 wt% admixed Cl (4.23 mol Cl/L). Kuzel's salt may occur for samples containing less admixed chloride.

D10) $MgCO_3$ (Magnesite)

Table D 7: Magnesite peak intensities for admixed salt samples relative to reference scan

		Maximum Peak Intensities					Peak height relative to Reference Peaks			
2 Theta	**$MgCO_3$ Peaks**[119]	**0Cl**	**NaCl**	**$CaCl_2$**	**$MgCl_2$**		**0Cl**	**NaCl**	**$CaCl_2$**	**$MgCl_2$**
32.7	1570	699	806	758	707		0.45	0.51	0.48	0.45
43.1	513	475	654	625	663		0.93	1.27	1.22	1.29

The magnesite peak referenced corresponds to a sample containing $(Mg_{1.98}, Fe_{0.01})C_{1.00}O_{3.00}$ and is shown below in comparison to the sample scans. Similar to calcite, the high intensity of the reference peak at 32.7° means that this peak would be the only one detectable making identification inconclusive. A higher substitution of Fe for Mg may modify the d-spacing in this compound resulting in altered peaks.

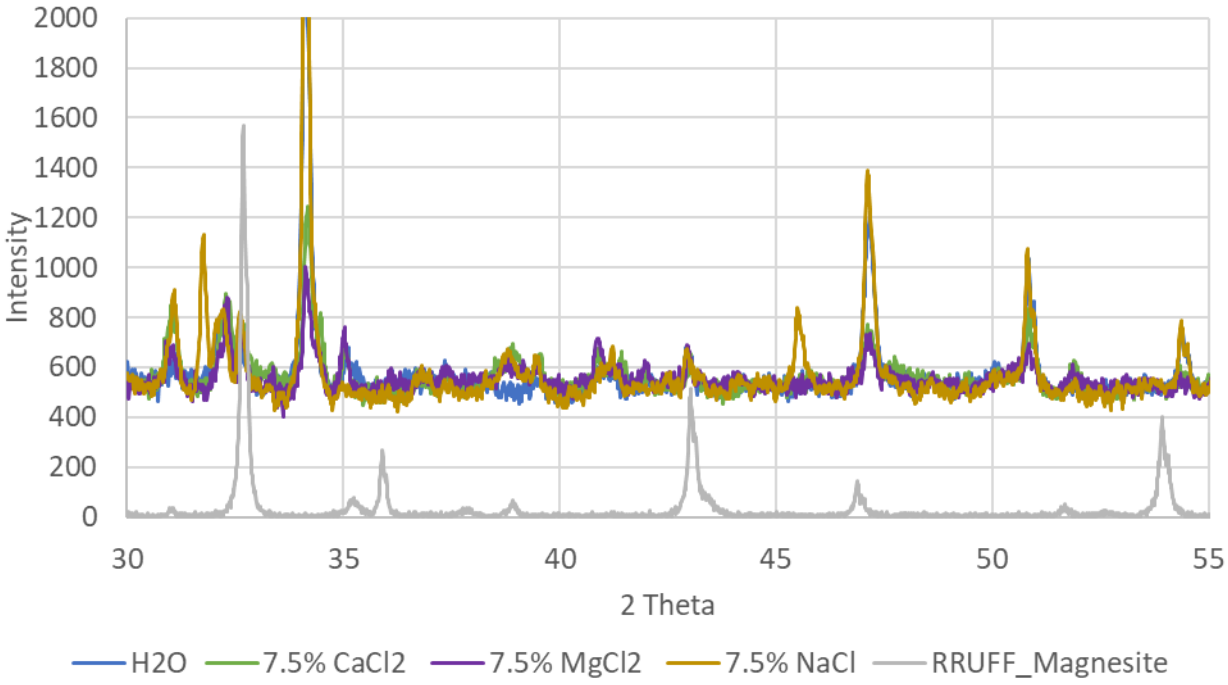

Figure D 5: Comparison of experimental xrd scans with Magnesite peaks from the RRUF database

D11) $Mg(OH)_2$ (Brucite)

Table D 8: Sample peak heights relative to reference $Mg(OH)_2$ peaks

	Approximate Peaks	Approximate Peaks					Peak height relative to Reference Peaks			
2 Theta	$Mg(OH)_2$ Reference	**0Cl**	**NaCl**	**$CaCl_2$**	**$MgCl_2$**		**0Cl**	**NaCl**	**$CaCl_2$**	**$MgCl_2$**
18.66	3597	521	521	500	588		0.14	0.14	0.14	0.16
38.08	1302	585	489	489	585		0.45	0.38	0.38	0.45
50.94	390.7	1040	997	772	632		2.66	**2.55**	**1.98**	**1.62**

Brucite does not appear to be present in sufficient quantities to appear on XRD scans for any samples.

D12) Oxychlorides

Oxychlorides and hydroxy chlorides were identified in the work of Peterson et al[35] and Julio-Betancourt and Hooton [36] formed from concrete or mortar exposed to $CaCl_2$ and $MgCl_2$ salt solutions. Because samples were submerged in high concentrations of $CaCl_2$ or $MgCl_2$ sufficient oxychloride salts were identified and isolated for xrd analysis. Since oxychlorides were not isolated in admixed salt samples there might not be sufficient salt crystals to appear on XRD scans.

Peterson et al focused-on calcium oxychloride salt formed on a cement sample at 5 °C. This salt was removed from the solution and immediately scanned in xrd (scan A below). Some oxychloride was removed from solution then dried for 10 minutes on a hot plate at 50 °C which resulted in the composition $Ca(OH)_2 \cdot CaCl_2 \cdot 2H_2O$ in scan B. The major peaks for both these scans do not align with any evident peaks for admixed salt cement samples.

Julio-Betancourt and Hooton investigated how oxychlorides might change under common preparation techniques like 38 °C for two weeks or 110 °C for 24 hours in addition to directly after removal from solution at 23 °C. Since cement samples for this work were not dried for a prolonged time at a high temperature the peaks corresponding to 110 °C have been omitted. The highest intensity peak for $3Mg(OH)_2 \cdot MgCl_2 \cdot 24H_2O + MgCl_2 \cdot 6H_2O$ (peak set E) occurs at approximately 63°, there is no increased intensity for cement with admixed $MgCl_2$ at this location.

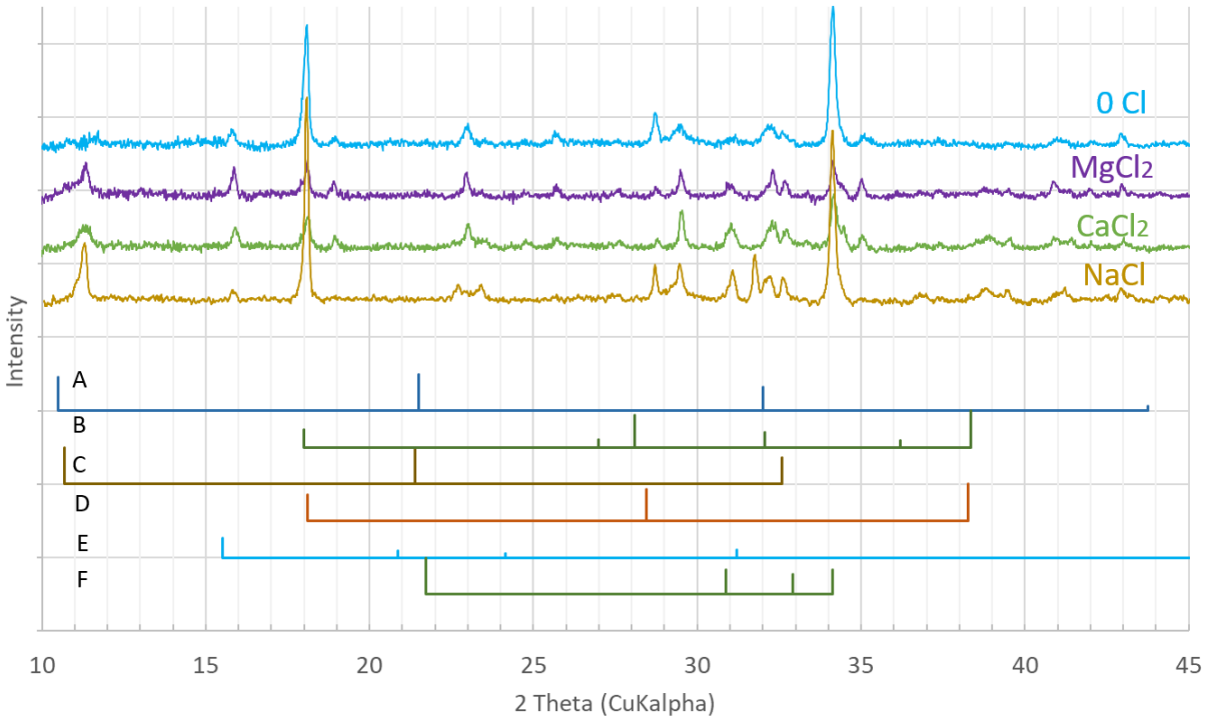

Figure D 6: Comparison of experimental xrd scans with peaks identified in literature where A) $3CaO{\cdot}CaCl_2{\cdot}15H_2O$ (wet) [35] B) $Ca(OH)_2{\cdot}CaCl_2{\cdot}2H_2O$ (dried) [35] C) $3Ca(OH)_2{\cdot}CaCl_2{\cdot}12H_2O$ (23 °C) [36] D) $3Ca(OH)_2{\cdot}CaCl_2{\cdot}0.1H_2O$ (38 °C) [36] E) $3Mg(OH)_2{\cdot}MgCl_2{\cdot}24H_2O$ + $MgCl_2{\cdot}6H_2O$ (23 °C) [36] F) $3Mg(OH)_2{\cdot}MgCl_2{\cdot}13H_2O$ + $MgCl_2{\cdot}6H_2O$ (38 °C) [36]